Investigations of Transition Metal Catalytic Cycles through Organometallic Studies

by

Joshua Thedford

A dissertation submitted in partial fulfillment
of the requirements for the degree of
Doctor of Philosophy
(Chemistry)
in the University of Michigan
2026

Doctoral Committee:

Professor Melanie S. Sanford, Chair
Assistant Professor Joshua A. Buss
Associate Professor Timothy Cernak
Professor John P. Wolfe

Joshua Thedford

thedford@umich.edu

ORCID iD: 0000-0003-4820-3694

© Joshua Thedford 2026

Dedication

I dedicate this thesis to my siblings, Jazzi, Christopher, and Matthew, and to my parents who I miss everyday, even if I don't say it enough.

Acknowledgements

Dr. Narke Norton is the reason I am in research today. As a young seventeen-year-old visiting the University of Georgia, he looked out for me and pointed me to the Young Scholar's Program, where I first did research. Not only that, but he has also stayed a steady and constant presence in my life. Thank you for all of your support.

Professor Aaron Thompson was my advisor in undergrad, and I can't thank him enough for allowing me to be in his lab as a freshman and simultaneously giving me the mentorship to learn soil chemistry while also giving me the space to learn and figure things out. That is the main reason I became interested in synthetic chemistry research. Thank you for helping me grow as a researcher. I also need to give a huge thanks to Dr. Nadia Noor, my mentor in the Thompson lab. Your patience and kind nature played such a huge role in why I enjoyed being in lab.

I would like to thank Professor Joshua Buss for allowing me to rotate in his lab and for allowing me to continue to stop him in the hallway for way-too-long conversions. I would like to thank Dr. Eric Wiedner at Pacific National Northwest Laboratory for being so helpful from the inception to the (near)end of this project, as well as always being such a calm presence. I would like to thank Dr. Fengrui Qu for collecting and sorting through all of my horrible crystals, as well as humoring random conversations. I would like to also thank Dr. Eugenio Alvarado for helping me with the random specific NMR experiments that I need and for not killing me for all the times I messed up in the NMR lab. I would finally like to thank my mentors when I started doing synthetic chemistry. Thank you to Dr. Hannah Vonesh for your patience and amazing mentorship, I don't think I could've made the switch from analytical chemistry to synthetic without you. Dr. Connor Brigham, thank you for your support in the Sanford lab. I appreciate the freedom you gave me to explore the project and allow me to become an independent researcher. And finally, thank you to Dr. Michela Maiola in the Buss lab who taught me most of what I know about inorganic research and for being a good friend during our time here.

I have to thank all the amazing people that I met at PNNL during my internship. Gayle, Krista, and Manuel, you guys are amazing labmates and I have to thank you for being so helpful

and personable in my time there. Evan, Alex, Jeff, Wendy, Taoshin, Nathaniel, Garam, Jay, Jay, Jim and Jim, thank you all for making my summer in Richland an unforgettable time. I couldn't imagine making such great friendship in so short of a time, and I hope I can play volleyball with yall again.

All of the people in and out of chemistry in Ann Arbor has made my time here so much richer. I would like to that Alex for being the best roommate/tennis partner/lunch advisor/friend a guy could ask for. And for bringing Arrhenius Tanabe Kim into all of our lives. I would like to thank Jake for always being down for getting coffee or hosting a watch party. You really kept me from closing myself up. I would also like to thank Cody for always being a great friend, even if for some completely unavoidable circumstances, I can never visit you. Thank you to Tenzin, Gonzalo, Cam and my mentor Mario for all our fun that we had and for putting up with my late-night naps. I would also like to thank Olivia for being my friend away from work. I will miss getting tea and watching open mics. I need to also deeply thank my best friends from undergrad. Marianne and Cynthia, yall have been such great friends for nearly a decade and I'm so proud to have you guys as my friends.

Professor Melanie Sanford was my advisor in graduate school and I couldn't have asked for a better mentor. She has taught me how to think critically and deeply at problems, as well as helping me gain more attention to detail. Even though my chemdraws are still not up to standard, we are miles better from where I started! Thank you for helping me grow as a chemist. Your unwavering support has been invaluable.

Melanie has fostered such an amazing lab, and I can't imagine spending five years here without you guys. Isaac and Maria were my sort of mentors and such wonderful guiding presences in the lab. Thank you to my mentee Zoe. Being able to mentor you guys has been a blessing and I'm very excited to see how far you go. Thank you, Frances, for being you. You are one of one and I'm so glad that we became friends. I would also like to thank Dan, Abdias. Sabrina, Julia, and Sammy for being the best friends and labmates that anyone could ask for.

Then of course, I have to thank my cohort, Taylor, Sabrina, Bobby, Emily, and Ila. Yall genuinely feel like siblings to me. In fact, I've seen some of your parents more than I've seen my own these past 5 years. Words cannot express how much I love you guys. There isn't another group of people that I would want to do my PhD with.

Table of Contents

Dedication ii

Acknowledgements iii

List of Tables ix

List of Figures xi

List of Schemes xv

Abstract xvii

Chapter 1 Introduction 1

1.1 Palladium-mediated Ary-Sulfur Coupling 2

1.1.1 Palladium-mediated Aryl-Sulfide Couplings 2

1.1.2 Palladium-mediated Aryl-Sulfinate Couplings 4

1.2 Copper-mediated aryl sulfur coupling 6

1.2.1 Copper-mediated Aryl-Sulfinate Couplings 7

1.3 Catalyst Activation 8

1.3.1 Base Metal Precatalysts 9

1.3.2 Fe(0) C-H activation 10

1.4 References 10

Chapter 2 Aryl-SCF_3 Coupling via Reductive Elimination from a Bipyridine-Ligated Palladium(II) Complex 16

2.1 Background 16

2.2 Synthesis of (4,4'-di-tert-butyl-2,2'bipyridine) Palladium (*p*-fluorophenyl)(halide) Complexes 17

2.3 Ligand Substitution of (dtbpy)Pd(*p*-fluorophenyl)(SCF_3) 20

2.4 Development of Ligand Promoted Aryl-SCF_3 Cross-Coupling Catalysis 24

2.5 Chemical Oxidation of (dtbpy)Pd(*p*-fluorophenyl)(SCF_3) 28

2.6 Photochemical Excitation of (dtbpy)Pd(*p*-fluorophenyl)(SCF_3) 32

2.7 Conclusion 33

2.8 Outlook 34

2.9 Experimental 36

2.9.1 Synthesis of Reagents 36

2.9.2 Palladium Complexes 37

2.9.3 Transmetalation Studies 40

2.9.4 Ligand Substitution/Reductive Elimination 41

2.9.5 Optimization of Catalysis 42

2.9.6 Synthesis of Organic Compounds 45

2.9.7 Oxidative Studies 46

2.9.8 Photochemical Studies 46

2.10 References 46

Chapter 3 Organometallic Investigations into Palladium-Mediated Aryl-Sulfinate Coupling 51

3.1 Background 51

3.2 Synthesis and Characterization of (4,4'-di-tert-butyl-2,2'-bipyridine) Palladium (*p*-fluorophenyl)(SO_2R) Complexes, R = CF_3, CF_2H, CFH_2, CH_3, and *para*-tolyl 53

3.3 *in situ* Phosphine Ligand Substitution and Reductive Elimination of (dtbpy)Pd(*p*-fluorophenyl)(SO_2R) Complexes 55

3.4 Synthesis and Transmetallation of Phosphine-ligated Palladium(II) (*p*-fluorophenyl) Halide Complexes with Sulfinates 61

3.5 Catalytic Developments of Aryl Halide Cross-Coupling with Sodium Sulfinates 63

3.6 Conclusion 69

3.7 Outlook 70

3.8 Experimental 71

3.8.1 Synthesis of Palladium Complexes 71

3.8.2 Ligand Substitution Study 73

3.9 References 74

Chapter 4 Mechanistic Elucidation of Copper-Mediated C-C and C-S Coupling of Directed Aryl Iodides and Sulfinates Salts 77

4.1 Background 77

4.2 Synthesis of (1,3-bis-(2,6-diisopropylphenyl)imidazolinium) Copper (sulfinate) Complexes 80

4.3 Stoichiometric Cross-Coupling of (1,3-bis-(2,6-Diisopropylphenyl)imidazolinium) Copper (sulfinate) with Aryl Iodides 82

4.4 Catalytic Development of Aryl-Sulfinate Cross-Coupling with IPrCuCl 87

4.5 Conclusion 88

4.6 Outlook 89

4.7 Experimental 92

4.7.1 Synthesis of Copper Species 92

4.7.2 Stoichiometric Oxidative Addition Reactions 94

4.7.3 10-CF_3 Time Study 94

4.7.4 10-Cl Control Reaction 94

4.7.5 Stoichiometric Transmetallation and Oxidative Addition Reactions 95

4.7.6 Silver-mediated Aryl-Sulfone Coupling 95

4.8 References 96

Chapter 5 Formation and Electrochemical Study of Fe(0) Phosphine Complexes from Bench-Stable Fe(II) Precatalysts 98

5.1 Background 98

5.2 Synthesis and Characterization of Dicationic Bidentate Phophosine Iron(II) Complexes 102

5.3 Comparison of Reactivity Modes of Iron(II) Complexes 105
5.4 Electrocatalysis with Iron(II) Precatalysts 114
5.5 Conclusion 115
5.6 Outlook 116
5.7 Experimental 118
5.7.1 Synthesis of Iron(II) Triflate Phosphine Species 118
5.7.2 Cyclic Voltammetry of Iron Species 121
5.7.3 Bulk Electrolysis of Iron Species 121
5.7.4 Chemical Reduction of Iron Species 122
5.7.5 Catalytic Reactions 122
5.8 References 123

List of Tables

Table 2.1[a] Time required for maximum conversion of **1-X**. [b]Mass balance was starting material **1-I** even after 24 h. Yields determined via ^{19}F NMR spectroscopy. 20

Table 2.2. Preliminary reaction optimization studies. Yields determined by ^{19}F NMR analysis. 25

Table 2.3. Oxidant Screen on **2**. Yields determined by ^{19}F NMR analysis..... 31

Table 2.4. Demonstration of rapid screening assay for transmetalation and reductive elimination of other sulfur nucleophiles. Yield determined by ^{19}F NMR spectroscopic analysis.35

Table 2.S1. Optimization of [M] and Phosphine Ligand (L) 42

Table 2.S2. Optimization of Pd source, Reagent/Catalyst Loading, and Temperature..... 43

Table 2.S3. Optimization of Pd Source..... 44

Table 2.S4. Optimization of Solvent..... 44

Table 2.S5. Optimization of Time, Temperature, and Atmosphere..... 45

Table 3.1. Yields of ligand screening assay, grouped by ligand class. Yields determined by ^{19}F NMR spectroscopy..... 56

Table 3.2. Desulfinylation and coupling of **8-*p*tol**. Yields determined by ^{19}F NMR spectroscopy..... 58

Table 3.3. Total deoxygenation considers each oxygen removed in the product(2 * sulfide% + sulfoxide%) of sulfinate complexes. Yields determined by ^{19}F NMR spectroscopy. 58

Table 3.4. Reaction of ligated Palladium aryl (psuedo)halide complexes with sulfinates at 120 °C. Yields determined by ^{19}F NMR spectroscopy. 63

Table 3.5. Literature conditions applied to other sulfinates and ligands. Yields determined by ^{19}F NMR spectroscopy. Cachi conditions are 1.2 equiv. Cs_2CO_3, 1.5 equiv. TBACl, 1.5 equiv sulfinate, 5 mol% Ligand and 2.5%mol Pd_2dba_3 in toluene under N_2 at 80 °C for 12hr. Shekar conditions are 5 mol% TDA, 5 mol% Ligand, 2.5 mol% Pd_2dba_3, and 1.5 equiv. sulfinate in toluene under N_2 at 80 °C for 12hr. *Reaction at 120 °C 64

Table 3.5. Effect of Buchwald ligand identity on cross-coupling of aryl triflates with sodium sulfinates. Conditions are 2 equiv of sulfinate, 10mol% ligand, 5mol% Pd_2dba_3 with a 1 hour

prestir at ambient temperature, no TDA, in toluene under N_2 at 80 °C for 12 hr. Yields determined by ^{19}F NMR spectroscopy. 67

Table 3.5. Matrix of sulfinate and electrophile cross-coupling with PAd_3 catalytic system. Conditions are 2 equiv. of sulfinate, 10mol% PAd_3, 5mol% Pd_2dba_3, in toluene under N_2 at 80 °C for 12hr. 69

Table 4.1. Reaction of 2-(2-pyridyl)-5-fluoro-phenyl iodide (**11**; 2 equiv) with IPrCu(SO_2R) complexes at 100 °C in THF. 83

Table 4.2. Flipped stoichiometry of reactions between **10-CF$_3$** and **11** as a function of reaction time. 84

Table 4.3. Stoichiometric reactions of **10** with 1 equiv of **11** in the presence of 2 equiv of $NaSO_2R$ in THF at 100 ºC. Yields determined by ^{19}F NMR spectroscopy using trifluoromethoxybenzene as a standard. 85

Table 4.4. Reaction of **10** with **11** with $NaSO_2R$ in the presence of $AgNTf_2$. Yields determined by ^{19}F NMR spectroscopy. *Isolated yield after workup (liquid/liquid extraction with dichloromethane and saturated aqueous sodium bicarbonate). 86

Table 4.5. Reaction **11** with 1 equiv of CuCl, 1 equiv of IPrCl, and 1 equiv of K_3PO_4 in the presence of 2 equiv of $NaSO_2R$ and 2 equiv of $AgNTf_2$. Yields determined by ^{19}F NMR spectroscopy. *Yield of putative Ag(I) complex. 87

Table 4.6. Equivalents screen of copper and silver in cross-coupling of **11** with $NaSO_2CF_2H$. For entries 1-3, IPrHCl and K_3PO_4 were added in 1:1 ratio of the CuCl. *In dark. **Yield of putative silver complex 88

List of Figures

Figure 1.1. Generic catalytic cycle..... 2

Figure 1.2. a. Sources of anionic SCF_3. b. Current palladium-catalyzed cross-coupling methodologies for Ar-SCF_3 4

Figure 1.3. a. Sulfinate salts are the common form of these moieties and the negative charge is delocalized across the O=S=O motif. b. Palladium-catalyzed aryl-sulfone cross-coupling from aryl halides and sodium sulfinates. 6

Figure 1.4. Crustal abundance of late transition metals.[31] 8

Figure 1.5. Utility of base metal precatalysts for reaction discovery and method development. Some examples of base metal precatalysts from the literature below. 9

Figure 1.6. Several iron phosphine precursors for C-H activation of unactivated organic compounds 10

Figure 2.1. Proposed catalytic cycle for ArX/$MSCF_3$ cross-coupling. 18

Figure 2.2. Ar–SCF_3 coupling results for BrettPhos derivatives. Conditions: 80 ºC, 24 h, 0.1 M **2** in THF, 1.5 equiv of ligand, N_2 atmosphere. Yield of **4a** and detection of **2-L** via ^{19}F NMR spectroscopy. 21

Figure 2.**3**. Ar–SCF_3 coupling results for P^{t}Bu$_3$ derivatives. Conditions: 80 °C, 24 hours, 0.1M of **(2)** in THF, 3 equiv of ligand, N_2 atmosphere. Yield of **4a** and detection of **2-L** via ^{19}F NMR spectroscopy..... 22

Figure 2.4. Ar–SCF_3 coupling results for phosphinoferrocene derivatives. Conditions: 80 °C, 24 h, 0.1M **2** in THF, 1.5 equiv of ligand, N_2 atmosphere. *Likely coordinated via -PPh_2 moiety. Yield of **4a** and detection of **2-L** via ^{19}F NMR spectroscopy..... 23

Figure 2.5. Ar–SCF_3 coupling results for XantPhos derivatives. Conditions: 80 °C, 24 h, 0.1 M of **2** in THF, 1.5 equiv of ligand, N_2 atmosphere. Yield of **4a** and detection of **2-L** via ^{19}F NMR spectroscopy..... 23

Figure 2.6. Time course for formation of **4a** at 80 ºC with selected L. Conditions: N_2, 0.1 M solution of **2** in THF. Reactions monitored via ^{19}F NMR spectroscopy..... 24

Figure 2.9. Optimized conditions for ArI, ArBr, and ArOTf substrates. Yields determined by ^{19}F NMR analysis..... 26

Figure 2.10. Scope of Pd/D^{t}BuPF-catalyzed trifluromethylthiolation. Yields reported as ^{19}F NMR yield (isolated yield). 27

Figure 2.11. Unreactive/modest yielding-substrates. Yields determined by ^{19}F NMR analysis. 28

Figure 2.12. Oxidatively-induced Ar-CF_3 reductive elimination from **2-CF$_3$** via Pd^{IV} intermediate **5** 28

Figure 2.13. Cyclic voltammogram (CVs) of **2** and **2-CF$_3$** in 0.5 M solution of KPF_6 in MeCN with a scan rate of 100 mV/s. Conditions: 0.071 cm^2 glassy carbon working electrode, platinum wire counter electrode, and Ag/Ag$^+$ reference electrode consisting of a 0.01 M $AgBF_4$ and 0.5 M KPF_6 solution in MeCN..... 29

Figure 2.14. Reaction of 2 with *m*-CPBA. Yields determined by ^{19}F NMR analysis..... 30

Figure 2.15. UV-Vis spectrum of **2 and 2-CF$_3$** in acetonitrile 32

Figure 2.16. Photoexcitation of **2** and **2-CF$_3$** at 370nm. Yield determined by ^{19}F NMR spectroscopic analysis 33

Figure 2.17. Synthesis of **2** and access to reductive elimination of **4a** via oxidative, photochemical, and steric means. 34

Figure 2.18. Proposed catalytic cycle for high-valent palladium cross-coupling of aryl boronic acids and metal SCF_3 species..... 36

Figure 3.1. a. Examples of C_{sp2}-Sulfones in molecules. b. Methods of synthesizing C_{sp2}-sulfones[4-7]..... 51

Figure 3.2. (a) Proposed Pd$^{0?II}$ catalytic cycle for C_{sp2}-SO_2R coupling. (b) Initial goal for this project 53

Figure 3.3. (a) Reaction of **1-I** and **1-Cl** with $NaSO_2CF_3$. (b) Synthesis of Pd(II)-SO_2R complexes with x-ray structures. (c) Literature reports of organometallic palladium sulfinate complexes. 54

Figure 3.4. Identification of arylated RockPhos (**7-K)** from stoichiometric and catalytic reactions 59

Figure 3.5. Crossover experiment of RockPhos catalysis and ligand assay. Yields determined by ^{19}F NMR spectroscopy. [a] 0 equiv of $NaSO_2CF_3$ was added. [b] 1 equiv of $NaSO_2CF_3$ was added. [c] 1 equivalent of $NaSO_2CH_3$ was added 61

Figure 3.5. a. Proposed catalytic cycle with the pathways in which these two organometallic studies probe the elementary steps. b. Synthesis of Ligated complexes 62

Figure 3.6. a. Demonstration of arylation of ᵗBuBrettPhos and the stepwise equilibrium of pre-arylated intermediates as reported from the Buchwald lab. b. Analogy of RockPhos-catalyzed aryl-sulfone coupling and sulfinates' role in promoting the equilibrium. 66

Figure 3.7. Proposed methodology of access to S^{II}, S^{IV}*, S^{VI} cross coupling of C_{sp2}-halides using palladium catalysis and phosphine deoxygenation 70

Figure 3.8. Summary of coupled sulfinate deoxygenation-reductive elimination attempts using Radosevich phosphine **7-Q** and XantPhos from various starting materials. 71

Figure 4.1. Group 11 catalyzed aryl-sulfone cross coupling reactions from the literature and the target reaction..... 78

Figure 4.2. Proposed catalytic cycles of copper(I/III)-catalyzed cross-coupling between aryl halides and metal sulfinate salts and desulfinylation pathway. 80

Figure 4.3. Optimized reaction conditions to form IPrCu(SO_2R). Single crystal X-ray structures of **10-CF_3** and **10-CF_2H** show that the sulfinate is bound through the oxygen. Yields are isolated after one recrystallization; additional product can be obtained through further recrystallizations of the mother liquor. 81

Figure 4.4. Different proposed roles of silver in the cross-coupling of aryl iodides with sulfinates. The left side demonstrates the most commonly implicated roles of silver in catalytic reactions, while the right side shows the less studied and more reactive roles that sivler can play. The upper half demonstrates Ag(0) pathways while the bottom half shows Ag(I) pathways. 90

Figure 4.5. A. Pd-catalyzed trifluoromethylation of aryl chlorides from the Buchwald lab using silyl sources of CF_3. B. General scheme of Langlois radical CF_3 production from $NaSO_2CF_3$ for trifluoromethylation of arenes. C. Proposed Lewis acid activation of copper-bound sulfinates to promote desulfinylation.. 91

Figure 5.1. (a) E–H bond activation at bis-ligated Fe(0) complexes. (b) Catalytic methods involving bis-ligated Fe(0) complexes..... 99

Figure 5.2. Chemical, thermal, and photochemical methods to access Fe(0) phosphine complexes. 101

Figure 5.3. Cyclic voltammograms of **A4**, **B4**, and **D1**.at 100mV dissolved in 0.1M $TBAPF_6$ in MeCN with 1mm glassy carbon disc working electrode, graphite rod counter electrode, and silver wire psuedo-reference electrode in a glass compartment connected with VyCor frit containing 0.1M $TBAPF_6$ in MeCN. Voltammograms were referenced to Fc/Fc^+ 104

Figure 5.4. UV-Vis spectra. Photochemical irradiation of iron(II) complexes at their most energetic UV-Vis feature (**D1**: 370nm, **A5**: 370nm, **A4**: UVB, **B5**: 390nm) for 24 h in MeCN showed no change. 105

Figure 5.5. ^{1}H and ^{31}P NMR spectra of electrochemical reductions of complex **B5**. Bulk electrolysis trace of constant potential electroreduction of 0.05 mmol of **B5** where on y-axis1, the proportion of current measured based on the initial current is plotted and on y-axis2, the amount of charged passed as a proportion of theoretical charge needed to reduce the amount of complex in the reaction is plotted. 107

Figure 5.6. (a) Electrochemical reduction of **A4** in 0.2 M LiOTf forming **A6** and **A7** but not *cis*-$(DMPE)_2Fe(H)(CH_2CN)$. (b) Proposed mechanism for formation of **A7**, resulting in deprotonated MeCN and downstream products. 109

Figure 5.7.^{1}H NMR spectra showing the hydride region of the electrolyte screen of the electroreduction of **A5.** 110

Figure 5.8. Deuterated solvent study with **A5**. Left side depicts the ^{1}H NMR (top) and ^{31}P NMR (bottom) constant potential bulk electrolysis of **A5** with TBAOTf electrolyte in MeCN-h_3 (1st) and MeCN-d_3 (2nd). Right side depicts the same data with bulk electrolysis using LiOTF electrolyte. 111

Figure 5.9. a. Electrochemical reduction of **B4** and **D1** in the presence of arene. b. ^{31}P NMR of benzonitrile, fluorobenzene, and benzene η^6- abducts with $(DCyPE)Fe^0$ 112

Figure 5.10. (a) Reaction of ^{t}BuMgCl with benzonitrile, forming a directed C-H activated substrate. (b) ^{1}H and ^{31}P NMR spectra of proposed C-H activated species. Coupling constant of 84.1 Hz. 114

Figure 5.11. (a) Scheme of DCyPE as chemical and electrochemical precatalysts. (b) Extended directing group scope and coupling partner scope 117

List of Schemes

Scheme 1.1. a. First reported transition-metal catalyzed aryl-sulfur cross-coupling from Migita and coworkers[3]. b. Organometallic palladium studies outline two of three key steps in the catalytic cycle[4]. 3

Scheme 1.2. Copper-mediated fluorination of aryl iodides at high temperatures and long reaction times to facilitate oxidative addition.[19] 7

Scheme 1.3. Copper-catalyzed aryl halide sulfinylation with limited sulfinate scope and gold-catalyzed C_{sp2}-I sulfinylation with limited electrophile scope. 8

Scheme 2.1. Synthesis of (dtbpy)Pd(*p*-FC_6H_4)(X) (X = I, Br, Cl; **1-X**). All yields are isolated. 18

Scheme 2.2. Synthesis and reactivity of (dtbpy)Pd(*p*-FC_6H_4)(SCF_3) (**2**). All yields are isolated. 19

Scheme 2.3. Pathway to Ar–SCF_3 coupling starting from **2** with diverse phosphine ligands (L) 21

Scheme 4.1. Stoichiometric fluorination[4] and fluoroalkylation[5] of directed aryl halides from IPrCu (pseudo)halide complexes. 79

Scheme 4.2. Transmetallation of **10-X** with $NaSO_2CF_3$ to form **10a** 80

Scheme 4.3. Reaction of $IPrCu^ICl$ with 2 equiv of **11** in THF at 100 °C for 15 h 84

Scheme 4.4. Attempts at C-H activation using **10** and a combination of Cs_2CO_3 and $AgNTf_2$. Formation of **10-CF_2H** identified from ^{19}F NMR 89

Scheme 4.6. Scope of attempted electrophiles with stoichiometric reactivity with **10b**. Yields determined by ^{19}F NMR spectroscopic analysis 91

Scheme 4.7. Substrate scope with candidates for expanded scope of directed aryl halides..... 92

Scheme 5.1. General synthesis of dicationic phosphine-ligated Fe(II) complexes. BF_4 complexes were synthesized but excluded from presentation for brevity. 103

Scheme 5.2. (a) Chemical reduction to activate **B5** for catalysis. 0.1 M reaction concentration. (b) Electrochemical reduction to activate **B5** for catalysis. Electrochemical portion was monitored by live constant potential electrolysis trace. When the appropriate amount of charge to reduce 0.01 mmol of **B5** was passed, and the trace showed two reduction events, the

electrolysis was stopped, electrodes removed, and the reaction was transferred to a new 20 mL vial to stir overnight. 0.1 mmol of substrate was used for both reactions. 115

Scheme 5.5. Cooperative chemical and photochemical proposal to access C-H borylation from bench-stable precatalysts. 118

Abstract

This thesis explores four transition-metal mediated cross-coupling reactions and investigates these reactions through the use of isolated organometallic complexes. The introduction of this thesis describes catalysis broadly and the specific classes of transformations targeted in this body of work.

Chapter 2 of this thesis investigates the cross-coupling of aryl groups and the trifluoromethanethiolate (SCF_3) anion with palladium. Aryl-sulfide cross-coupling is well-explored but this unique SCF_3 unit has not shared in the same spotlight. Novel palladium species were synthesized to act as model complexes of proposed intermediates in the catalytic cycle. From these model complexes the transmetallation of the SCF_3 anion was investigated as a function of countercation and as a function of Pd-halide. From here, we find that the tetramethylammonium (TMA) cation is the most productive cation and that transmetallation occurs at ambient temperatures with all halides using this $TMASCF_3$ salt. This transmetallated complex was then used as a model complex for reductive elimination. A ligand assay was developed to rapidly investigate the productivity of a wide screen of ligands. We found that D^{t}BuPF and XantPhos were the best ligands in this stoichiometric study. These stoichiometric results were used to develop a catalytic method using $TMASCF_3$ and D^{t}BuPF. Furthermore, this transmetallated complex was used to investigate oxidatively induced reductive elimination through the screening of oxidants. We find that $NOPF_6$ and radical dication tris-(aryl amine) cyclopropeniums as the most productive oxidants. Finally, we photoexcite that model complex and find that photo-induced reductive elimination is also productive.

Chapter 3 takes the ligand assay developed in chapter 2 and applies it to a much more difficult reaction, aryl-sulfone cross-coupling. A series of (dtbpy)Pd^{II}(Ar)(sulfinate) complexes were synthesized, and a combinatorial screen of ligands was performed. In this study we identify a XantPhos, RockPhos, and PAd_3 as ligands of interest based on reductive elimination and literature catalysis. We developed cross-over experiments using these model complexes that uncover *in situ* functionalization of RockPhos that enables productive chemistry. We then make

RockPhos and XantPhos palladium complexes and find that the XantPhos complexes reactivity mirros catalysis, but the RockPhos complexes reactivity does not. We then investigate catalysis by screening sulfinates and develop reasonings for catalytic behavior based on stoichiometric results.

Chapter 4 investigates copper(I/III) reactivity as a method of forging ary-sulfone bonds. A series of novel NHC-copper-sulfinate complexes were synthesized. Their reactivity with directed aryl iodides was investigated and it was found that all sulfinates coupling >95% yield except for SO_2CF_3 which desulfinylates and forms the C-C coupled product. Tandem transmetallation, oxidative addition, and reductive elimination were investigated. Electron-rich sulfinates performed decently and the fluorinated sulfinates did not. Silver(I) salts were investigated as transmetallating reagents in these reactions, and it was found that the silver salts performed coupling of the fluorinated sulfinates without the help of copper.

Finally, Chapter 5 investigates the start of the catalytic cycle, catalyst activation using iron(II) phosphine complexes to reach the highly reactive iron(0) phosphine complexes that perform C-H activation on a variety of substrates. Novel bench-stable dicationic iron(II) phosphine complexes bearing bis disubstituted phosphinoethane ligands were synthesized and characterized. Electrochemical reduction and chemical reduction were employed to access the iron(0) species and their behavior during the reduction was studied. The bis diphenylphosphinoethane iron(II) complex was found to be an effective precatalyst in both chemical and electrochemical C-H alkenylation reactions.

Chapter 1 Introduction

Transition metal catalysis is a fundamental pillar of modern civilization. Efficient synthetic routes to bioactive molecules, fertilizers, and polymers are crucial for supporting our society, and all of these are enabled by transition metal catalysis. Organic molecules containing aryl or heteroaryl groups are particularly important in pharmaceutical and agrochemical development.[1] While the use of metal catalysts for the functionalization of aromatic-containing molecules is a mature field, there are significant unanswered questions, incomplete areas, and underexplored domains.

Transition metal catalyzed functionalizations of arenes most commonly involve the reaction of an aryl halide electrophile with a carbon or heteroatom-based nucleophile. While these couplings have been realized with a diverse array of nucleophilic coupling partners, there remain some that have not been fully realized. This thesis specifically targets these couplings between aryl halides and sulfur containing nucleophiles including fluorinated sulfides (like SCF_3^-) and sulfinates (SO_2R^-).

A majority of transition metal catalyzed arene cross coupling catalytic cycles, especially those of the late transition metals, are similar. First (and often overlooked), a metal pre-catalyst is activated to enter the catalytic cycle. Next, the coupling partners become bound to the activated metal center through **oxidative addition** of the arene electrophile and **transmetallation** of the nucleophile. Finally, the coupling partners undergo **reductive elimination** to form the target aryl–X bond, **Figure 1.1**

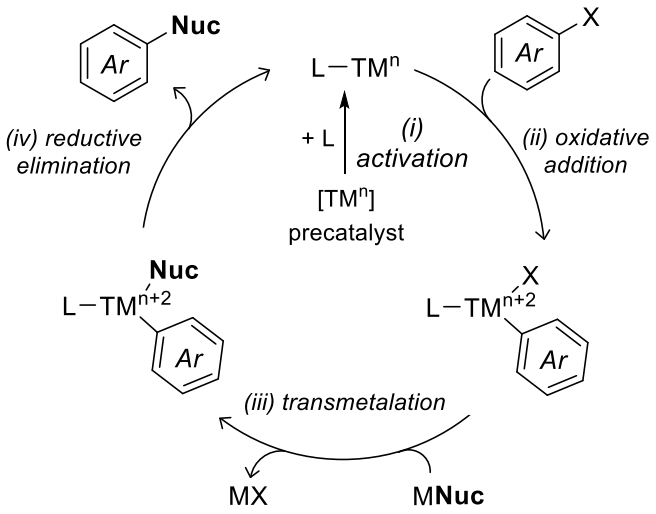


Figure 1.1. Generic catalytic cycle (TM = transition metal)

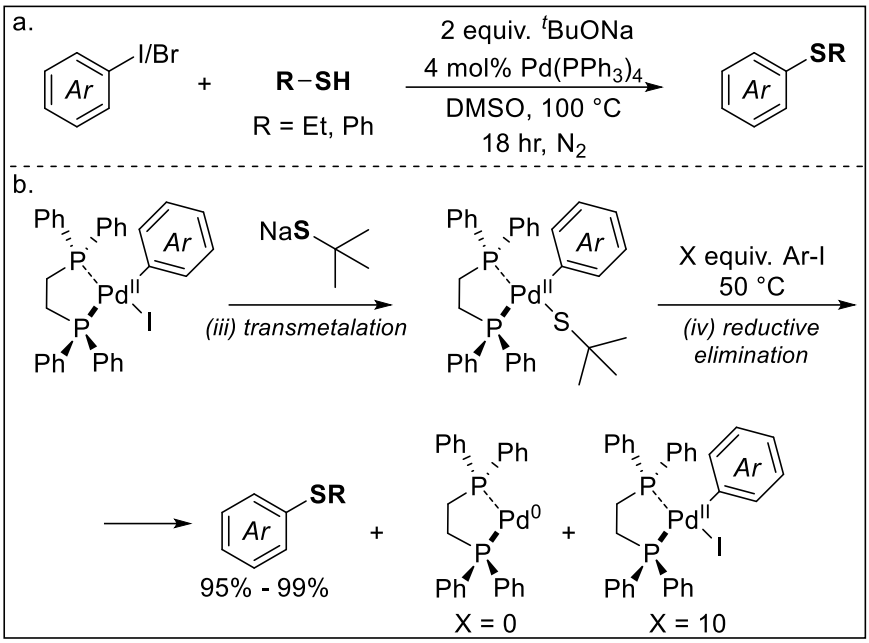
Each of these reactions involves an organometallic intermediate, and the catalytic cycle is largely defined by the most kinetically difficult reaction – or elementary step – often called the rate-limiting step. This thesis focuses on coupling reactions that are underdeveloped and uses the synthesis and reactivity of targeted organometallic complexes to interrogate and identify ligands that promote these challenging steps.

1.1 Palladium-mediated Ary-Sulfur Coupling

Transition metal catalyzed functionalizations of arenes are dominated by palladium. Palladium catalysts exhibit exceptional reactivity for coupling aryl halides with nucleophilic organic compounds and a majority of heteroatoms, including amines, alcohols, and sulfides. However, these transformations, particularly Aryl–S couplings maintain key limitations that are addressed in this thesis.[2]

1.1.1 Palladium-mediated Aryl-Sulfide Couplings

The first report of a palladium-catalyzed cross-coupling of an aryl halide with a sulfide nucleophile was in 1978 from Migita and coworkers.[3] The authors showed that $Pd(PPh_3)_4$ is an effective pre-catalyst for coupling aryl iodides/bromides with thiophenol and ethanethiol in the presence of ^{t}BuONa at 100 °C in DMSO, **Scheme 1.1a**.



Scheme 1.1. (a) First reported transition-metal catalyzed aryl-sulfur cross-coupling.[3] (b) Organometallic palladium studies establish the feasibility of key steps in the catalytic cycle.[4]

Several decades later in 1995, Baranano and Hartwig[4] performed the first organometallic investigations into the palladium mediated coupling of aryl sulfides. They demonstrated that (DPPE)Pd(Ar)(I) undergoes transmetallation with NaS^{t}Bu and that this is followed by by thermally-induced Aryl–S bond-forming reductive elimination, **Scheme 1.1b**. Trapping of Pd^0 with either PPh_3 or diphenylacetylene proved essential for achieving >95% yield of the sulfide. ArI could also be used as the trapping agent to re-form the starting organometallic complex. Free energy relationship plots varying substituents on the aryl group show a δ_I (inductive) value of 1.7 and δ_r (resonance) value of 5.0 for reductive elimination, showing that this ligand serves as the electrophile. Overall, this study showed that Pd complexes can perform transmetallation, reductive elimination, and oxidative addition stoichiometrically, thus outlining a catalytic cycle for aryl-sulfide cross-coupling.

Soon after this, a variety of additional palladium-catalyzed methodologies for Aryl–S coupling began to appear.[6a-c] All of these methods featured low (≤3 mol%) catalyst loading and high functional group compatibility. Subsequent developments improved or innovated on these methods.[7a-d] For instance in 2006, Hartwig showed that Josiphos enables the coupling of a thiol + base mixture with diverse ArX electrophiles (X = I, Br, Cl, OTf, and OTs) with high turnover

numbers (≥10,000). A year later, Lee showed that 0.3 equiv of a tri(organothiolate) indium species serves as as a competent nucleophile source with a $Pd(OAc)_2$ and XantPhos catalytic system.[7b] In general, a wide range of solvents and bases are compatible as well as sterically/electronically varied ligands (including PPh_3[2], D^{i}PrPF[6b], $DPPF_7$[c], XantPhos[7a], and N-heterocyclic carbenes)[7d]

A commonality of nearly all of these methods is that the R group on the sulfur has minimal effect on catalytic efficiency. The only exception to this is the trifluoromethanethiolate anion (SCF_3) . This nucleophile is desirable in bioactive molecules due to its high lipophillicity and moderately electron withdrawing nature.[8] However, cross-coupling with SCF_3^- is not as facile as the other sulfide systems for a few reasons. It is a relatively weak nucleophile due to the inductive effects of the CF_3 group. Additionally, SCF_3 salts can be difficult to access. Some of the first examples were mercury salts that were challenging to prepare.[9] In 2003, Yagupolskii and coworkers reported a series of novel cations (TMA, Cs, (crown ether)Cs), which greatly advanced the field.[10] In 2008, the Buchwald group developed and commercialized the light-sensitive $AgSCF_3$ reagent and reported the first aryl halide cross-coupling. This reaction uses the sensitive palladium pre-catalyst $(COD)Pd(CH_2SiMe_3)_2$, **Figure 1.2b**.[11]

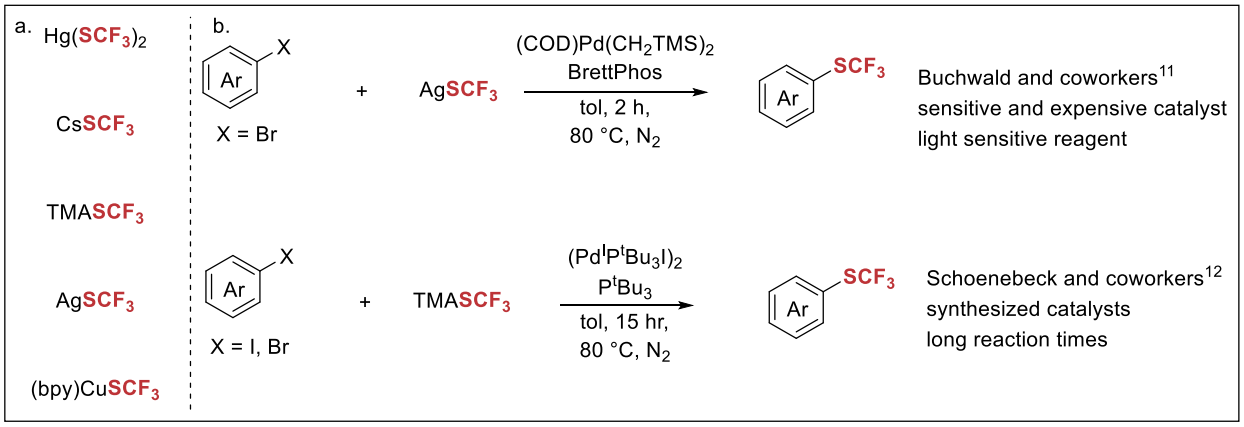


Figure 1.2. a. Sources of anionic SCF_3. b. Current palladium-catalyzed cross-coupling methodologies for Ar-SCF_3

Subsequently, Schoenebeck and coworkers[12] reported the use of a Pd^I dimer as an efficient pre-catalyst for the coupling of aryl iodides and bromides with tetramethylammonium trifluoromethanethiolate, one of the novel salts that Yagupolskii and coworkers reported, which also saw use in a few Ni-catalyzed methodologies.[13] Along with this smaller set of developed

methodologies, there are no reported mechanistic investigations into this transformation on the typical Pd(0/II) manifold. Chapter 2 demonstrates the first of these mechanistic studies, along with organometallic investigations into other reaction modalities.

1.1.2 Palladium-mediated Aryl-Sulfinate Couplings

The palladium-catalyzed cross-coupling of aryl sulfides is facile; in contrast, the palladium-catalyzed cross-coupling of aryl sulfones is not. Sulfinates are very weak nucleophiles, owing to the high oxidation state of the sulfur center and the resonance structure that delocalizes the negative charge of the sulfinate onto the oxygen. The direct analogy to the thiol chemistry would be sulfinic acids, but these acids are quite strong and are mostly utilized as the deprotonated salts, **Figure 1.3a**. This weak nucleophilicity makes both reductive elimination and transmetallation more difficult. Consistent with these challenges, there are only two reports of palladium-catalyzed cross-coupling of aryl halides and metal sulfinates. Cacchi and coworkers published 2002 and 2004 reports of a Pd-XantPhos system capable of coupling aryl and vinyl iodides, bromides, and triflates with sodium *p*-tolyl sulfinate ($NaSO_2$*p*-tol) using cesium carbonate and tetrabutylammonium chloride form a more reactive sulfinate *in situ*.[14] Twelve years later, the Shekar group at AbbVie published the palladium-catalyzed coupling of aryl triflates with sodium trifluoromethanesulfinate using a Pd-RockPhos system.[15] This reaction is highly effective but very specific, as it exhibits unusually extreme sensitivity to changes in the ligand. It is also essentially only works with triflates. The reactivity trend of Ar-OTf > Cl >> Br led the the authors to conclude that transmetallation is the rate-limiting step for this reaction. However, detailed mechanistic studies were not conducted, and no other sulfinate salts (alkyl or aryl) were reported for this method.

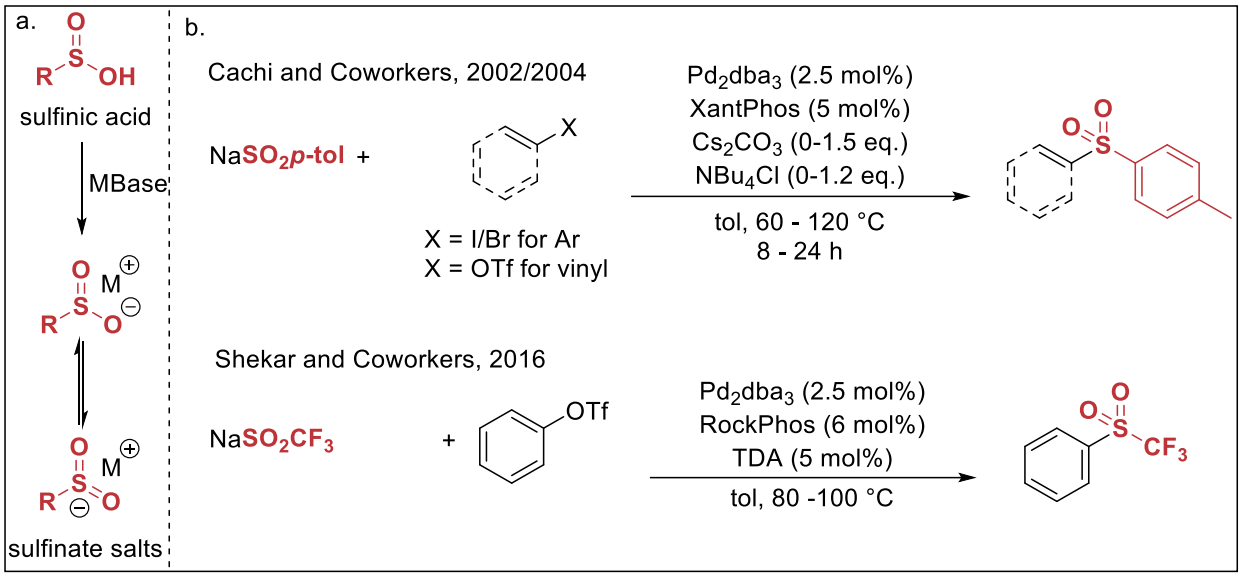


Figure 1.3. (a) Sulfinic acids, sulfinate salts, and resonance structures. (b) Palladium-catalyzed synthesis of aryl-sulfones from aryl halides and sodium sulfinates.

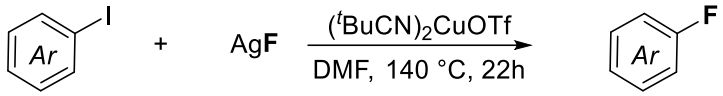
In comparison to the sulfides, these transformations show extreme sensitivity to the R group on sulfur. In fact, there are no examples of alkyl sulfinates in these methods. Furthermore, the ligand scope is very restricted. Only three ligands have been reported to give over 25% yield – XantPhos (SO_2Ar)[14], RockPhos (SO_2CF_3), and AdRockPhos (SO_2CF_3).[15] Despite this clear gap in the field and the utility of aryl sulfones in pharmaceuticals and agrochemicals, there has not been any mechanistic investigation into these transformations. Chapter 3 unveils detailed mechanistic studies to understand and develop new Pd-catalyzed Ar-SO_2R cross-couplings.

1.2 Copper-mediated aryl sulfur coupling

Palladium is the most popular transition-metal catalyst for the functionalization of arenes in academia and industry.[16] However, palladium is a precious metal and is mined in only a few countries, some of which are politically unstable. Additionally, the mining of palladium often has drastic adverse environmental effects. This negative environmental impact along with volatility in its already high prices has led to an intensive search for alternatives.[17] Copper is a very popular transition metal in industry for several reasons. Its high earth abundance and relative ubiquity make for predictable availability and pricing. Additionally, copper is a productive catalyst in a number of valuable transformations. Many of the famous palladium catalyzed C_{sp2}-N, and C_{sp2}-O cross-

couplings have now been replicated and in some respects improved upon with copper catalytic systems.[18]

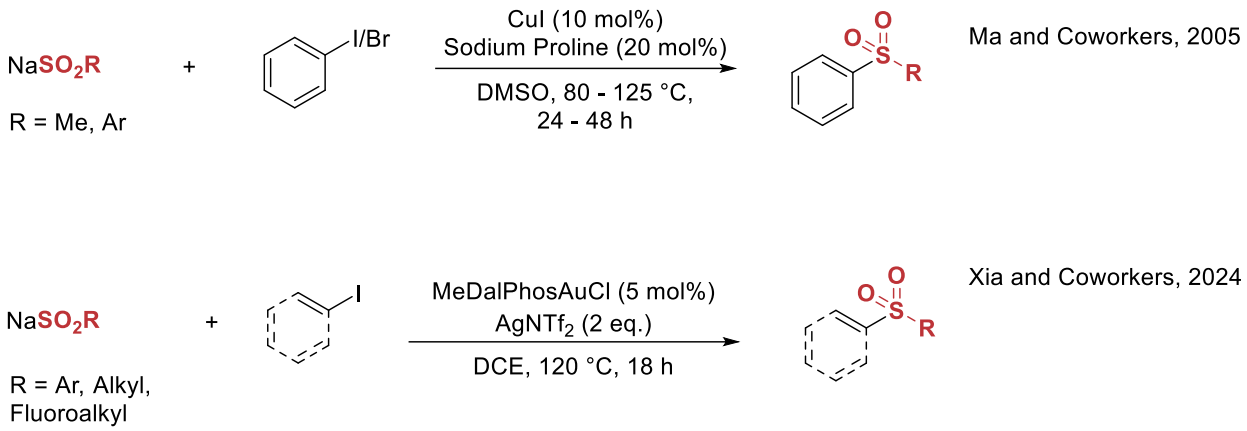
On top of sourcing benefits, copper exhibits divergent reactivity trends from palladium. Unlike Pd, copper readily mediates C_{sp2}–F bond-forming reductive elimination without the need for specialized ligands. On the other hand, copper catalysts often struggle with oxidative addition, even with relatively activated aryl iodides. This behavior is exemplified in pioneering work from Hartwig and Fier[19] where a copper salt with no ligand performs aryl-fluoride cross coupling with aryl iodides but requires 140 °C for moderately good yields due to slow oxidative addition. This change in metal behavior introduces new challenges in ligand design but also opens up new avenues for productive chemistry.



Scheme 1.2. Copper-mediated fluorination of aryl iodides at high temperatures and long reaction times to facilitate oxidative addition.[19]

1.2.1 Copper-mediated Aryl-Sulfinate Couplings

The first cross-coupling of a metal alkyl sulfinate with an aryl group come from Ma and coworkers in 2005.[20] The methodology features prolinate as a ligand and CuI as a precatalyst. $NaSO_2CH_3$ and $NaSO_2$*p*-tol could be coupled with aryl iodides and bromides in DMSO. This landmark study demonstrates copper's ability to promote reductive elimination reactions that cannot be achieved at palladium. Nineteen years later, the Xia group followed this report by employing a gold catalyst to couple various C_{sp2}-I with aryl, alkyl, and fluoroalkyl sulfinates.[21] Gold is the 3rd row congener of copper and carries some of its characteristics, such as facile reductive elimination. This methodology is even more restricted on the aryl side, as only iodides are tolerated and electronics on the aryl group have a significant effect on yield. This report is exciting, but gold suffers from the same or elevated price and environmental drawbacks as palladium. To date, there have not been any mechanistic investigations of these reactions at Cu nor efforts to expand the Cu catalyzed transformations with fluoroalkyl sulfinate nucleophiles or aryl chloride electrophiles. Chapter 4 investigates organometallic copper species to understand more about the mechanisms of these aryl-sulfone forming reactions.



Scheme 1.3. Copper-catalyzed aryl halide sulfinylation with limited sulfinate scope and gold-catalyzed C_{sp2}-I sulfinylation with limited electrophile scope.

1.3 Catalyst Activation

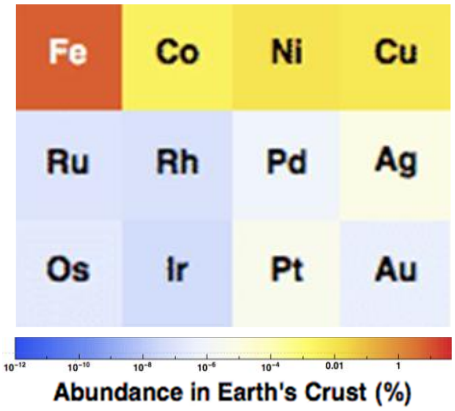


Figure 1.4. Crustal abundance of late transition metals.[31]

In a similar vein to copper, the two other 1st row late transition metals – Fe and Ni – are particularly sought after as an earth-abundant, green, politically-insensitive alternatives to precious metals. Reactivity wise, base metals can promote many similar transformations as noble metals, perform similar reactions with differing selectivity, and perform chemistries that are distinct from noble metal reactivity. However, these benefits of base metals often come at the expense of well-understood mechanisms, broad ligand options, low catalyst loadings, fewer side reactions, and mild conditions, characteristics that are typical of the noble metals.[22] While these issues are solvable and have been addressed in certain systems, base metals have a unique hurdle that stifles investigations into optimizing base metal reactivity, selectivity, and mechanistic study. The active

species of most of these base metals are highly air and water sensitive.[23] This is due to the fact that the active species are most often low oxidation state metals. Metals in a low oxidation state have a wealth of electrons that engage in productive chemistry. Unfortunately, those electrons are also available for deleterious reactions, especially with air or water. As such, both reaction development campaigns and mechanistic studies suffer from increased time and cost associated with the storage and handling of these reactive metal species. A highly attractive way to address these storage and handling issues would be to develop bench stable base metal precatalysts, which brings us to the first step in any catalytic reaction – precatalyst activation.

1.3.1 Base Metal Precatalysts

There are a few base metal precatalysts in literature. The Engle and Cornella groups have made significant progress in bench stable Ni^0 sources, while the Chirik group has reported a series of Co^I and Fe^I precatalysts. Typically, these precatalysts are activated *via* ligand substitution or heating. Electrochemistry is a powerful field with many applications, but it is under-utilized in base metal catalysis for chemical synthesis. Recent work in this field from the Ackermann and Derosa groups demonstrate the power and selectivity that electrochemistry can impart on transition metal catalysis.[24]

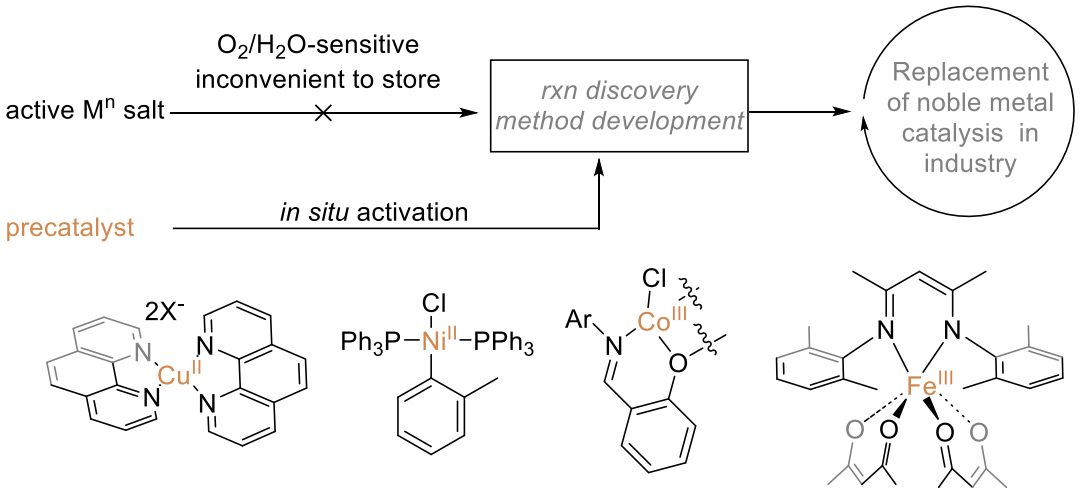


Figure 1.5. Utility of base metal precatalysts for reaction discovery and method development. Some examples of base metal precatalysts from the literature below.

1.3.2 Fe(0) C-H activation

When Fe(0) is bound to four phosphine ligands, these species have been shown to perform H-SiR_3,[25] $B(OR)_2$,[26] $C_{sp,sp2,sp3}$[27,28] bond activation, even promoting the C-H activation of pentane! However, there have been few methodologies reported that take advantage of this reactivity, with only two catalytic cycles developed. In the 58 years since the first report of this chemistry, there are only four iron phosphine sources utilized in the literature. Three of them are bis-ligated phosphinoethane Fe species with methyl, ethyl and phenyl substituents (DMPE, DEPE[29], DPPE, respectively). The other is a mono-ligated (DPPE)$FeBr_2$[30] species. In each of these cases, the iron is activated to form Fe(0) via a photochemical, chemical, or thermal induced reduction. The Fe(II) pre-catalysts amenable to these reduction processes are often quite difficult to handle due to light-sensitivity and bench-instability, as well as the need for pyrophoric reagents in their synthesis. Chapter 5 discusses our efforts to create bench stable iron phosphine precatalysts for use in chemical and electrochemical C-H activation.

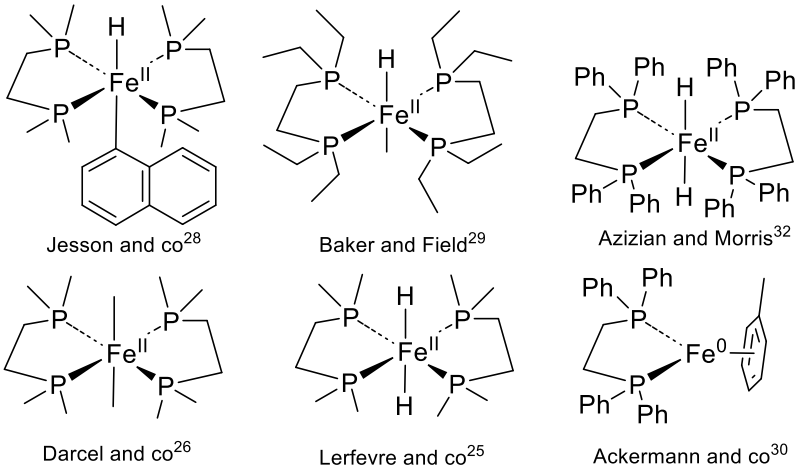


Figure 1.6. Several iron phosphine precursors for C-H activation of unactivated organic compounds

1.4 References

1. Lovering, F.; Bikker, J.; Humblet, C. "Escape from Flatland: Increasing Saturation as an Approach to Improving Clinical Sucess", *J. Med. Chem*. **2009**, 52, 21, 6752–6756

2. Fernandez-Rodriguez, M. A.; Shen, Q.; Hartwig, J. F. "A General and Long-Lived Catalyst for the Palladium-Catalyzed Coupling of Aryl Halides with Thiols". *J. Am. Chem. Soc*., **2006**, 128, 2180–2181
3. Kosugi, M.; Shimizu, T.; Migita, T. "Reactions of Aryl Halides with Thiolate Anions in the Presence of Catalytic Amounts of Tetrakis(Triphenylphosphine)Palladium – Preparation of Aryl Sulfides" *Chemistry Letters*, **1978**, 13-14
4. Baranano, D.; Hartwig, J. "Carbon-Heteroatom Bond-Forming Reductive Elimination. Mechanism, Importance of Trapping Reagents, and Unusual Electronic Effects during Formation of Aryl Sulfides" *J. Am. Chem. Soc.*, **1995**, 117, 2937-2938
5. For a review on metal-catalyzed Carbon-Sulfur bond forming reactions before 2000, see Kondo, T.; Mitsudo, T. "Metal-Catalyzed Carbon-Sulfur Bond Formation", *Chem. Rev.*, **2000**, 100, 3205-3220
6. Early palladium-catalyzed aryl-sulfide cross-coupling: (a) Schopfer, U.; Schlapbach, A.; "A general palladium-catalysed synthesis of aromatic and heteroaromatic thioethers", *Tetrahedron*, **2001**, 57, 3069-3073; (b) Murata, M.; Buchwald, S. L. "A general and efficient method for the palladium-catalyzed cross-coupling of thiols and secondary phosphines", *Tetrtahedron*, **2004**, 60, 7397-7403; (c) Itoh, T.; Mase, T. "A General Palladium-Catalyzed Coupling of Aryl Bromides/Triflates and Thiols", *Org. Lett*, **2004**, 6, 4587-4590
7. Later palladium-catalyzed aryl-sulfide cross-coupling: (a) Fernandez-Rodriguez, M. A.; Shen, Q.; Hartwig, J. F. "A General and Long-Lived Catalyst for the Palladium-Catalyzed Coupling of Aryl Halides with Thiols", *J. Am. Chem. Soc.*, **2006**, 128, 2180-2181; (b) Lee, J-Y.; Lee, P. H. "Palladium-Catalyzed Carbon-Sulfur Cross-Coupling Reactions with Indium Tri(organothiolate) and Its Application to Sequential One-Pot Processes", *J. Org. Chem.*, **2008**, 73, 7413-7416; (c) Okauchi, T.; Kuramoto K.; Mitamura, M. "Facile Preparation of Aryl Sulfides Using Palladium Catalysis under Mild Conditions", *Synlett*, **2010**, 19, 2891-2894; (d) Bastug, G.; Nolan, S. P. "Carbon-Sulfur Bond Formation Catalyzed by [Pd(^{i}Pr^{*OMe})(cin)Cl] (cin = cinnamyl)", *J. Org. Chem.*, **2013**, 78, 9303-9308
8. (a) Hansch, C.; Leo, A.; Unger, S. H.; Kim, K. H.; Nikiaitani, D.; Lien, E. J. "Aromatic substituent constants for structure-activity correlations". *J. Med. Chem.* **1973**, 16, 11, 1207–1216. (b) Leroux, F.; Jeschke, P.; Schlosser, M.; "α-Fluorinated Ethers, Thioethers,

and Amines: Anomerically Biased Species". *Chem. Rev.* **2005**, 105, 3, 827–856. (c) Leroux, F. R.; Manteau, B.; Vors, J-P.; Pazenok, S. "Trifluoromethyl ethers – synthesis and properties of an unusual substituent". *Beilstein J. Org. Chem.* **2008**, 4, No. 13. DOI: 10.3762/bjoc.4.13. (d) Hardy, M. A.; Chachignon, H.; Cahard, D. "Advances in Asymmetric Di-and Trifluoromethylthiolation, and Di- and Trifluoromethoxylation Reactions". *Asian J. Org. Chem.* **2019**, 8, 5, 591-609.

9. Brandt, G. A. R.; Emeleus, H. J.; Haszeldine, R. N. "Organometallic and Organometalloidal Fluorine Compounds. Part III.* Trifluoromethyl Derivatives of Sulphur.", *J. Org. Chem.*, **1952**, 2198-2205
10. Tyrra, W.; Naumann, D.; Hoge, B.; Yaguploskii, Y. L.; "A new synthesis of trifluoromethanethiolates—characterization and properties of tetramethylammonium, cesium and di(benzo-15-crown-5)cesium trifluoromethanethiolates". *J. Fluorine Chem.* **2003**, 119, 1, 101-107
11. Teverovskiy, G.; Surry, D. S.; Buchwald, S. L. "Pd-Catalyzed Synthesis of Ar-SCF_3 Compounds under Mild Conditions". *Angew. Chem., Int. Ed.* **2011**, 50, 32, 7312-7314
12. Yin, G.; Kalvet, I.; Schoenebeck, F. "Trifluoromethylthiolation of Aryl Iodides and Bromides Enabled by a Bench-Stable and Easy-To-Recover Dinuclear Palladium(I) Catalyst". *Angew. Chem., Int. Ed.* **2015**, 54, 23, 6809-6813
13. (a) Zhang, C-P.; Vicic, D. A. Nickel-catalyzed synthesis of aryl trifluoromethyl sulfides at room temperature. *J. Am. Chem. Soc.* **2012**, *134*, 183-185. (b) Yin, G.; Kalvert, I.; Englert, U.; Schoenebeck, F. Fundamental studies and development of nickel-catalyzed trifluoromethylthiolation of aryl chlorides: Active catalytic species and key roles of ligand and traceless MeCN additive revealed. *J. Am. Chem. Soc.* **2015**, *137*, 4164-4172. (c) Durr, A.; Yin, G.; Kalvet, I.; Napoly, F.; Schoenebeck, F. Nickel-catalyzed trifluoromethylthiolation of Csp^2-O bonds. *Chem. Sci.*, **2016,** 7, 1076-1081
14. (a) Cachi, S.; Fabrizi, G.; Goggiamani, A.; Parisi, L. M. "Unsymmetrical Diaryl Sulfones through Palladium-Catalyzed Coupling of Aryl Iodides and Arenesulfinates", *Org. Lett.*, **2002**, 4, 4719–4721; (b) Cachi, S.; Fabrizi, G.; Goggiamani, A.; Parisi, L. M.; Bernini, R.; "Unsymmetrical Diaryl Sulfones and Aryl Vinyl Sulfones through Palladium-Catalyzed Coupling of Aryl and Vinyl Halides or Triflates with Sulfinic Acid Salts", *J. Org. Chem.*, **2004**, 69, 5608–5614
15. Smyth, L. A.; Phillips, E. M.; Chan, V. S.; Napolitano, J. G.; Henry, R.; Shekar, S. "Pd-Catalyzed Synthesis of Aryl and Heteroaryl Triflones from Reactions of Sodium Triflinate with Aryl (Heteroaryl) Triflate", *J. Org. Chem.*, **2016**, 81, 3, 1285–1294
16. Lopez, O.; Padron, J. M. "Iridium- and Palladium-Based Catalysts in the Pharmaceutical Industry.", *Catalysts* **2022**, 12, 2, 164

17. (a) Rahman, A.; Uahengo, V.; Daniel, L. S. Green chemistry concept: Applications of catalysis in pharmaceutical industry. *Glob Drugs Therap*, **2017**, 2, 4, 1-6; (b) Church, C.; Crawford, A.; Minerals and the Metals for the Energy Transition: Exploring the Conflict Implications for Mineral-Rich, Fragile States, *The Geopolitics of the Global Energy Transition. Lecture Notes in Energy*, **2020,** 73, 279-304; (c) Yarochevsky, A. A.; Abundances of chemical elements in the Earth's crust, *Geochemistry International*, **2006**, 44, 48-55; (d) Busacca. C. A.; Fandrick, D. R.; Song, J. J.; Senanayake, C. H. The Growing Impact of Catalysis in the Pharmaceutical Industry, *Adv. Synth. Catal.,* **2011**, 353, 11-12, 1825-1864
18. (a) Bhunia, S.; Pawar, G> G>; Kumar, S. V.; Jiang, Y.; Ma, D. "Selected Copper-Based Reactions for C-N, C-O, C-S, and C-C Bond Formation", *Angew. Chem. Int. Ed.*, **2017**, 56, 16136-16179; (b) Evano, G.; Blanchard, N.; Toumi, M. "Copper-Mediated Coupling Reactions and the Their Applications in Natural Products and Designed Biomolecules Synthesis", *Chem. Rev.*, **2008**, 108, 8, 3054-3131
19. Fier, P. S.; Hartwig, J. F. "Copper-Mediated Fluorination of Aryl Iodides", *J. Am. Chem. Soc.*, **2012**, 134, 26, 10795–10798
20. Zhu. W; Ma. D. "Synthesis of Aryl Sulfones via L-Proline-Promoted CuI-Catalyzed Coupling Reaction of Aryl Halides with Sulfinic Acid Salts", *J. Org. Chem.*, **2005**, 70, 2696-2700
21. Zhang, L.; Du. W.; Wu, J.; Yang, R.; E. X.; Wang, J.; Xia, Z. " Au(I)/Au(III)-Catalyzed Sulfonylation of Aryl Iodides for the Synthesis of Various Functionalized Aryl Sulfones", *Org. Lett.*, **2024**, 26, 9413-9418
22. (a) Hayler, J.D; Leahy, D.K.; Simmons, E.M. A Pharmaceutical Industry Perspective on Sustainable Metal Catalysis. *Organometallics* **2019**, 38, 1, 36–46; (b) Sherry, B. D.; Furstner, A. The Promise and Challenge of Iron-Catalyzed Cross Coupling, *Acc. Chem. Res.,* **2008**, 41, 11, 1500-1511; (c) Han, F. Transition-metal-catalyzed Suzuki–Miyaura cross-coupling reactions: a remarkable advance from palladium to nickel catalysts, *Chem. Soc. Rev.,* **2013**, 42, 5270-5298; (d) Cahiez, G.; Moyeux, A.; Cobalt-Catalyzed Cross-Coupling Reactions, *Chem. Rev.*, **2010**, 110, 3, 1435-1462; (e) Margarita, C.; Andersson, P. G. Evolution and Prospects of the Asymmetric Hydrogenation of Unfunctionalized Olefins, *J. Am. Chem. Soc.* 2017, 139, 4, 1346–1356; (f) Wu, K.; Doyle, A. G. Parameterization of phosphine ligands demonstrates enhancement of nickel catalysis via remote steric effects, *Nature Chem.*, **2017**, 9, 779-784; (g) Monnier, F.; Taillefer, M.

Catalytic C-C, C-N, and C-O Ullmann-Type Coupling Reactions, *Angew. Chem. Int. Ed.*, **2009**, 48, 6954-6971

23. Docherty, J. H.; Peng, J.; Dominey, A. P.; Thomas, S. P. Activation and discovery of earth-abundant metal catalysts using sodium tert-butoxide, *Nature Chem.* **2017**, 9, 595-600
24. For recent examples of transition metals in electrosynthetic systems see : (a) Li, Y.; Liu, S.; Yuan, B.; Graw, N.; Ackermann, L. "Construction of remote dual stereocenters by electrochemical cobalt-catalyzed enantioselective desymmetrization", *Nat. Comm.*, **2026**, 17, 743; (b) Hinrichs, F.; Purushothaman, R.; Ackermann, L. "Nickelaelectro-Catalyzed Glycosyl-Donor Activation Enabling α-*C*-Alkenyl Glycoside Assembly", *Org. Lett.* **2025**, 27, 11714–11718; (c) Okamoto, K.; Homolle, S. L.; von Munchow, T.; Peters, S. E.; Trienes, S.; Oliveira, J. C. A.; Ackermann, L.; (d) Parnitzke, B.; Lalisse, R.; Gerhardt, E.; Maity, T.; Liu, Y.; Xuan, X.; Gutierrez, O.; Derosa, J. "Mediator- Enabled Co-Catalyzed *Z*-Selective Semihydrogenation via Hydride-Free Multisite Proton-Coupled Electron Transfer", *ACS Catal.*, **2026**, 16, 203-210; (e) Xuan, Z.; Gerhardt, E.; Parnitzke, B.; Dersoa, J. "Electroreductive Iron Catalysis Enabled by Redox Mediator: Alkyne Semi-Hydrogenation as a Model System", *ACS Catal.*, **2025**, 15, 13904-13909
25. Neumann, T.; Wowk, V.; Djebbar, F.; Chamoreau, L.; Lefevre, G. " Iron-Mediated Si-H Bond Activation: Synthesis, Characterization and Spectral Properties of a Series of $Fe^{II}(H)(SiR_3)(dmpe)_2$ Complexes", *Inorg. Chem.*, **2025**, 64, 22251-22261
26. Dombray, T.; Werncke, C. G.; Jiang, S.; Grellier, M.; Vendier, L.; Bontemps, S.; Sortais, J.; Sabo-Etienne, S.; Darcel, C. "Iron-Catalyzed C-H Borylation of Arenes", *J. Am. Chem. Soc.*, **2015**, 137, 4062-4065
27. Whittlesey, M. K.; Mawby, R. J.; Osman, R.; Perutz, R. N.; Field, L. D.; Wilkinson, M. P.; George, M. W. "Transient and Matrix Photochemistry of $Fe(dmpe)_2H_2$ (dmpe = $Me_2PCH_2CH_2PMe_2$): Dynamics of C-H and H-H Activation", *J. Am. Chem. Soc.*, **1993**, 115, 8627-8637
28. Ittel, S. D.; Tolman, C. A.; English. A. D.; Jesson, J. P. "The Chemistry of 2-Naphthyl Bis[bis(dimethylphosphino)ethane] Hydride Complexes of Fe, Ru, and Os. 2. Cleavage of sp and sp^3 C-H, C-O, and C-X Bonds. Coupling of Carbon Dioxide and Acetonitrile", *J. Am. Chem. Soc.*, **1978**, 7577-7585

29. Baker, M. V.; Field, L. D. “Reversible Metalation of Alkyl and Aryl Groups by a Coordinatively Unsaturated Iron Complex”, *J. Am. Chem. Soc.*, **1986**, 5, 821-823
30. Surke, M.; Simon, M. M.; Oliveira, J. C. A.; Ackermann, L. “Well-Defined Iron(0) Precatalysts for Grignard-Free C-H Alkenylation at Room Temperature”, *ACS Catal.*, **2025**, 12676-12683
31. Figure modified from https://periodictable.com/Properties/A/CrustAbundance.st.log.wt.html
32. Azizian, H.; Morris, R. “Photochemical Synthesis and Reaction of $FeH(C_6H_4PPhCH_2CH_2PPh_2)(PPh_2CH_2CH_2PPh_2)$”, *Inorg. Chem.*, **1983**, 22, 6-9

Chapter 2 Aryl-SCF_3 Coupling via Reductive Elimination from a Bipyridine-Ligated Palladium(II) Complex[a]

2.1 **Background**

The installation of fluorine-containing substituents onto (hetero)aromatic rings is a powerful approach for modulating the binding affinity, distribution, and metabolism of bioactive molecules.[1] One example is the SCF_3 group, whose unique physiochemical properties have led to its incorporation into a variety of agrochemical and pharmaceutical candidates.[2] Aryl-SCF_3 groups are also valuable as alternatives to aryl-CF_3 moieties, since molecules containing carbon-fluoroalkyl bonds are under regulatory pressure in the European Union.[3] As a result, the development of general, mild, and user-friendly catalytic methods to access aryl–SCF_3 ($ArSCF_3$) moieties remains an active area.[4,5,6,7,8,9]

Pioneering reports by Buchwald[10] and Schoenebeck[11] demonstrated the feasibility of Pd(0/II)-catalyzed cross-coupling between (hetero)aryl halides (ArX; X = I, Br) and $MSCF_3$ (M = Ag, NMe_4) to form $ArSCF_3$ products. However, despite the promise of these methods, their broader application has been limited by a combination of the need for sensitive and/or designer palladium pre-catalysts, a narrow range of viable ligands (Brettphos and P^tBu_3), the need for expensive and light-sensitive $AgSCF_3$, and/or incompatibility with certain classes of electrophiles (*e.g.*, (hetero)aryl triflates). We hypothesized that these limitations stem, at least in part, from a dearth of detailed information about the impact of $MSCF_3$ salt, phosphine ligand structure, and Pd precursor on the rate, selectivity, and side products associated key steps of the catalytic cycle.

High valent Pd catalytic cycles [Pd(II/IV) or Pd(I/III)] could also offer potential, but these have been underexplored in this field. For instance, palladium(II/IV) catalysis has been shown to enable challenging reductive elimination reactions like Ar-CF_3 and Ar-F couplings.[12] However, to

[aa] The cyclic voltammagrams of **2** and **2-CF3** were collected by Zoe Watchel. Additionally, the reaction of **2** with CP^{*++} was also performed by Zoe Watchel. The crystal structure of **1-Br**, **1-Cl**, **2**, and **3** were collected and solved by Dr. Fengrui Qu.

date, Ar-SCF_3 reductive elimination from Pd(IV) has not been reported . This is largely due to a lack of access to Pd–SCF_3 complexes, as well as a limited range of reliable and powerful oxidants required to access high-valent Pd complexes. Pioneering work from Ball and coworkers[13] demonstrated the use of inner-sphere chemical oxidants to form Pd(IV)-(Ar)(CF_3) complexes from (dtbpy)Pd^{II}(Ar)(CF_3) (dtbpy = di-*tert*-butylbipyridine), and these underwent facile Ar-CF_3 reductive elimination at 60 ºC. We hypothesize that an analogous approach can be pursued with Pd(Ar)(SCF_3) to study Ar-SCF_3 coupling at high valent Pd centers.

This Chapter describes mechanistic organometallic studies designed to compare palladium-phosphine catalysts and $MSCF_3$ reagents for the coupling of aryl (pseudo)halides with $MSCF_3$. Systematic investigations of transmetalation with different $MSCF_3$ salts reveal that NMe_4SCF_3 provides the optimal combination of fast and chemoselective transmetalation with (dtbpy)Pd(Ar)(X) to generate (dtbpy)Pd(Ar)(SCF_3) (dtbpy = 4,4'-di-*tert*-butylbipyridine; Ar = 4-fluorophenyl). This latter complex is used as a versatile precursor for studying phosphine ligand effects in Ar–SCF_3 reductive elimination from Pd^{II}. In addition, this complex is leveraged to establish the feasibility of oxidatively-induced and photochemically-promoted Ar–SCF_3 coupling via higher valent Pd intermediates.

2.2 **Synthesis of (4,4'-di-tert-butyl-2,2'bipyridine) Palladium (*p*-fluorophenyl)(halide) Complexes**

Proposed Catalytic Cycle. A proposed catalytic cycle for the palladium(0/II)-catalyzed coupling of aryl halides with $MSCF_3$ is shown in **Figure 2.1**.[10,11] Oxidative addition of ArX at Pd^0 (step i) affords Pd^{II}(Ar)(X) intermediate **A**. Transmetalation with $MSCF_3$ (step ii) yields Pd^{II}(Ar)(SCF_3) (**B**). Finally, Ar–SCF_3 bond-forming reductive elimination (step iii) releases the product and regenerates the Pd^0 catalyst. Step i is common across many cross-coupling reactions and has thus been widely studied with a variety of palladium(0) pre-catalysts and phosphine ligands.[14] In contrast, steps ii and iii have not been investigated in detail with SCF_3. Key open questions include: (1) what is the optimal combination of [M] and (pseudo)halide (X) for fast and selective transmetalation at Pd^{II}?; (2) what phosphine ligands (L) effectively promote Ar–SCF_3 reductive elimination from LPd^{II} complexes?; and (3) how does phosphine ligand structure impact reactivity and rates in the reductive elimination step?

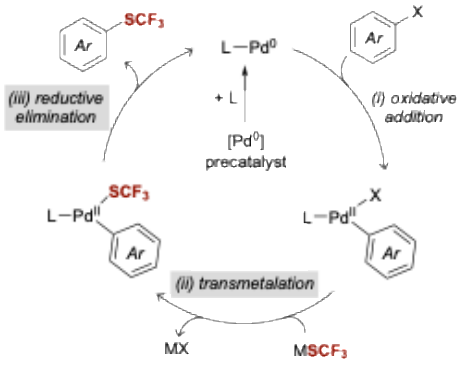
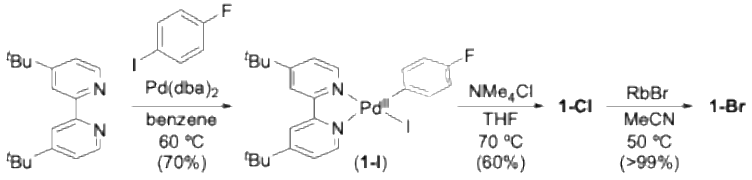


Figure 2.1. Proposed catalytic cycle for ArX/$MSCF_3$ cross-coupling.

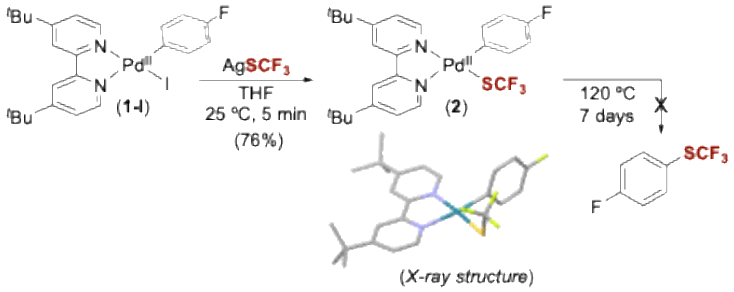
Transmetalation. We first sought to investigate transmetalation between $MSCF_3$ and (dtbpy)Pd^{II}(Ar)(X) (**1**) (dtbpy = 4,4'-di-*tert*-butylbipyridine; Ar = 4-fluorophenyl) as a function of M and X. Complex **1** was selected as a model Pd^{II} complex based on previous work from our group with related MCF_3 nucleophiles.[12] The starting material (dtbpy)Pd(*p*-FC_6H_4)(I) (**1-I**) was prepared in 70% yield via oxidative addition of *p*-FC_6H_4I at $Pd(dba)_2$ (dba = dibenzylidene acetone) in the presence of 1.5 equiv of dtbpy (**Scheme 2.1**).**Error! Bookmark not defined.** The treatment of **1-I** with excess NMe_4Cl in THF afforded the chloride analogue **1-Cl** in 60% yield. The bromide complex **1-Br** was isolated in quantitative yield from the reaction of **1-Cl** with 3 equiv of RbBr (**Scheme 2.1**).



Scheme 2.1. Synthesis of (dtbpy)Pd(*p*-FC_6H_4)(X) (X = I, Br, Cl; **1-X**). All yields are isolated.

An authentic sample of the transmetalation product, **2**, was prepared via the reaction of **1-I** with $AgSCF_3$ in THF (**Scheme 2.2**). Within 5 min at room temperature the color changed from light red to deep orange, and (dtbpy)Pd(*p*-FC_6H_4)(SCF_3) (**2**) was isolated in 76% yield after stirring overnight. This air and moisture stable orange solid and was characterized by ^1H, ^{13}C, and ^{19}F NMR spectroscopy, elemental analysis, and X-ray crystallography. It is the first reported Pd^{II}

complex containing an SCF_3 group, as well as the first crystallographically characterized group 10 complex containing both SCF_3 and aryl ligands. Isolated samples of **2** are stable to heating up to 120 ºC for ≥7 days in THF, indicating that Ar–SCF_3 reductive elimination has a high activation barrier with the bipyridine ligand.



Scheme 2.2. Synthesis and reactivity of (dtbpy)Pd(*p*-FC_6H_4)(SCF_3) (**2**). All yields are isolated.

We studied transmetalation between **1-I** and $MSCF_3$ as a function of [M], using $AgSCF_3$, NMe_4SCF_3, (dtbpy)$CuSCF_3$, $CsSCF_3$, and $CsSCF_3$•15-c-5 (15-c-5 = bisbenzo-15-crown-5). Among these, $AgSCF_3$ is a commercial reagent, while the others were synthesized in 1-3 steps via literature procedures.[6a,15] $AgSCF_3$ and NMe_4SCF_3 were used previously in the Buchwald[10] and Schoenebeck[11] methods, respectively. Each reaction was monitored by ^{19}F NMR spectroscopy to: (i) establish the overall yield of **2**; (ii) identify side products; and (iii) establish the time required for complete conversion (**Table 2.1**).

Overall, the yield of **2** ranged widely, from 48% with (dtbpy)Cu(SCF_3) to ~80% with $AgSCF_3$ and $CsSCF_3$ to ≥99% with $CsSCF_3$•15-c-5 and NMe_4SCF_3. The major identifiable side product was (dtbpy)Pd(SCF_3)$_2$ (**3**), which is expected to be a dead end in catalysis. With (dtbpy)Cu(SCF_3), **3** was formed in ~5% yield, and the remainder of the mass balance was unreacted starting material **1-I** (45%). With $AgSCF_3$, **3** was formed in 10% yield, while $CsSCF_3$ led to a different unidentified side product in ~25% yield. Finally, $CsSCF_3$•15-c-5 afforded only traces (~1%) of **3**, and this side product was not detected with NMe_4SCF_3.

Table 2.1. Reactivity of **1** with different $MSCF_3$ reagents



entry	M	X	yield 2	yield 3	time[a]
1	NMe_4	I	>99%	<1%	10 min
2	Cs	I	76%	<1%	5 min
3	Cs-15-c-5	I	99%	1%	30 s
4	Ag	I	80%	10%	30 s
5	(dtbpy)Cu	I	48%[b]	5%	1 day
6	NMe_4	Br	>99%	<1%	10 min
7	NMe_4	Cl	>99%	<1%	30 s

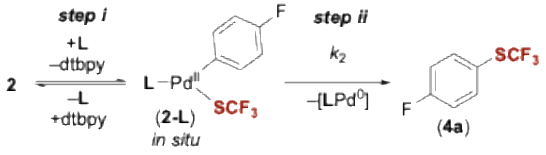
[a] Time required for maximum conversion of **1-X**. [b]Mass balance was starting material **1-I** even after 24 h. Yields determined via ^{19}F NMR spectroscopy.

Nearly all the $MSCF_3$ reagents afforded complete conversion of **1-I** within 30 min at 25 ºC. The Ag and Cs•15-c-5 salts reacted fastest (30 s), while $CsSCF_3$ and NMe_4SCF_3 proceeded to full conversion within 10 min. The Cu complex reacted slowest, requiring ~30 min to achieve the final yield of 48% which did not change over 24 h. Based on these results, we selected NMe_4SCF_3 as the $MSCF_3$ source to move forward due to its clean reactivity (>99% yield, no detectable side products) and relatively fast rate of transmetalation (~10 min at room temperature). The yields and rates of transmetalation between NMe_4SCF_3 and (dtbpy)Pd(*p*-FC_6H_4)(X) were also compared as a function of the halide (X = Cl, Br, I). In all cases, transmetalation was fast at room temperature (≤10 min), with Cl > Br ~ I (**Table 2.1**, entries 1, 6, and 7).

2.3 **Ligand Substitution of (dtbpy)Pd(*p*-fluorophenyl)(SCF_3)**

We next evaluated the rate and yield of Ar–SCF_3 reductive elimination as a function of the supporting ligand (L), to establish ligand classes and structural features leading to rapid and high-yielding Ar–SCF_3 coupling. To avoid the need to isolate individual LPd(Ar)(SCF_3) complexes (**2-**

L in **Scheme 2.3**), we generated these species *in situ* via the reaction of L with **2** (**Scheme 2.3**, step i). Since **2** is inert towards reductive elimination, the product (**4a**) can only be formed from **2-L** (**Scheme 2.3**, step ii). ^{19}F NMR spectroscopy was used to monitor these reactions with four distinct classes of ligands.



Scheme 2.3. Pathway to Ar–SCF_3 coupling starting from **2** with diverse phosphine ligands (L)

Initial studies focused on BrettPhos derivatives, since BrettPhos was the first ligand reported for Pd-catalyzed aryl trifluoromethylthiolation.[10] The treatment of **2** with 1.5 equiv BrettPhos under our assay conditions (0.1 M in THF for 24 h) afforded **4a** in 6% yield at 25 ºC and 37% yield at 80 ºC (**Figure 2.2**). The putative intermediate **2-BrettPhos** was not detected at either temperature. Upon increasing to 3 equiv of BrettPhos under otherwise identical conditions, **2-Brettphos** was detected, but the yield of **4a** increased only slightly to 39%. This result indicates that the rate of reductive elimination (rather than the rate or equilibrium for ligand substitution) is the main factor limiting product formation in this system. The impact of substitution on the biaryl ring was assessed by changing L to XPhos and CyJohnPhos (**Figure 2.2**). Both gave much lower yields of **4a** than BrettPhos (13% and 6%, respectively, at 80 ºC), and intermediate **2-L** was not detected in either case.

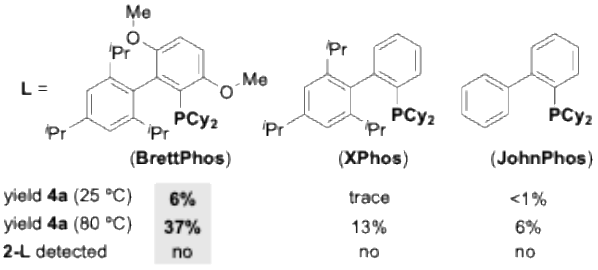


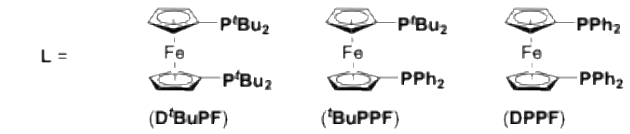
Figure 2.2. Ar–SCF_3 coupling results for BrettPhos derivatives. Conditions: 80 ºC, 24 h, 0.1 M **2** in THF, 1.5 equiv of ligand, N_2 atmosphere. Yield of **4a** and detection of **2-L** via ^{19}F NMR spectroscopy.

We next examined P^{t}Bu$_3$, which was employed by Schoenebeck for Pd-catalyzed aryl trifluoromethylthiolation.[11] Under the standard conditions, **4a** was formed in 13% yield at 25 ºC and >99% yield at 80 ºC (**Figure 2.3**). Again, the putative intermediate (**2-P^{t}Bu$_3$**) was not detected by ^{19}F NMR. Comparable reactivity was observed with P^{t}Bu$_2$Ph, with 10% and >99% yield of **4a** at 25 and 80 ºC and no detectable **2-P^{t}Bu$_2$Ph**. Further replacing *t*-butyl substituents with phenyls resulted in a dramatic drop-off in yield (24% and <1% yield of **4a** at 80 ºC with P^{t}BuPh$_2$ and PPh$_3$, respectively). In these cases, intermediate **2-L** was detected, indicating that Ar–SCF$_3$ reductive elimination is the slow step with these smaller phosphines.

L =	P^{t}Bu$_3$	P^{t}Bu$_2$Ph	P^{t}BuPh$_2$	PPh$_3$
yield **4a** (25 ºC)	**13%**	10%	3%	<1%
yield **4a** (80 ºC)	**>99%**	>99%	24%	<1%
2-L detected	no	no	yes	yes

Figure 2.**3**. Ar–SCF$_3$ coupling results for P^{t}Bu$_3$ derivatives. Conditions: 80 °C, 24 hours, 0.1M of **(2)** in THF, 3 equiv of ligand, N$_2$ atmosphere. Yield of **4a** and detection of **2-L** via ^{19}F NMR spectroscopy.

Our previous work showed that phosphinoferrocene ligands promote challenging Ar–CF$_3$ bond-forming reductive elimination reactions at Pd^{II}, with di-*t*-butylphosphinoferrocene (D^{t}BuPF) affording the fastest rates and highest yields.[16] This led us to hypothesize that D^{t}BuPF and derivatives would also be effective for Ar–SCF$_3$ coupling. Indeed, D^{t}BuPF showed higher reactivity than either BrettPhos or P^{t}Bu$_3$, affording 35% yield of **4a** at room temperature and 99% yield at 80 ºC (**Figure 2.4**). Replacing one of the -P^{t}Bu$_2$ groups with a -PPh$_2$ (^{t}BuPPF) had minimal impact on reactivity, but diphenylphosphinoferrocene (DPPF) afforded dramatically lower yield of **4a**. Intermediate **2-L** was observed with both ^{t}BuPPF and DPPF, although in the former case it is likely the smaller phenyl substituted phosphine that is bound to the Pd center.



yield **4a** (25 ºC)	**35%**	26%	<1%
yield **4a** (80 ºC)	**>99%**	>99%	29%
2-L detected	no	yes*	yes

Figure 2.4. Ar–SCF_3 coupling results for phosphinoferrocene derivatives. Conditions: 80 °C, 24 h, 0.1M **2** in THF, 1.5 equiv of ligand, N_2 atmosphere. *Likely coordinated via -PPh_2 moiety. Yield of **4a** and detection of **2-L** via ^{19}F NMR spectroscopy

A final set of studies focused on XantPhos and derivatives, since this ligand class is known to be effective for other challenging reductive elimination reactions.[17] Xantphos exhibited a different profile compared to the successful ligands from above. First, **4a** was formed in >99% yield over 2 h *at room temperature*. Second, the ligand substitution intermediate **2-Xantphos** was generated in quantitative yield after 5 min at 25 ºC and then decayed over 2 h to form **4a**. The rate and yield of Ar–SCF_3 coupling was significantly attenuated upon moving to the less rigid analogues DPEPhos and DPPEE (**Figure 2.5**).

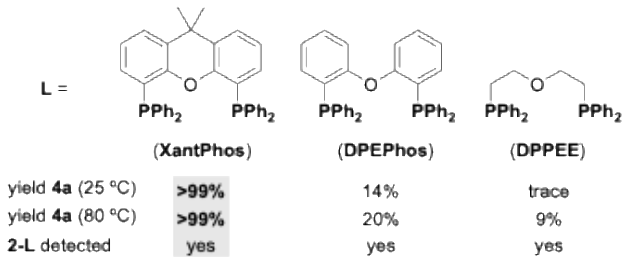


Figure 2.5. Ar–SCF_3 coupling results for XantPhos derivatives. Conditions: 80 °C, 24 h, 0.1 M of **2** in THF, 1.5 equiv of ligand, N_2 atmosphere. Yield of **4a** and detection of **2-L** via ^{19}F NMR spectroscopy.

We also conducted time studies at 80 ºC with 5 representative ligands, XantPhos, D^{t}BuPF, P^{t}Bu$_3$, Brettphos, and DPPF. These data show that XantPhos, D^{t}BuPF, and P^{t}Bu$_3$ all react rapidly at 80 ºC, affording essentially quantitative yield within 1 h. Notably, comparable rates have been reported for Ar-CF_3 reductive elimination from analogous XantPhos, D^{t}BuPF, and P^{t}Bu$_3$ $Pd^{II}(Ar)(CF_3)$ complexes at this temperature.**Error! Bookmark not defined.**[17] In contrast, Brettphos and DPPF showed dramatically slower rates, with minimal formation of **4** after 1 h and slow conversion over 24 h.

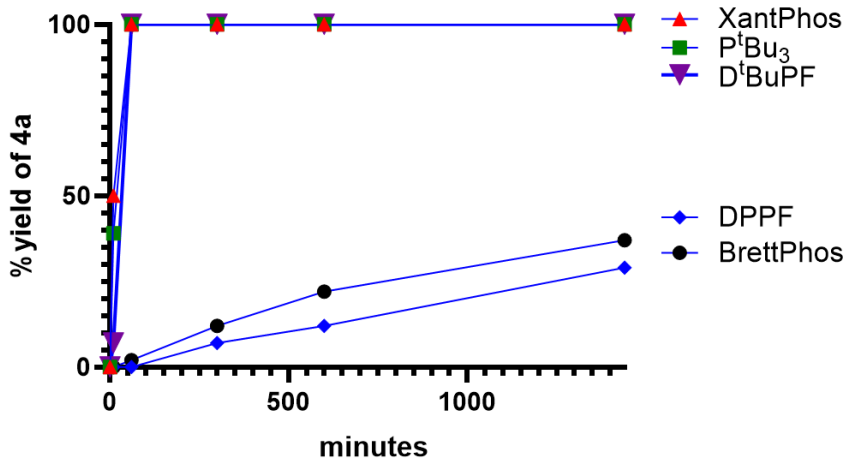


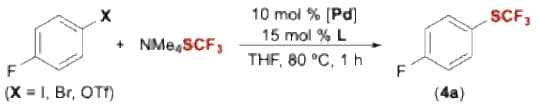
Figure 2.6. Time course for formation of **4a** at 80 ºC with selected L. Conditions: N_2, 0.1 M solution of **2** in THF. Reactions monitored via ^{19}F NMR spectroscopy

2.4 **Development of Ligand Promoted Aryl-SCF_3 Cross-Coupling Catalysis**

We next sought to leverage lessons learned from the stoichiometric studies to achieve $Pd^{II/0}$-catalyzed Ar-SCF_3 coupling reactions that address limitations of previous methods. The coupling of 4-fluoroiodobenzene with NMe_4SCF_3 (the optimal reagent for transmetalation) was selected as model reaction for translating the stoichiometric studies to catalysis. The objectives of catalyst screening were two-fold: (1) to compare the performance of the ligands identified in **Figures 2.3-6**; and (2) to address limitations of previous methods, including the requirement for expensive and/or specialized pre-catalysts [$(COD)Pd(CH_2SiMe_3)_2$ or $Pd^{I}_2(I)_2(P^tBu_3)_2$] as well as incompatibility with aryl triflate electrophiles. We initially evaluated six ligands that were effective for Ar–SCF_3 reductive elimination: BrettPhos, Xantphos, D^{t}BuPF, ^{t}BuPPF P^{t}Bu$_3$, and P^{t}Bu$_2$Ph. $(COD)Pd(CH_2SiMe_3)_2$ was used as the precatalyst, mimicking Buchwald's initial report of Pd-catalyzed trifluoromethylthiolation.[10] As expected based on the literature report,[10] BrettPhos performed well under these conditions, affording 91% yield of **4a** (**Table 2.2**, entry 1). D^{t}BuPF and Xantphos, ligands that have not been previously reported for this transformation, afforded >99% yield (entries 2 and 3). In contrast, P^{t}Bu$_3$, P^{t}Bu$_2$Ph, and ^{t}BuPPF gave much lower yields (37-66%; entries 4-6).

The same set of ligands was next examined using $Pd(dba)_2$ (dba = dibenzylidene acetone), a significantly cheaper and more stable pre-catalyst. With BrettPhos, the yield of **4a**

dropped dramatically to just 32% (entry 7), reflecting well-documented challenges in ligand substitution of dba with this ligand.[18] In contrast, Xantphos and D^{t}BuPF maintained yields of >90% (entries 8 and 9) with $Pd(dba)_2$.[19] Upon moving from the aryl iodide to the analogous bromide, D^{t}BuPF significantly outperformed Xantphos (63% versus 15%, respectively; entries 13 and 14), leading us to move forward with D^{t}BuPF.



entry	L	[Pd]	X	yield 4a
1	Brettphos	$(COD)Pd(CH_2SiMe_3)_2$	I	91%
2	Xantphos	$(COD)Pd(CH_2SiMe_3)_2$	I	99%
3	D^{t}BuPF	$(COD)Pd(CH_2SiMe_3)_2$	I	99%
4	^{t}BuPPF	$(COD)Pd(CH_2SiMe_3)_2$	I	66%
5	P^{t}Bu$_3$	$(COD)Pd(CH_2SiMe_3)_2$	I	37%
6	P^{t}Bu$_2$Ph	$(COD)Pd(CH_2SiMe_3)_2$	I	39%
7	Brettphos	$Pd(dba)_2$	I	32%
8	Xantphos	$Pd(dba)_2$	I	92%
9	D^{t}BuPF	$Pd(dba)_2$	I	99%
10	^{t}BuPPF	$Pd(dba)_2$	I	72%
11	P^{t}Bu$_3$	$Pd(dba)_2$	I	22%
12	P^{t}Bu$_2$Ph	$Pd(dba)_2$	I	6%
13	Xantphos	$Pd(dba)_2$	Br	15%
14	D^{t}BuPF	$Pd(dba)_2$	Br	63%

Table 2.2. Preliminary reaction optimization studies. Yields determined by ^{19}F NMR analysis.

The Pd^0/D^{t}BuPF-catalyzed reaction was further optimized with respect to pre-catalyst structure, solvent, catalyst loading, reagent stoichiometry, concentration, and time. Ultimately, changing the solvent to dioxane and the reaction temperature to 110 ºC enabled efficient and high yielding trifluoromethylthiolation of both the aryl bromide and aryl triflate substrates using 4 mol

% Pd and 6 mol % D^{t}BuPF. The corresponding aryl iodide reacted at 80 ºC under analogous conditions.

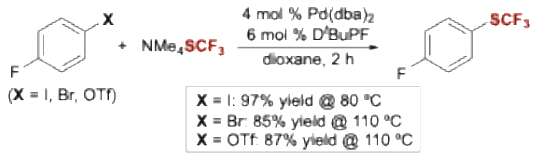


Figure 2.9. Optimized conditions for ArI, ArBr, and ArOTf substrates. Yields determined by ^{19}F NMR analysis

A series of (hetero)aryl iodide, bromide, and triflate substrates were evaluated under the optimized conditions, and the results are summarized in **Figure 2.10**. Functional groups including 3º-anilines (**4l**), aldehydes (**4e**), esters (**4g**), and 3º-amides (**4h**) as well as a variety of heterocycles (**4i**, **4m**, **4n**, **4q**, **4s**) proved compatible. Sterically hindered electrophiles with mono- and di-substitution at the *ortho*-position was well tolerated (**4j, 4k**). In examples where different electrophiles were compared, the aryl iodide, -bromide, and -triflate afforded similar yields (**4a-c**). Functional groups/products that have not been demonstrated in previous Pd-catalyzed trifluorothiomethylation methods, including alkynes (**4f**, **4t**), sulfones (**4p**), and silyl groups (**4o**) were well-tolerated. 2-Bromostyrene was converted to the corresponding vinyl-trifluoromethylthiolate **4r** in good yield. Notably, the starting material was a ~9 : 1 mixture of the E : Z isomers, but only the E product was formed (with unreacted Z-2-bromostyrene remaining). Finally, **4t**, the -SCF_3 analogue of a positron emission tomography tracer for imaging the metabotropic glutamate receptor subtype 5, was accessed in 70% isolated yield from the corresponding aryl bromide.

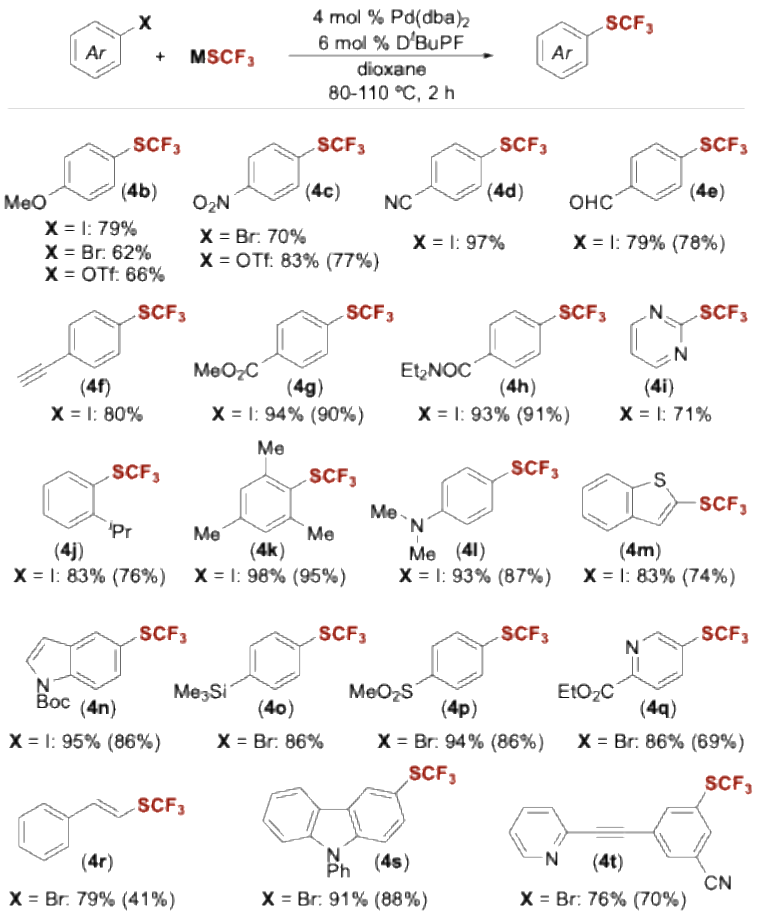


Figure 2.10. Scope of Pd/D^{t}BuPF-catalyzed trifluromethylthiolation. Yields reported as ^{19}F NMR yield (isolated yield).

Finally, we sought to establish the limitations of this transformation. As shown in **Figure 2.11**, aryl iodide substrates containing -OH and -NH functional groups, including phenols, anilines, carboxylic acids, amides, and boronic acids, generally afforded low or no yield of the trifluoromethylthiolated product. While pyridine and pyrimidine heterocycles were tolerated, imidazole derivatives were not compatible. An N-alkyl pyrazole gave modest 41% yield, but the NH analogue showed no reaction under analogous conditions. Notably, while similar limitations were not explicitly discussed in previous reports of Pd-catalyzed trifluoromethylthiolation,[10,11] none of these substrates/functional groups were successfully demonstrated. Control studies in the absence of Pd revealed that TMASCF$_3$ completely decomposes over 24 h at 80 ºC in the presence of many of these substrates (4-iodoaniline, 5-iodoindole, 4-bromophenyl boronic acid, 4-iodobenzamide, 4-iodoimidazole, 4-iodopyrazole), which explains their poor performance in this

transformation. Finally, 4-fluorophenyl chloride and 4-chlorobenzonitrile gave <5% product, even at 130 ºC, while more activated 2-chloropyrimidine afforded modest (24%) trifluorothiomethylation at 110 ºC.

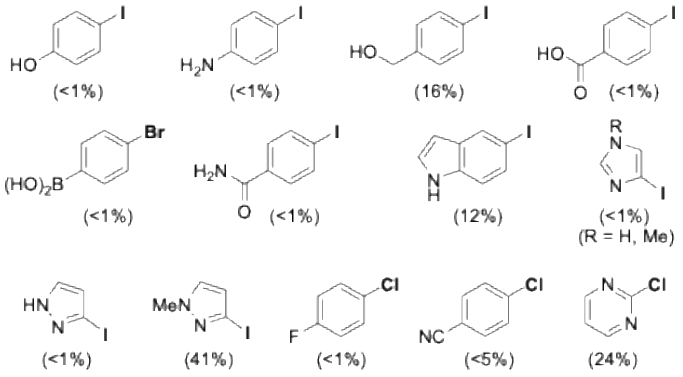


Figure 2.11. Unreactive/modest yielding-substrates. Yields determined by ^{19}F NMR analysis.

In summary, this study describes the use of organometallic studies to drive reagent and ligand selection for Pd(0/II)-catalyzed aryl trifluorothiomethylation reactions. In particular, di-*tert*-butylbipyridine (dtbpy) palladium(II) complexes served as readily available and stable precursors for studying the key transmetalation and reductive elimination steps of the catalytic cycle. This ultimately led to the identification of $Pd(dba)_2$ and di-*t*-butylphosphinoferrocene (D^{t}BuPF) as an effective pre-catalyst/ligand combination for the trifluorothiomethylation of diverse aryl bromides, -iodides, and -triflates. Moving forward, we anticipate that this approach will be effective for identifying transmetalating reagents, ligands, and catalysts for other challenging Pd-catalyzed R–X coupling reactions.

2.5 **Chemical Oxidation of (dtbpy)Pd(*p*-fluorophenyl)(SCF_3)**

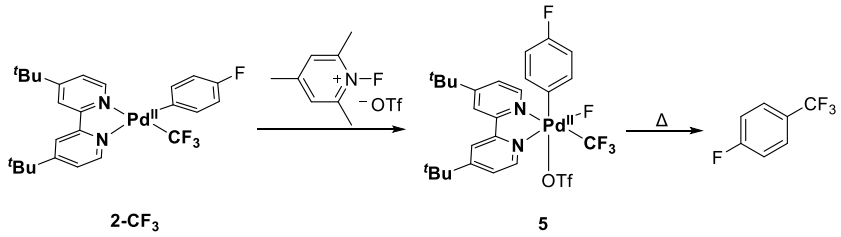


Figure 2.12. Oxidatively-induced Ar-CF_3 reductive elimination from **2-CF_3** via Pd^{IV} intermediate **5Error! Bookmark not defined.**

In parallel with studying thermally promoted reductive elimination from Pd^{II}, we also evaluated oxidatively and photochemically-induced Ar–SCF_3 coupling. In 2012, Ball and coworkers[12]**Error! Bookmark not defined.** demonstrated that the analogous **2-CF$_3$** complex reacts with *N*-fluoro-2,4,6-trimethyl-pyridinium triflate (NFTPT) to afford an isolable Pd(IV) intermediate **5** (**Figure 2.12**). Upon heating to 60 ºC, **5** undergoes Ar–CF_3 bond-forming reductive elimination to furnish 4-fluorotrifluorotoluene. We sought to study analogous reactivity at the Pd^{II}(Ar)(SCF_3) complex **2**. We first used cyclic voltammetry (CV) to compare the oxidation potential of **2** to that of **2-CF$_3$** (**Figure 2.13**). The CVs were acquired in 0.5 M KPF_6 in acetonitrile with a scan rate of 100 mV/s. This complex shows an onset oxidation potential of 0.86 V vs Ag/Ag^+, which is over 250 mV lower than that of **2-CF$_3$** (>1.1 V vs Ag/Ag^+). We hypothesize the lower oxidation potential of **2** is due to a higher amount of electron density on the palladium center, due to the fact that SCF_3 is less electron-withdrawing than CF_3. Overall, these data suggest that high valent Pd should be accessible by treatment of **2** with a variety of chemical oxidants.

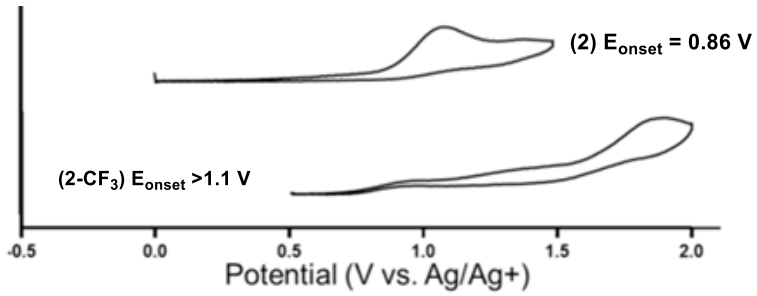


Figure 2.13. Cyclic voltammogram (CVs) of **2** and **2-CF$_3$** in 0.5 M solution of KPF_6 in MeCN with a scan rate of 100 mV/s. Conditions: 0.071 cm^2 glassy carbon working electrode, platinum wire counter electrode, and Ag/Ag^+ reference electrode consisting of a 0.01 M $AgBF_4$ and 0.5 M KPF_6 solution in MeCN.

To test this proposal, we reacted **2** with a series of different oxidants in acetonitrile at room temperature (**Table 2.3**). The goals of this study were to (i) establish the feasibility and yield of Ar–SCF_3 coupling as a function of oxidant and (ii) detect high valent Pd intermediates during these transformations. Two types of oxidants were employed: (1) inner-sphere oxidants, which oxidize the Pd^{II} through the chemical addition of two X-type ligands to the Pd^{II} center, and (2) outer-sphere oxidants, which transfer an electron hole to the Pd center. In general, no high valent Pd

intermediates were observed by ^{19}F NMR spectroscopy in these transformations, likely because Ar–SCF_3 bond forming reductive elimination is fast from high valent Pd centers.

Inner sphere oxidants were first evaluated, starting with NFTPT, the reagent used by Ball with **2-CF$_3$**. In less than an hour at ambient temperature, **2** was completely consumed to afford **4a** in 30% yield, as determined by ^{19}F NMR spectroscopic analysis (**Table 2.2**). The remainder of the SCF_3 mass balance consisted of unidentified Pd–SCF_3 complexes. Notably, these did not lead to more of product **4a** upon heating, indicating that they are not $Pd^{IV}(Ar)(SCF_3)$ species.

Another inner sphere oxidant – *m*-CPBA (*meta*-chloroperoxybenzoic acid) – reacted rapidly with **2** in MeCN at ambient temperature, forming a bright red solution. The target Ar-SCF_3 product formed in 13% yield along with 5% of F_3CS-SCF_3 and 13% unreacted **2**. The remaining mass balance consisted of a myriad of side products, including Pd(Ar)(X) complexes bearing $S(O)CF_3$ (13%) and SO_2CF_3 (6%) as X-type ligands along with two unknown Pd-SCF_3 complexes (-25 ppm in the crude ^{19}F NMR spectrum) (**Figure 2.14**). The former derive from O-atom transfer from the peroxide reagent, and the synthesis and reactivity of analogous complexes will be discussed in detail in Chapter 3 of this thesis.

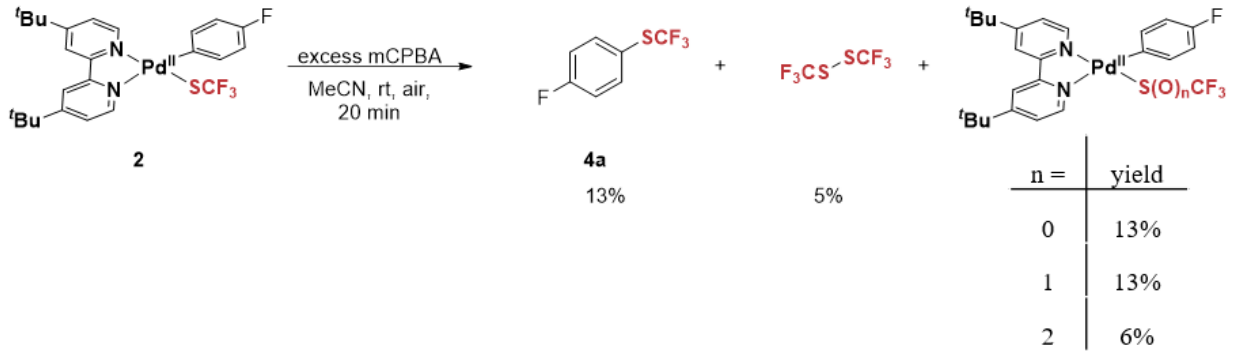
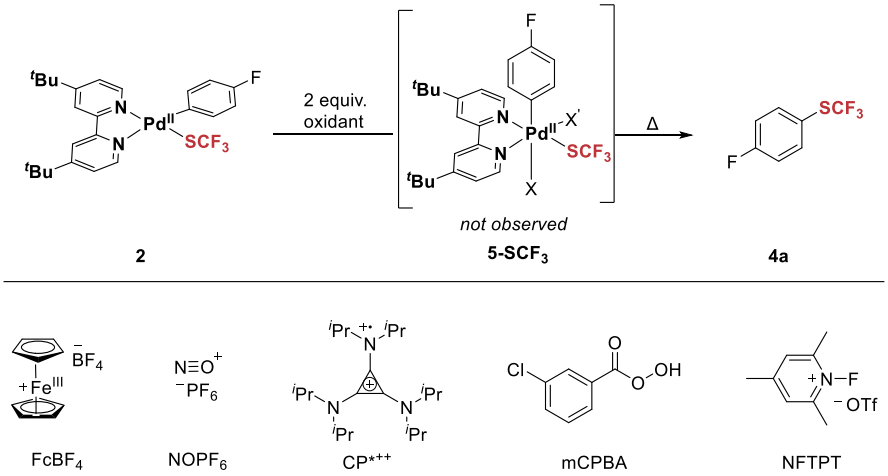


Figure 2.14. Reaction of 2 with *m*-CPBA. Yields determined by ^{19}F NMR analysis.

Outer sphere oxidants were next examined for promoting Ar-SCF_3 coupling from **2**. Ferrocenium tetrafluoroborate was not competent in this transformation, returning unreacted starting material **2**. This is consistent with its oxidation potential (0.003 V vs Ag/Ag^+) being more than 800 mV lower than the E_{onset} of **2**. In contrast, higher potential outer sphere oxidants – $NOPF_6$

(entry 2) and the trisaminocyclopropenium radical dication $\mathbf{CP}^{\bullet++}$ (entry 3) – afforded 47% and 60% yield of **4a**, respectively. The major side product characterized in these transformations was $F_3CS\text{-}SCF_3$ (8% yield with both oxidants). While the exact mechanism for the formation of this side product has not been elucidated, it likely involves radical extrusion of SCF_3 from the palladium center.



entry	oxidant	potential	yield 4a	Yield $(SCF_3)_2$
1	$FcBF_4$	0.03 V	0%	0%
2	$NOPF_6$	0.94 V	47%	8%
3	CP^{*++}	0.92 V	60%	8%
4	mCPBA	*via* O^{2-}	13%	5%
5	NFTPT	*via* F-, OTf-	30%	trace

Table 2.3. Oxidant Screen on **2**. Yields determined by ^{19}F NMR analysis.

2.6 **Photochemical Excitation of (dtbpy)Pd(*p*-fluorophenyl)(SCF_3)**

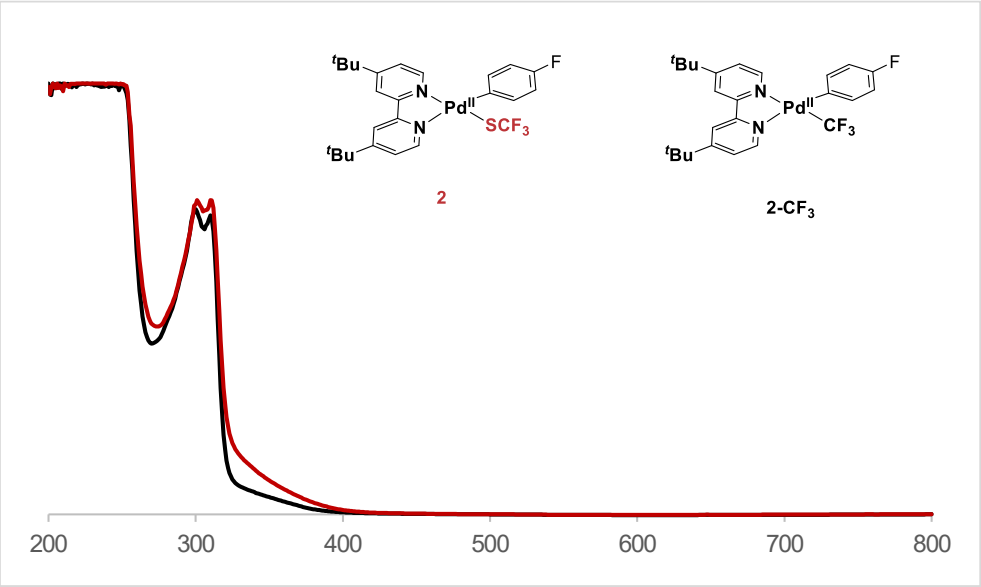
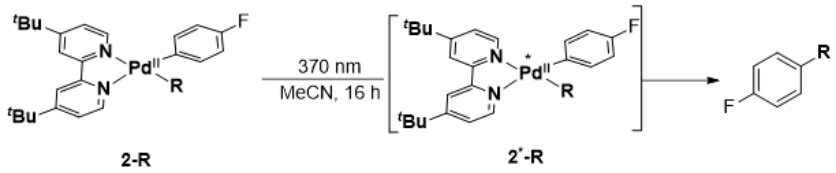


Figure 2.15. UV-Vis spectrum of **2 and 2-CF_3** in acetonitrile

Finally, photo-induced reductive elimination from complex **2** was explored. While direct excitation of palladium(II) complexes is not commonly invoked in photocatalytic systems, palladium has been used in photochemistry.[20] Furthermore, the di-tert-butylbipyridine ligand is featured in a wide variety of first-row transition-metal photoredox catalyses.[20] A UV-Vis spectrum of **2** was acquired (**Figure 2.15**), and this complex shows a strong absorption peak at 306 nm that tails into the near UV region. **2-CF_3** shows a nearly identical UV-Vis trace, suggesting that the feature is based on either the dtbpy-Pd excitation or Pd-*para*-fluorophenyl excitation. As such, a solution of **2** in acetonitrile was irradiated with 370 nm Kessel lamps for 4 h in both air and under N_2-atmosphere. During this irradiation, the color changed from light yellow to dark orange with yellow precipitates for the reaction conducted under air. The reaction conducted under N_2 turned a very dark black or brown. However, analysis of the crude reaction mixture via ^{19}F NMR spectroscopy showed both reactions produced **4a** in high yields, 78% and 72%, respectively. The difference in color is likely due to O_2 from the atmosphere oxidizing the resulting Pd(0) species from after the reductive elimination to a Pd(II) species, which are often yellow and orange, **Figure 2.16**. Despite having a nearly identical UV-Vis trace to **2**, **2-CF_3** did not reductively eliminate upon photoexcitation. This exciting preliminary result suggests photocatalytic Ar-SCF_3 coupling

methods could be accessible and represent an exciting area for future exploration. To the best of our knowledge, this is the first report demonstrating photo-induced reductive elimination from a (dtbpy)Pd complex.



Entry	R	Atmosphere	Yield	Notes
1	**CF_3**	air	0%	light orange
2	**CF_3**	N_2	0%	orange
3	**SCF_3**	air	78%	orange w/ solids
4	**SCF_3**	N_2	72%	black w/ solids

Figure 2.16. Photoexcitation of **2** and **2-CF_3** at 370 nm. Yield determined by ^{19}F NMR spectroscopic analysis

2.7 **Conclusion**

In summary, Chapter 2 describes thermal, oxidative, and photochemical reductive elimination reactions from (dtbpy)Pd^{II}(Ar)(SCF_3) (**2**) to form Ar–SCF_3 products. Complex **2** facilitated: (1) screening of sterically bulky phosphine ligands for thermal reductive elimination pathways, (2) evaluation of inner and outer sphere oxidants for oxidatively-induced reductive elimination, and (3) photoinduced Ar–SCF_3 bond-formation. These studies identified a novel catalytic system for the cross-coupling of aryl-trifluoromethylthiolates, leveraged tris(amino)cyclopropenium radical dications as powerful and chemoselective oxidants, and unlocked palladium(II) photochemistry.

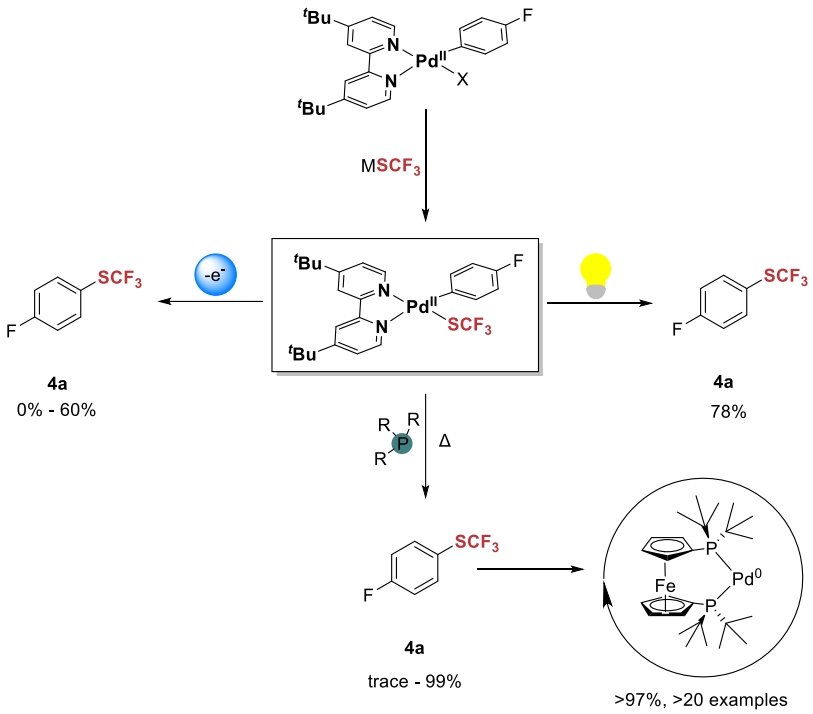
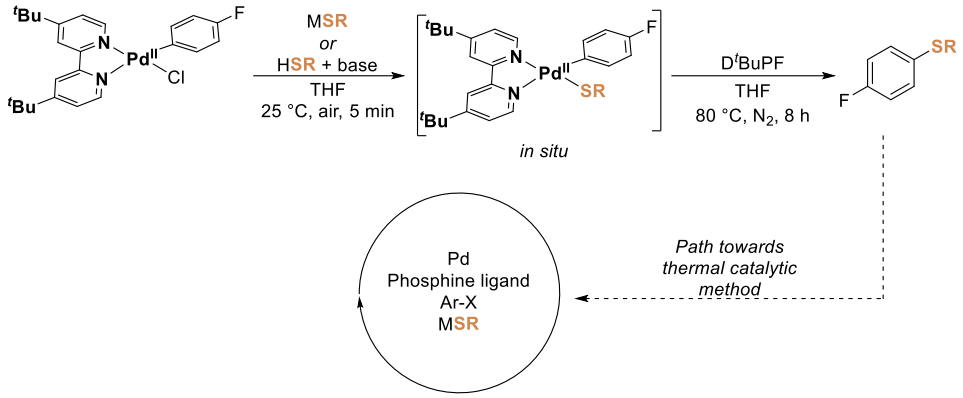


Figure 2.17. Synthesis of **2** and access to reductive elimination of **4a** via oxidative, photochemical, and thermal means.

2.8 **Outlook**

Moving forward, we propose several additional catalytic methods that could be accessed by leveraging the approaches described above. First, continuing with the thermal reductive elimination, we envision substituting CF_3S^- with different anionic coupling partners and conducting analogous reductive elimination studies to find appropriate ligand candidates for palladium(0/II) catalysis. Furthermore, based on the rapid rate of transmetalation at **1-Cl, 1-Br, and 1-I,** we envision a protocol in which **1-X** is the starting complex, transmetalation with the desired cross-coupling partner anion is performed *in situ*, and this reaction mixture is then combined with stock solutions of different ligands. This protocol takes advantage of rapid transmetalation at the halogen complexes and the lability of the dtbpy ligand in the presence of electron rich phosphines. Successes from this rapid organometallic assay can be followed up by studying each step alone as described in **2.2** and **2.3** and then translated to catalysis. Preliminary data in **Table 2.4** show the feasibility of this approach. The proposed *in situ* protocol was performed using $NaSCH_3$ and K_3PO_4·HSPh as transmetalating partners in conjunction with D^{t}BuPF as the ligand. This protocol furnished 4-fluorothioanisole and 4-fluorothiophenol in 25%

and 12% yield, respectively, demonstrating the utility of this rapid protocol as a first pass assay for identifying compatible cross-coupling conditions.



entry	Nucleophile	Base	yield
1	$TMASCF_3$	N/A	71%
2	$NaSCH_3$	N/A	25%
3	HSPh	K_3PO_4	12%

Table 2.4. Demonstration of rapid screening assay for transmetalation and reductive elimination of other sulfur nucleophiles. Yield determined by ^{19}F NMR spectroscopic analysis.

To date, there are no catalytic methodologies that use high-valent or photo-excited palladium centers for Ar–SCF_3 cross-coupling. The knowledge gained from the oxidant studies and UV-Vis studies provides a pathway for the development of such procedures. Because oxidative addition into aryl-halide bonds at palladium(II) is not well precedented, catalytic methods will likely require a different aryl source. Boronic acids are known to transmetalate at Pd(II) in the presence of base and thus could serve as the source of aryl groups. As shown in **Figure 2.18**, starting from (dtbpy)$Pd(Cl)_2$ and $CsSCF_3$ or $TMASCF_3$ could allow the SCF_3 anion play two roles: (1) as a transmetalating reagent to form a Pd^{II}–SCF_3 intermediate and (2) as a base to promote boronate transmetalation. Subsequently, a strong oxidant such as CP^{*++} could oxidize the resulting $Pd^{II}(Ar)(SCF_3)$ intermediate, leading to oxidatively-induced Ar–SCF_3 coupling.

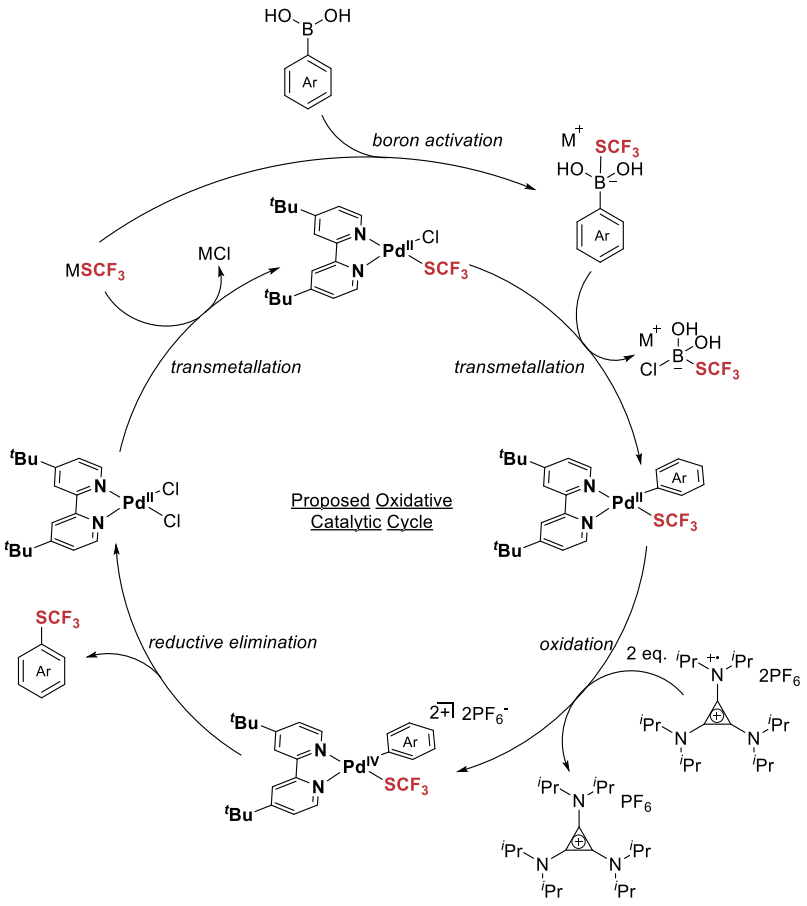
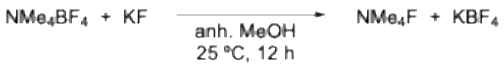


Figure 2.18. Proposed catalytic cycle for high-valent palladium cross-coupling of aryl boronic acids and metal SCF_3 species.

2.9 Experimental

2.9.1 Synthesis of Reagents

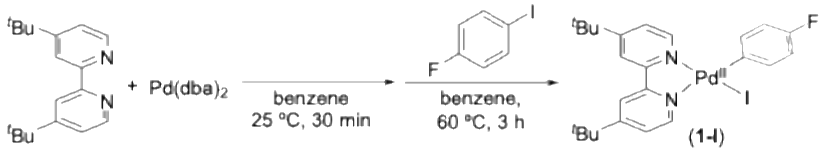
Trifluoromethylthiolate reagents with various counterions [NMe_4,[14] Cs,[14] (bisbenzo-15-crown-5)Cs[14]] were synthesized using literature procedures. Tetramethylammonium fluoride for the synthesis of NMe_4SCF_3 was prepared as described below.



An oven dried 100 mL flask was charged with a large stir bar and KF (3.36 g, 57.9 mmol, 1 equiv), sealed with a rubber septum, and then dried while stirring at 150 ºC under vacuum for 1 day. An

oven-dried, 250 mL, 3-neck flask was charged with a large stir bar and tetramethylammonium tetrafluoroborate (9.32 g, 57.9 mmol, 1 equiv). The two outer necks were sealed with a rubber septum and a solid ground glass stopper. The middle neck was connected to a Schlenk line using a ground glass adapter. The NMe_4BF_4 was dried by stirring under vacuum at room temperature for 1 day. Anhydrous methanol (250 mL) was refluxed over 2 g of ground magnesium shavings and then distilled under nitrogen. This freshly distilled methanol was added to each flask via syringe (50 mL each). The KF solution was then added to the NMe_4BF_4 solution via syringe. The resulting mixture was stirred at room temperature overnight under N_2. An oven-dried 2-neck round bottom flask ("receiving flask") was connected to a Schlenk line using a ground glass adapter. The second neck was attached to a swivel frit, which was then connected to the reaction flask. The reaction mixture was filtered via swivel frit to remove KBF_4, affording a methanolic solution of NMe_4F in the receiving flask. The MeOH was removed by vacuum distillation, leaving the NMe_4F product as a white power. The NMe_4F was transferred into a 100 mL round-bottom flask in a N_2-filled glovebox, and the solid was stirred under vacuum at 100 ºC for 3 days.

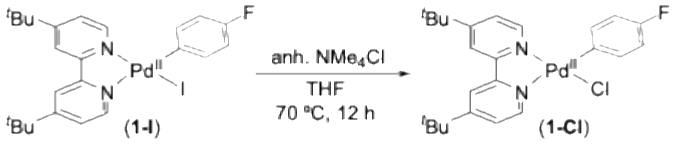
2.9.2 **Palladium Complexes**



Complex 1-I. A literature preparation was followed[4] with some modification in the purification procedure. Under nitrogen, $Pd(dba)_2$ (1000 mg, 1.74 mmol, 1.0 equiv) was weighed into a reaction flask along with 4,4'-Di-*tert*-butylbipyridine (dtbpy, 699 mg, 2.61 mmol, 1.5 equiv). This was dissolved in benzene (~0.2 M solution based on Pd). The resulting mixture was stirred at 25 ºC for 30 min. 4-Fluoro-iodobenzene (1550 mg, 6.98 mmol, 4 equiv) was added, and the solution was warmed to 60 ºC for 3 h. Under ambient air, the reaction mixture was filtered through a plug of Celite, washing with benzene. It was then filtered through a plug of silica gel, washing with benzene. The solvent was removed under reduced pressure until a solid powder remained, and the residue was washed with diethyl ether and hexanes (~100 mL each) to remove residual dibenzylidene acetone (dba). The remaining solid was dried under vacuum and then purified via chromatography on silica gel using an eluent of 12% EtOAc in hexanes. This chromatographic purification removed $(dtbpy)Pd(I)_2$ (dark red). Product **1-I** was obtained as a light orange solid

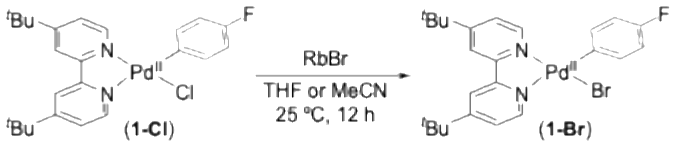
(739 mg, 71% yield). This procedure was effective starting with between 100 mg and 2 g of $Pd(dba)_2$, with yields ranging from 65-85%. THF could also be used as a solvent, but the purification worked better with benzene.

Note: The chromatographic purification was very important for the transmetallation studies to ensure that any complex **3** observed derives from **1-I** and not from residual $(dtbpy)Pd(I)_2$.



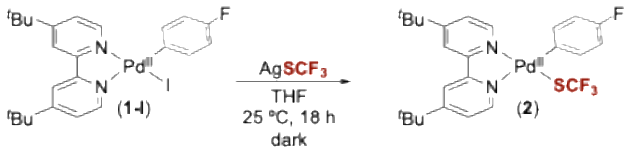
Complex 1-Cl. In air, a 20 mL vial was charged with **1-I** (813 mg, 1.36 mmol, 1 equiv) and anhydrous TMACl (1480 mg, 13.6 mmol, 10 equiv). THF (15 mL) was added, and the vial was capped and sealed with electrical tape. The dark orange heterogeneous mixture was heated at 70 ºC for 15 h, during which time it changed color to light yellow with a white precipitate. The reaction mixture was filtered through a plug of celite and concentrated under vacuum, and the resulting solids were purified via column chromatography on silica gel using an eluent of 15% EtOAc in hexane. Notably, under these conditions residual **1-I** elutes first, followed closely by **1-Cl**. The product **1-Cl** was obtained as a white solid (423 mg, 62% yield). This procedure was effective starting with between 50 and 800 mg of **1-I**, with yields ranging from 60-70%. Single crystals suitable for XRD were obtained by slow diffusion of hexane into a THF solution of **1-Cl** at room temperature or from precipitation of **1-Cl** from a solution of 15% EtOAc in hexane at room temperature.

^{1}H NMR (600 MHz, CD_2Cl_2) δ 9.03 (d, J = 5.7 Hz, 1H), 8.07 (dd, J = 4.5, 2.0 Hz, 2H), 7.85 (d, J = 6.0 Hz, 1H), 7.59 (dd, J = 5.7, 1.9 Hz, 1H), 7.35-7.29 (multiple peaks, 3H), 6.85 (m, 2H), 1.45 (s, 9H), 1.40 (s, 9H). **^{13}C NMR** (126 MHz, CD_2Cl_2) δ 163.84 (d, J = 46.7 Hz), 161.05 (d, J = 238.8 Hz), 156.41, 153.68, 151.09, 148.90, 144.04 (d, J = 2.6 Hz), 135.59 (d, J = 5.6 Hz), 123.83, 123.74, 118.96, 118.22, 113.68, 113.52, 35.56, 35.52, 30.19, 30.01. **^{19}F NMR** (564 MHz, CD_2Cl_2) δ -123.19 (tt, J = 9.8, 6.3 Hz). **Elemental Analysis** calc'd C 57.04%; H 5.58%; N 5.54%. Found: C 57.11%; H 5.63%; N 5.51%.



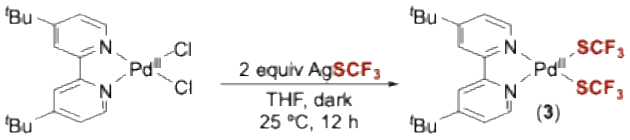
Complex 1-Br. In air, a 20 mL vial was charged with **1-Cl** (100 mg, 0.2 mmol, 1 equiv) and RbBr (98 mg, 0.6 mmol, 3 equiv), and the solids were then dissolved in THF or MeCN (5 mL). The vial was capped, and the reaction was stirred for 12 h at 25 ºC. This resulted in a yellow solution with a white precipitate, which was filtered through a plug celite, washing with THF. The solvent was removed under reduced pressure to yield a faint yellow solid (109 mg, 99% yield). Single crystals suitable for XRD were obtained by slow diffusion of hexane into THF solution of **1-Cl** at room temperature.

^{1}H NMR (600 MHz, CD_2Cl_2) δ 9.21 (d, *J* = 5.7 Hz, 1H), 8.03 (dd, *J* = 5.0, 2.0 Hz, 2H), 7.73 (d, *J* = 6.0 Hz, 1H), 7.58 (dd, *J* = 5.7, 1.9 Hz, 1H), 7.35-7.28 (multiple peaks, 3H), 6.86 (m, 2H), 1.44 (s, 9H), 1.39 (s, 9H). **^{13}C NMR** (126 MHz, CD_2Cl_2) δ 163.60 (d, *J* = 25.8 Hz), 160.85 (d, *J* = 238.9 Hz), 156.12, 153.69, 150.36, 149.90, 142.30 (d, *J* = 2.5 Hz), 135.79 (d, *J* = 5.6 Hz), 123.71, 123.62, 118.77, 118.15, 113.58, 113.43, 35.36, 35.35, 30.00, 29.84. **^{19}F NMR** (564 MHz, CD_2Cl_2) δ -123.56 (tt, *J* = 10.3, 6.2 Hz). **Elemental Analysis** calc'd C 52.43%; H 5.13%; N 5.10%. Found: C 52.37%; H 5.12%; N 5.17%.



Complex 2. In a N_2-filled glovebox, a 20 mL vial was charged with **1-I** (199 mg, 0.33 mmol, 1 equiv), $AgSCF_3$ (76.6 mg, 0.366 mmol, 1.1 equiv), THF (18 mL), and a stir bar. The vial was sealed and wrapped in electric tape to minimize exposure to light. The reaction was stirred overnight at 25 ºC. Under ambient air, the reaction mixture was filtered through a plug of Celite, washing with THF. It was then filtered through a plug of silica, washing with THF and DCM. The resulting yellow solution was concentrated under vacuum to form an oily solid that was purified by column chromatography with 15% EtOAc in hexane. The product was obtained as a light-yellow powder (143 mg, 76% yield). Single crystals suitable for single crystal XRD were obtained from by both slow diffusion of hexane into THF at room temperature and from precipitation from a solution of 15% EtOAc in hexane at room temperature.

^{1}H NMR (600 MHz, CD_2Cl_2) δ 9.14 (d, *J* = 5.7 Hz, 1H), 8.07 (m, 2H), 7.65 (d, *J* = 6.0 Hz, 1H), 7.63 (dd, *J* = 5.7, 1.9 Hz, 1H), 7.37-7.30 (multiple peaks, 3H), 6.88 (dd, *J* = 9.8, 8.5 Hz, 2H), 1.46 (s, 9H), 1.40 (s, 9H). **^{13}C NMR** (126 MHz, CD_2Cl_2) δ 164.16 (d, *J* = 1.2 Hz), 160.82 (d, *J* = 238.9 Hz), 155.93, 154.28, 150.36, 149.36, 144.60 (d, *J* = 2.6 Hz), 136.00 (d, *J* = 5.6 Hz), 136.00 (q, *J* = 303.0 Hz), 123.77, 123.68, 118.82, 118.55, 113.93, 113.78, 35.56, 35.53, 30.18, 30.03. **^{19}F NMR** (564 MHz, CD_2Cl_2) δ -21.41 (s, 3F), -123.27 (tt, *J* = 9.8, 6.4 Hz, 1F). **Elemental Analysis** calc'd C 52.59%; H 4.94%; N 4.91%. Found: C 52.58%; H 4.99%; N 4.98%.



In a N_2-filled glovebox, a 20 mL vial was charged with $AgSCF_3$ (98.6 mg, 0.47 mmol, 2.1 equiv). This vial was removed from the box and then charged with (dtbpy)Pd(Cl)$_2$[12] (100 mg, 0.23 mmol, 1 equiv). The solids were suspended in THF (5 mL), and the reaction was stirred for 30 min at room temperature, leading to a light-yellow solution with an off-white precipitate. This mixture was filtered through a plug of celite, washing with THF. The solvent was removed under reduced pressure, and the residue was recrystallized from 20% EtOAc in hexane to afford **3** as a light-yellow solid (126 mg, 97% yield). Single crystals suitable for XRD were obtained by slow diffusion of hexane into THF at room temperature or from precipitation from a solution of 20% EtOAc in hexane at room temperature.

^{1}H NMR (600 MHz, CD_2Cl_2) δ 9.45 (d, *J* = 6.0 Hz, 2H), 8.04 (d, *J* = 2.0 Hz, 2H), 7.67 (dd, *J* = 6.1, 2.0 Hz, 2H), 1.45 (s, 18H). **^{13}C NMR** (126 MHz, CD_2Cl_2) δ 165.62, 155.96, 150.05, 134.69 (q, *J* = 304.0 Hz), 124.06, 119.24, 35.76, 30.08. **^{19}F NMR** (564 MHz, CD_2Cl_2) δ -23.13. **Elemental Analysis** calc'd C 41.64%; H 4.19%; N 4.86%. Found: C 41.65%; H 4.38%; N 4.89%.

2.9.3 Transmetalation Studies

General Procedure I (for $AgSCF_3$, NMe_4SCF_3 and $CsSCF_3$). In a N_2-filled glovebox, a 4 mL vial was charged with a stir bar and $MSCF_3$ (3 equiv, 0.01 mmol). In a 4 mL vial, **1-X** (0.013 mmol) and trifluoromethoxybenzene (0.013 mmol) were dissolved in THF (2 mL). This stock

solution (0.5 mL) was added, and the reaction was stirred for the appropriate time (30 s, 200 s, or 600 s). Around 5 s before the end of each time, the reaction mixture was drawn into a syringe, a 0.22 micron syringe filter with a needle was attached to the syringe, and the mixture was filtered into an NMR tube. Because the salts are (mostly) insoluble, the reaction stops at this point. The sample was analyzed by ^{19}F NMR spectroscopy using 16 scans and 1 second relaxation delay, referencing to trimethoxybenzene (at -57.54 ppm).

Note: The Ag and Cs salts are not completely removed filtration. This impacts the chemical shifts, integrations, and peak shapes in the NMR spectra.

General Procedure 2 (for c_2CsSCF_3 and dtbpyCuSCF$_3$). In a N_2-filled glovebox, a 4 mL vial was charged with a stir bar, $MSCF_3$ (0.013 mmol), and THF (1 mL). In a 4 mL vial, **1-X** (0.013 mmol) and trifluoromethoxybenzene (0.013 mmol) were dissolved in THF (1 mL) and sealed with a Teflon-lined septum cap. To a screw-cap NMR tube was added 0.25 mL of the $MSCF_3$ solution. The NMR tube was sealed with a Teflon-lined septum cap, and this NMR tube along with the **1-X** stock solution were carried to the NMR spectrometer. 0.25 mL of the **1-X** stock solution was drawn up with a N_2-purged syringe and injected into the screw-cap NMR tube that was then immediately inserted into the NMR spectrometer. ^{19}F NMR spectra were acquired at 30 s, 300 s, and 600 s.

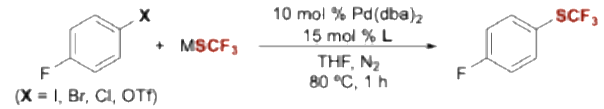
2.9.4 Ligand Substitution/Reductive Elimination

General Procedure for Time Studies: In a N_2-filled glovebox, a 0.01 M stock solution **2** and trifluoromethoxybenzene in THF was prepared and portioned into NMR tubes (0.5 mL per NMR tube). A ^{19}F NMR spectrum was acquired as a t = 0 measurement. A 0.03 M stock solution of ligand in THF was prepared. This solution (0.25 mL) was then added to the NMR tube. The NMR tube was heated at 80 ºC, and ^{19}F NMR spectra were acquired at t = 10, 60, 120, 360, 600, 1440, 4320, and 8640 min.

General Procedure for 24 h time point: In a N_2-filled glovebox, a 0.01 M stock solution **2** and trifluoromethoxybenzene in THF was prepared and portioned into NMR tubes (0.5 mL per NMR tube). A ^{19}F NMR spectrum was acquired as a t = 0 measurement. A 0.03 M stock solution of ligand in THF was prepared. This solution (0.25 mL) was then added to the NMR tube. The NMR tube was equilibrated at 25 ºC or 80 ºC, and a ^{19}F NMR spectrum was acquired at t = 24 h.

2.9.5 Optimization of Catalysis

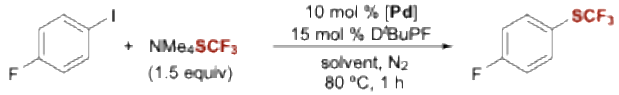
Table 2.S1. Optimization of [M] and Phosphine Ligand (L)



entry	$MSCF_3$[a]	ligand	X	yield (%)[b]
1	Ag	XantPhos	I	trace
2	Ag	XantPhos	Br	trace
3	Ag	XantPhos	Cl	0
4	Ag	XantPhos	OTf	0
5	Cs	XantPhos	I	91
6	Cs	XantPhos	Br	0
7	Cs	XantPhos	Cl	0
8	Cs	XantPhos	OTf	0
9	Cs	D^{t}BuPF	I	46
10	Cs	D^{t}BuPF	Br	17
11	Cs	D^{t}BuPF	Cl	0
12	Cs	D^{t}BuPF	OTf	trace
13	NMe_4	XantPhos	I	90
14	NMe_4	XantPhos	Br	15
15	NMe_4	XantPhos	Cl	0
16	NMe_4	XantPhos	OTf	86
17	NMe_4	^{t}BuPPF	I	72
18	NMe_4	BrettPhos	I	32
19	NMe_4	P^{t}Bu$_3$	I	22
20	NMe_4	P^{t}Bu$_2$Ph	I	6
21	NMe_4	D^{t}BuPF	I	99
22	NMe_4	D^{t}BuPF	Br	63
23	NMe_4	D^{t}BuPF	Cl	0
24	NMe_4	D^{t}BuPF	OTf	39
25	c2Cs	D^{t}BuPF	I	trace
26	dtbpyCu	D^{t}BuPF	I	8

[a] 1.5 equiv $MSCF_3$. [b]Yields determined by ^{19}F NMR spectroscopy.

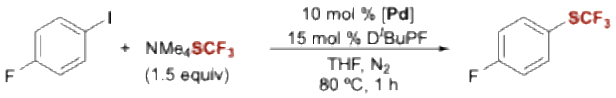
Table 2.S2. Optimization of Pd source, Reagent/Catalyst Loading, and Temperature



entry	SCF_3 loading (equiv)	Pd source	Pd loading (mol %)	solvent	ligand[b]	temp (°C)	time (h)	X	yield (%)[b]
1	1.5	$Pd(dba)_2$	10	THF	D'BuPF	80	1	I	99
2	1.3	$Pd(dba)_2$	10	THF	D'BuPF	80	1	I	99
3	1.1	$Pd(dba)_2$	10	THF	D'BuPF	80	1	I	99
4	1.0	$Pd(dba)_2$	10	THF	D'BuPF	80	1	I	46
11	1.5	$(COD)Pd(CH_2TMS)_2$	10	THF	D'BuPF	80	1	I	99
12	1.5	$(COD)Pd(CH_2TMS)_2$	10	THF	P'Bu$_3$	80	1	I	37
13	1.5	$(COD)Pd(CH_2TMS)_2$	10	THF	BrettPhos	80	1	I	91
14	1.5	$(COD)Pd(CH_2TMS)_2$	10	THF	XantPhos	80	1	I	99
5	1.5	$Pd(dba)_2$	4	THF	D'BuPF	80	1	I	97
6	1.5	$Pd(dba)_2$	1	THF	D'BuPF	80	1	I	55
7	1.5	$Pd(dba)_2$	1	dioxane	D'BuPF	110	2	I	56
8	1.5	$Pd(dba)_2$	4	dioxane	D'BuPF	110	1	Br	91
9	1.5	$Pd(dba)_2$	4	dioxane	D'BuPF	110	1	OTf	87
10	1.5	$Pd(dba)_2$	4	dioxane	XantPhos	80	1	I	92
11	1.5	$(COD)Pd(CH_2TMS)_2$	4	dioxane	D'BuPF	80	1	I	93
12	1.5	$(COD)Pd(CH_2TMS)_2$	4	dioxane	P'Bu$_3$	80	1	I	49
13	1.5	$(COD)Pd(CH_2TMS)_2$	4	dioxane	BrettPhos	80	1	I	88
14	1.5	$(COD)Pd(CH_2TMS)_2$	4	dioxane	XantPhos	80	1	I	95

[a] 1.5 equiv of ligand relative to [Pd]. [b] Yields determined by ^{19}F NMR spectroscopy.

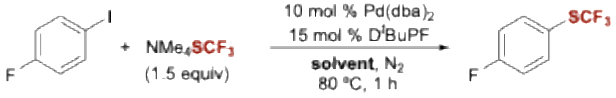
Table 2.S3. Optimization of Pd Source



entry	Pd source	yield (%)[a]
1	$Pd(dba)_2$	99
2	$Pd_2(dba)_3$	88
3	$Pd(OAc)_2$	49
4	$(COD)Pd(CH_2TMS)_2$	68
5	Buchwald G3	35
6	**1-I**	>109
7	**1-Br**	>109
8	**1-Cl**	>109
9	**2**	>109
10	**3**	54

[a] Yields determined by ^{19}F NMR spectroscopy.

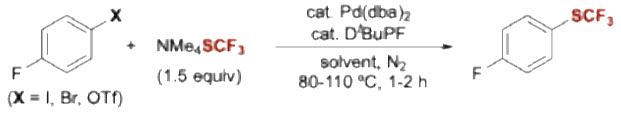
Table 2.S4. Optimization of Solvent



entry	solvent	yield (%)[a]
1	THF	99
2	MeCN	18
3	toluene	15
4	acetone	55
5	dioxane	99

[a] Yields determined by ^{19}F NMR spectroscopy.

Table 2.S5. Optimization of Time, Temperature, and Atmosphere



entry	Pd loading (mol %)[a]	solvent	temp (°C)	time (h)	atmosphere	halide	yield (%)[b]
1	10%	THF	80	1	N_2	Br	63
2	10%	THF	80	2	N_2	Br	87
3	10%	dioxane	80	1	N_2	I	99
4	10%	dioxane	110	1	N_2	Br	85
5	10%	dioxane	110	1	N_2	OTf	87
6	1%	dioxane	80	1	N_2	I	55
7	1%	dioxane	110	2	N_2	I	56
8	4%	dioxane	110	1	N_2	Br	91
9	4%	dioxane	110	1	N_2	OTf	87
10	10%	dioxane	80	1	air	I	3

[a]1.5 equiv of ligand relative to $Pd(dba)_2$. [b]Yields determined by ^{19}F NMR spectroscopy.

2.9.6 Synthesis of Organic Compounds

General Procedure A. In a N_2-filled glovebox, a vial was charged with 4 mol % of $Pd(dba)_2$, 6 mol % of D^{t}BuPF, 1.5 equiv of NMe_4SCF_3, 1 equiv of aryl halide, 1 equiv of trifluoromethoxybenzene (internal standard), and dioxane (0.2 M). The vial was capped, wrapped in electric tape, removed from the glovebox, placed in an 80 °C (iodide) or 110 °C (bromide, triflate) hotplate and stirred at 600 rpm for 2 h.

General Procedure B. In a N_2-filled glovebox, a vial was charged with 4 mol % of $Pd(dba)_2$, 6 mol % of D^{t}BuPF, 1.5 equiv of NMe_4SCF_3, 1 equiv of trifluoromethoxybenzene (internal standard), and dioxane (0.4 M relative to aryl halide). The vial was sealed with a septum cap, wrapped in electric tape, and removed from the glovebox. Outside the glovebox, 1 equiv of liquid aryl halide was added as a 0.4 M solution in dioxane. The vial was then placed in an 80 °C (iodide) or 110 °C (bromide, triflate) hotplate and stirred at 600 rpm for 2 h.

Workup Procedure. The vials were placed in a freezer for a few minutes to cool to room temperature. Small scale reactions (<1.0 mL) were filtered using a 0.45 micron syringe filter. Larger scale reactions were vacuum filtered through a plug of celite. The crude mixtures were then analyzed by ^{19}F NMR spectroscopy, with the trifluoromethoxybenzene set to -57.54 ppm. The filtered reaction mixtures were then concentrated under vacuum, and $ArSCF_3$ products were purified via column chromatography on silica gel.

2.9.7 Oxidative Studies

General Procedure for oxidative reaction: In a nitrogen filled glovebox, a 20 mL vial was charged with **2**, 2-fluorobiphenyl, and MeCN (1 mL). An aliquot of this solution (~0.4 mL) was added to an NMR tube. The NMR tube was sealed and removed from the glovebox, and an 19F NMR spectrum was obtained to determine the ratio of the complex to internal standard. The NMR sample was brought back into the box and combined with the original solution. In a 4 mL vial, oxidant was dissolved in MeCN 0.5 mL. The solution of the complex
and internal standard was added dropwise to the solution of oxidant. The resulting mixture was shaken for 15 s, then allowed to stand for 20 min. A ^{19}F NMR spectrum was acquired.

2.9.8 Photochemical Studies

General Procedure for photochemical reaction: In a N_2-filled glovebox or in air, a clear 4mL vial was charged with **2**, an ^{19}F NMR standard ($PhOCF_3$), a stir bar, and 1mL of MeCN. The vial was capped, sealed, and placed in a Kessil photobox was two 370 nm Kessil lamps at 100% and the photobox fan on to stir for 4 hours. An ^{19}F NMR was acquired.

2.10 References

1. (a) Purser, S.; Moore, P. R.; Swallow, S.; Gouverneur, V. Fluorine in medicinal chemistry. *Chem. Soc. Rev.* **2008**, *37*, 320-330. (b) Jeschke, P. Recent developments in fluorine-containing pesticides. *Pest Mgmt. Sci.* **2023**, *80*, 3065-3087.

2. (a) Hansch, C.; Leo, A.; Unger, S. H.; Kim, K. H.; Nikiaitani, D.; Lien, E. J. Aromatic substituent constants for structure-activity correlations. *J. Med. Chem.* **1973**, *16*, 1207-1216. (b) Leroux, F.; Jeschke, P.; Schlosser, M. α-Fluorinated ethers, thioethers, and amines: Anomerically biased species. *Chem. Rev.* **2005**, *105*, 827-856. (c) Leroux, F. R.; Manteau, B.; Vors, J-P.; Pazenok, S. Trifluoromethyl ethers – Synthesis and properties of an unusual substituent. *Beilstein J. Org. Chem.* **2008**, *4*, DOI: 10.3762/bjoc.4.13. (d) Xu, X.-H.; Matsuzaki, K.; Shibata, N. Synthetic methods for compounds having CF_3–S units on carbon by trifluoromethylation, trifluoromethylthiolation, triflylation, and related reactions. *Chem. Rev.* **2014**, *115*, 731-764. (e) Xiong, H.-Y.; Pannecoucke, X.; Besset, T. Recent advances in the synthesis of SCF_2H- and SCF_2FG-containing molecules. *Chem. Eur. J.* **2016**, *22*, 16734-16749. (f) Hardy, M. A.; Chachignon, H.; Cahard, D. Advances in asymmetric di-and trifluoromethylthiolation, and di- and trifluoromethoxylation Reactions. *Asian J. Org. Chem.* **2019**, *8*, 591-609.

3. (a) Erickson, B. E. EU proposal would ban 10,000 PFAS. *Chem. Eng. News* **2023**, *101*. (b) Tiedje, J. M.; et. al. Emerging contaminants: A one health perspective. *The Innovation* **2024**, *5*, 100612.

4. Zheng, H.; Huang, Y.; Weng, Z. Recent advances in trifluoromethylthiolation using nucleophilic trifluoromethylthiolating reagents. *Tetrahedron Lett.* **2016**, 57, 1397-1409.

5. For examples of Ni-catalyzed aryl-trifluoromethylthiolation, see: (a) Zhang, C-P.; Vicic, D. A. Nickel-catalyzed synthesis of aryl trifluoromethyl sulfides at room temperature. *J. Am. Chem. Soc.* **2012**, *134*, 183-185. (b) Yin, G.; Kalvert, I.; Englert, U.; Schoenebeck, F. Fundamental studies and development of nickel-catalyzed trifluoromethylthiolation of aryl chlorides: Active catalytic species and key roles of ligand and traceless MeCN additive revealed. *J. Am. Chem. Soc.* **2015**, *137*, 4164-4172. (c) Durr, A.; Yin, G.; Kalvet, I.; Napoly, F.; Schoenebeck, F. Nickel-catalyzed trifluoromethylthiolation of Csp^2-O bonds. *Chem. Sci.*, **2016,** 7, 1076-1081. (d) Gravatt, C. S.; Johannes, J. W.; King, E. R.; Ghosh, A. Photoredox-mediated, nickel-catalyzed trifluoromethylthiolation of aryl and heteroaryl iodides. *J. Org. Chem.* **2022**, *87*, 8921-8927.

6. For examples of Group 11-mediated aryl-trifluoromethylthiolation, see: (a) Weng, Z.; He, W.; Chen, C.; Lee, R.; Tan, D.; Lai, Z.; Kong, D.; Yuan, Y.; Huang. K. An air-stable copper reagent for nucleophilic trifluoromethylthiolation of aryl halides. *Angew. Chem. Int. Ed.* **2012**, *52*, 1548-1552. (b) Tran, L. D.; Popov, I.; Daugulis, O. Copper-promoted sulfenylation of sp^2 C–H bonds. *J. Am. Chem. Soc.* **2012**, *134*, 18237-18240. (c) Zhang, C-P.; Vicic, D. Oxidative Trifluoromethylthiolations of aryl boronic acids using a copper/O_2-based protocol. *Chem. Asian J.*, **2012**, 7. 1756-1758 (d) Yang, Y.; Xu, L.; Yu, S.; Liu, X.; Zhang, Y.; Vicic, D. A. Triphenylphosphine-mediated deoxygenative reduction of CF_3SO_2Na and its application for trifluoromethylthiolation of aryl iodides. *Chem. Eur. J.* **2015**, *22*, 858-863. (e) Mudshinge, S.; Yang, Y.; Xu, B.; Hammond, G. B.; Lu, Z. Gold (I/III)-catalyzed trifluoromethylthiolation and trifluoromethylselenolation of organohalides. *Angew. Chem., Int. Ed*. **2022**, *61*, e202115687.

7. Co-catalyzed aryl-trifluoromethylthiolation: Lopez-Resano, S.; Martinez de Salinas, S.; Garces-Pineda, F. A.; Moneo-Corcuera, A.; Galan-Mascaros, J. R.; Maseras, F.; Perez-Temprano, M. H. Redefining the mechanistic scenario of carbon−sulfur nucleophilic coupling via high-valent Cp^*Co^{IV} species. *Angew. Chem., Int. Ed.* **2021**, *60*, 11217-11221.

8. For examples of free radical and electrophilic aryl-trifluoromethylthiolation, see: (a) Guyon, H.; Chachignon, H.; Cahard, D. CF_3SO_2X (X = Na, Cl) as reagents for trifluoromethylation, trifluoromethylsulfenyl-, -sulfinyl- and -sulfonylation. Part 1: Use of CF_3SO_2Na. *Beilstein J. Org. Chem.* **2017***, 13,* 2764-2799. (b) Shao, X.; Xu, C.; Lu, L.; Shen, Q. Shelf-stable electrophilic reagents for trifluoromethylthiolations. *Acc. Chem. Res*. **2015**, 48, 1227-1236. (c) Barata-Vallejo, S.; Bonsei, S.; Postigo, A. Late stage trifluoromethylthiolation strategies for organic compounds. *Org. Biomol. Chem.* **2016**, *14*, 7150-7182. (c) Xu, W.; Wang, W.; Liu, T.; Xie, J.; Zhu, C. Late-stage trifluoromethylthiolation of benzylic C–H bonds. *Nature Commun.* **2019**, *10*, 4867. (d) Shen, Q. A toolbox of reagents for trifluoromethylthiolation: from serendipitous findings to rational design. *J. Org. Chem*. **2023**, 88, 3359-3371.

9. Teverovskiy, G.; Surry, D. S.; Buchwald, S. L. Pd-catalyzed synthesis of $ArSCF_3$ compounds under mild conditions. *Angew. Chem., Int. Ed.* **2011**, *50*, 7312-7314.

10. Yin, G.; Kalvet, I.; Schoenebeck, F. Trifluoromethylthiolation of aryl iodides and bromides enabled by a bench-stable and easy-to-recover dinuclear palladium(I) catalyst. *Angew. Chem., Int. Ed.* **2015**, *54*, 6809-6813.

11. Zhang, B.; Yan, X.; Guo, S. Synthesis of Well-Defined High-Valent Palladium Complexes by Oxidation of Their Palladium(II) Precursors. *Chem. Eur. J.* **2020**, 26, 9430-9444

12. Ball, N. D.; Kampf, J. W.; Sanford, M. S. Aryl−CF_3 bond-forming reductive elimination from palladium(IV). *J. Am. Chem. Soc*. **2010**, *132*, 2878-2879.

13. Rio, J.; Liang, H.; Perrin, M-E. L.; Perego, L. A.; Grimaud, L.; Payrd, P-A. We already know everything about oxidative addition to Pd(0): Do we? *ACS Catal*. **2023**, 13, 11399-11421.

14. Tyrra, W.; Naumann, D.; Hoge, B.; Yaguploskii, Y. L. A new synthesis of trifluoromethanethiolates—Characterization and properties of tetramethylammonium, cesium, and di(benzo-15-crown-5)cesium trifluoromethanethiolates. *J. Fluorine Chem.* **2003**, *119*, 101-107.

15. Ferguson, D. M.; Bour, J. R.; Canty, J. W.; Sanford, M. S. Stoichiometric and catalytic aryl-perfluoroalkyl coupling at tri-*tert*-butylphosphine palladium(II) complexes. *J. Am. Chem. Soc.* **2017**, 139, 34, 11662-11665.

16. Ferguson, D. M.; Bour, J. R.; Canty, A. J.; Kampf, J. W.; Sanford, M. S. Aryl–CF_3 coupling from phosphinoferrocene-ligated palladium(II) complexes. *Organometallics* **2019**, *38*, 519-526.

17. (a) Grushin, V. V.; Marshall, W. J. Facile Ar−CF_3 bond formation at Pd. Strikingly different outcomes of reductive elimination from [$(Ph_3P)_2Pd(CF_3)Ph$] and [(Xantphos)Pd(CF_3)Ph]. *J. Am. Chem. Soc.* **2006**, *128*, 12644-12645. (b) Keaveney, S. T.; Schoenebeck, F. Palladium-catalyzed decarbonylative trifluoromethylation of acid fluorides. *Angew. Chem. Int. Ed.* **2018**, *57*, 4073-4077.

18. (a) Amatore, C.; Broeker, G.; Jutand, A.; Khalil, F. Identification of the effective palladium(0) catalytic species generated *in situ* from mixtures of $Pd(dba)_2$ and bidentate phosphine ligands. Determination of their rates and mechanism in oxidative addition. *J. Am. Chem. Soc.* **1997**, *119*, 5176-5185. (b) Biscoe, M. R.; Fors, B. P.; Buchwald, S. L. A new class of easily activated palladium precatalysts for facile C–N cross-coupling reactions and the low temperature oxidative addition of aryl chlorides. *J. Am. Chem. Soc.* **2008**, *130*, 6686-6687.

19. Complex **2** also serves as a viable pre-catalyst with Xantphos and D^{t}BuPF (affording quantitative yield in both cases), with the added advantage that it is air and moisture stable.

20. Chan, Y. A.; Perry, I. B.; Bissonnette, N. B.; Buksh, B. F.; Edwards, G. A.; Frye, L. I.; Garry, O. L.; Lavagnino, M. N.; Li, B. X.; Liang, Y.; Mao, E.; Millet, A.; Oakley, J. V.; Reed, N. L.; Sakai, H. A.; Seath. C. P.; MacMillan, D. W. C. Metallaphotoredox: The Merger of Photoredox and Transition Metal Catalysis. *Chem. Rev*. **2022**, 122, 1485-1542

Chapter 3 Organometallic Investigations into Palladium-Mediated Aryl-Sulfinate Coupling

3.1 Background

Aryl sulfones represent an underutilized functional group in the fields of medicinal and agricultural chemistry. While more abundant than their reduced cousin, the sulfoxide, sulfones are dwarfed in their presence in pharmaceuticals and agrochemicals by their fully reduced analogue, the sulfide.[1] In comparison to sulfides, sulfones are significantly more electron withdrawing. Additionally, sulfones are tetrahedral, thus projecting in 3D space and impeding pi-stacking interactions that can adversely affect solubility. Depending on the organic substituents on the sulfone, the oxygen atoms can also act as H-bond acceptors, thus broadening the range of potential enzyme or receptor interactions.[2]

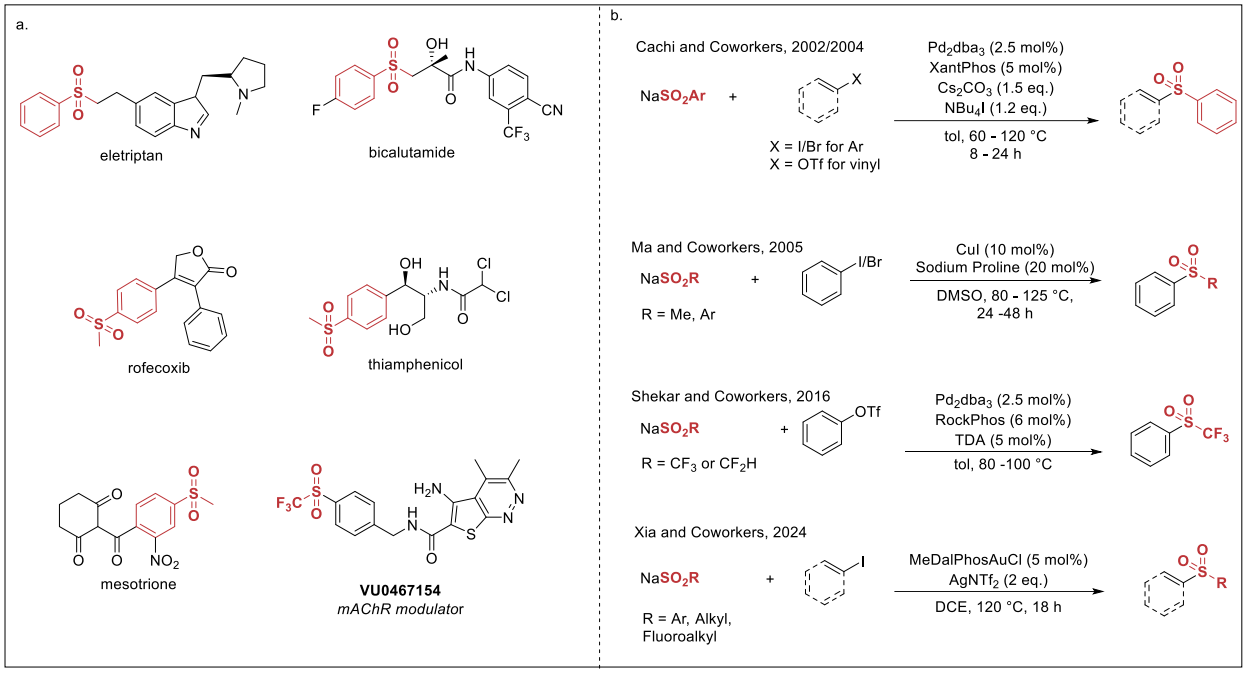


Figure 3.1. a. Examples of C_{sp2}-Sulfones in molecules. b. Methods of synthesizing C_{sp2}-sulfones[4-7]

Traditionally, sulfone functional groups are synthesized by first forming the sulfide, then exhaustively oxidizing the sulfur.[3] However, this method exhibits poor functional group compatibility and limits the possibility of late-stage functionalization. Since 2004, there have been just four transition metal catalyzed methods reported to achieve C_{sp2}-SO_2R coupling, **Figure 3.1.b**.[4-7] Among these, two involve palladium-based catalysts, and two involve group 11 metals (see Chapter 4 for further discussion of these transformations). While impressive, none of these methods are general with respect to sulfinate or electrophile scope. Despite these clear gaps in the literature, in the past 22 years there has been a startling lack of advancement in this area, both in new methods development or in mechanistic understanding of the challenges associated with these transformations. Unlike the sulfide chemistry, there is not an obvious trend where the most electron-deficient sulfinate is the most difficult to couple. Based on our studies in Chapter 2 using organometallic complexes to probe elementary steps of a Pd(II) catalytic system, we sought to use a similar approach to tackle C_{sp2}-SO_2R coupling at Pd.

We initially hypothesized that the dearth of $Pd^{0/II}$-catalyzed methodologies for C_{sp2}-SO_2R cross-coupling stems from a confluence of properties of sulfinates and palladium species that make developing competent catalytic systems a delicate balancing act. While the overall mechanism for the two known methods – by Cachi and Shekar – is likely similar (**Figure 3.2.a**), the differences in electrophile and nucleophile scope likely stem from ligand effects, with Shekar using Rockphos and Cachi using XantPhos. Additionally, we initially reasoned that reductive elimination was the rate-limiting step, thus restricting the usable ligand set for these transformations. Overall, our initial goal for this project was to synthesize (dtbpy)Pd(*p*-F-Ph)(SO_2R) complexes and evaluate several classes of ligands for reductive elimination to help guide the development of a general catalytic system for C_{sp2}-SO_2R bond formation from C_{sp2}-halides and metal sulfinate salts, **Figure 3.2.b**

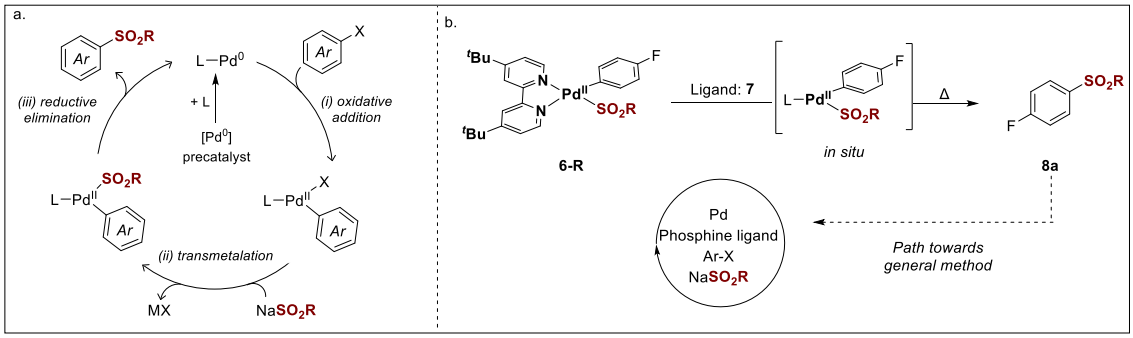


Figure 3.2. (a) Proposed $Pd^{0?II}$ catalytic cycle for C_{sp2}-SO_2R coupling. (b) Initial goal for this project

3.2 Synthesis and Characterization of (4,4'-di-tert-butyl-2,2'-bipyridine) Palladium (*p*-fluorophenyl)(SO_2R) Complexes, R = CF_3, CF_2H, CFH_2, CH_3, and *para*-tolyl

In comparison to the trifluoromethylthiolate salts discussed in Chapter 2, the sulfinates are much more stable and commercially available. All commercially available sulfinates are purchasable as a sodium salt, the CF_3 derivative is also available as a potassium salt, while the CF_3, CF_2H, and ^{i}Pr substituents can be obtained from commercial sources as zinc salts. The aryl and fluoroalkyl sulfinate salts are air-stable, while the alkyl sulfinates undergo oxidation to the sulfonate salt upon extended exposure to air. Most of these MSO_2R salts are insoluble in non-polar organic solvents, although THF does dissolve $NaSO_2CF_3$ and $NaSO_2CF_2H$.

The treatment of **1-I** with $NaSO_2CF_3$ afforded **6-CF$_3$** in low (<20%) yield. The conversion does not increase significantly with increased equivalents of the sulfinate salt. However, the addition of 1.1 equiv of $AgBF_4$, $AgPF_6$, AgOTf, or Ag_2CO_3 drove this reaction to full conversion by abstracting the iodide and formation of a cationic palladium species with an open site for the sulfinate to coordinate. **6-CF$_3$** was isolated in 48% yield after purification by column chromatography on silica gel with 20% ethyl acetate in hexane as the eluant. Single crystals were obtained via slow diffusion of hexane into a THF solution of **6-CF$_3$**. The x-ray crystal structure of this complex reveals that the sulfinate is bound to Pd^{II} through the sulfur atom.

The observation of incomplete transmetallation with **1-I** is similar what was observed in Chapter 2 with $CsSCF_3$ and $CuSCF_3$. In those systems, **1-Cl** showed much more efficient transmetallation with all of the SCF_3 salts, so we sought to employ it in this study. The reaction of **2-Cl** with 2 equiv of $NaSO_2CF_3$ resulted in full consumption of the starting complex after 15 h at

ambient temperature in THF. Performing this reaction in dichloromethane, where both $NaSO_2CF_3$ and the resulting NaCl are insoluble but the Pd complexes are soluble, was similarly effective, and the residual salts were removed using a celite filter or syringe filter. Evaporation of the solvent from the filtrate afforded **6-CF$_3$** in 84% yield. This product was clean and did not require further purification via column chromatography. This procedure was successfully applied to prepare **6-CF$_2$H**, **6-CFH$_2$**, **6-CH$_3$**, and **6-*p*-tol**.

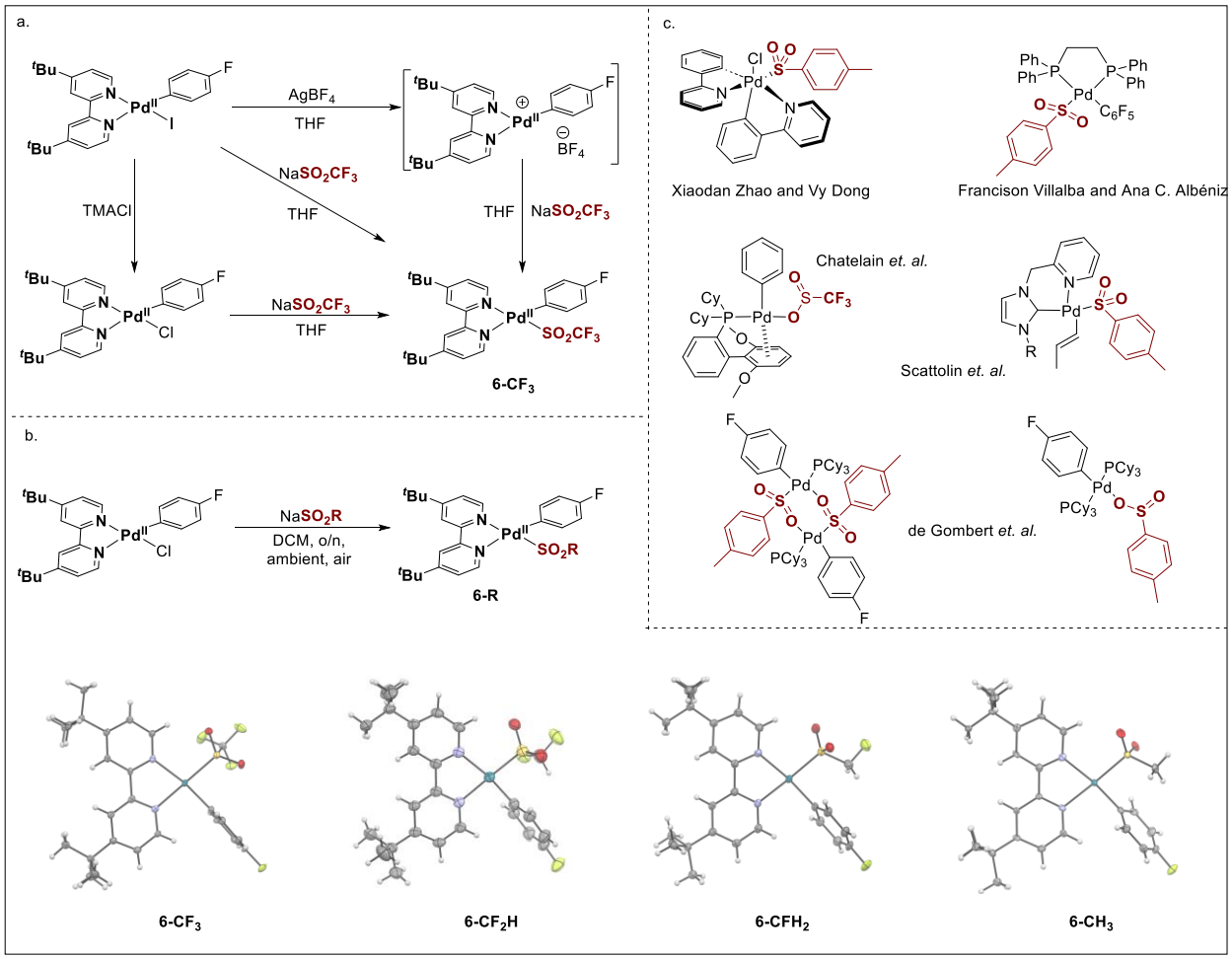


Figure 3.3. (a) Reaction of **1-I** and **1-Cl** with $NaSO_2CF_3$. (b) Synthesis of Pd(II)-SO_2R complexes with x-ray structures. (c) Literature reports of organometallic palladium sulfinate complexes.

All of the complexes **6-R** have the sulfinate ligand bound to palladium though sulfur. S-binding is well-precedented in the literature for palladium-sulfinate complexes. Within the Cambridge Crystallographic Data Centre, there are six examples of organometallic complexes containing a palladium-(SO_2) bond. Four of them (all with -SO_2*p*-tol) have the sulfinate bound

through the sulfur atom, and these are ligated with mono[8]- or bidentate[9] phosphines, a bidentate NHC-pyridine[10], or two cyclometalated phenylpyridine ligands[11]. In contrast, two complexes contain O-bound sulfinates – one with SPhos as the ligand[12] and SO_2CF_3 as the sulfinate and one with a bridging SO_2*p*-tol and PCy_3 as the supporting ligand.[8] The two structures from de Gombert et al are synthesized from the transmetallation of a sulfinate salt onto a palladium center. The Pd(IV) complex is formed via the addition of a strong $ClSO_2$*p*-tol electrophile to a Pd(II) complex. The remaining three of these are formed by the oxidative addition of palladium into a C_{sp2}-S(O_2) bond The underlying mechanism of what determines O-bound vs. S-bound in this system is not well understood, as several different ligands, sulfinates, and synthetic pathways led to different binding modes.

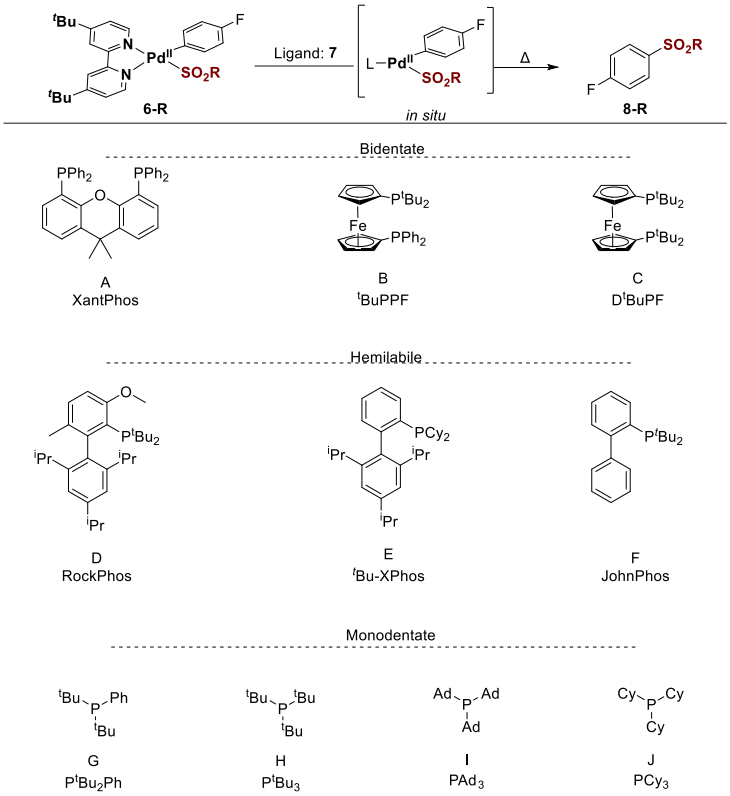
3.3 *in situ* Phosphine Ligand Substitution and Reductive Elimination of (dtbpy)Pd(*p*-fluorophenyl)(SO_2R) Complexes

We next evaluated the effect of ligand on C_{sp2}-SO_2R bond-forming reductive elimination from complex **6-SO_2R**. Because we are investigating five different sulfinates and the prior literature methodologies have demonstrated that there are significant differences in the behavior of the sulfinates, we sought to investigate a wide range of ligand classes, as well as a significant sampling of ligand within each of these classes. We employed the same *in situ* ligand assay developed in Chapter 2 to perform a combinatorial screen.

Ligand selection was guided by (i) the literature reports of C_{sp2}-SO_2R coupling and (ii) the successful ligands from the SCF_3 chemistry in Chapter 2. Bulky bidentate phosphine ligands, Buchwald-type phosphine ligands, and monodentate phosphine ligands were chosen, as shown in **Table 3.1**. These classes provide a continuum of mono- and bidentate ligands, where the hemilabile Buchwald ligands can be both mono- and bidentate. Additionally, D^{t}BuPF can also act as a monodentate ligand with a hemilabile group, according to ^{31}P NMR observations in a related system.[13]

Screening was conducted by reacting **6-R** with 2 equiv of ligand in toluene at 120 ºC. Toluene was chosen because it is the solvent in both the Cachi and Shekar reports. All ligands led to a color change upon addition, suggesting that ligand substitution is occurring. Additionally, the formation of palladium black was observed in all of the reaction vessels, indicating that the Pd is reduced. However, overall reductive elimination to form C_{sp2}-SO_2R proved to be extremely difficult. **6-*p*tol** was by far the most productive complex. **7A** gave **8-*p*tol** in quantitative yields, as

expected because it is the operative ligand in the Cachi catalysis. **7B** and **7C** gave moderate yields, but clearly lower. This data is in contrast to results from Chapter 2 where all three of these ligands gave **4a** in high yields from the analogous study. Bulky monodentate phosphines **7H** and **7I** also gave the organic product in high yields, 67% and 83% respectively. The Buchwald ligands, **D-F**, gave very low yields (0-4%). However there seems to be a trend of increasing yields as the Buchwald ligands trends towards true monodentate ligands (from **7F** to **7G**).

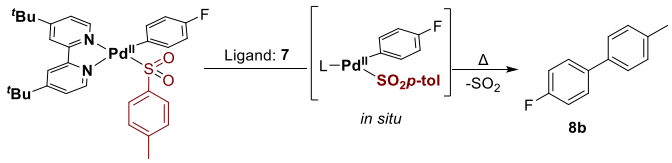


Ligand, 7	8a-CF_3	8a-CF_2H	8a-CFH_2	8a-CH_3	8a-*p*-tol
A	0	6	26	59	>99%
B	0	7	43	65	33
C	0	3	10	7	22
D	2	<1	0	0	0
E	3	2	2	<1	<1
F	4	11	4	2	4
G	1	9	7	<1	18
H	13	29	15	5	67
I	31	63	44	6	83
J	0	0	0	0	<1

Table 3.1. Yields of ligand screening assay, grouped by ligand class. Yields determined by ^{19}F NMR spectroscopy.

For the series of C_{sp3} sulfinates (R = CH_3, CFH_2, CF_2H, and CF_3), no obvious trends are observed. XantPhos (**7A**), the ligand used in the Cachi catalysis with $NaSO_2$*p*-tol, promoted reductive elimination with SO_2CH_3 and SO_2CFH_2 with 59% and 27% yield, respectively. However, SO_2CHF_2 and SO_2CF_3 gave low yields of 6% and <1% with this ligand. A similar trend was observed for ^{t}BuPPF (**7B**), although the yields were slightly higher across-the-board (65%, 43%, 7%, and <1%, respectively). The bulky monodentate ligands P(*t*-Bu)$_3$ (**7H**) and PAd_3 (**7I**) showed the opposite trend, affording moderate to good yields with the fluorinated sulfinates. For instance, P(*t*-Bu)$_3$ gave 13%, 29%, and 15% yield for SO_2CF_3, SO_2CHF_2, and SO_2CH_2F, respectively, while PAd_3 afforded even higher yields of 31%, 63%, and 44% yield for this same series. In contrast, both were barely effective for the non-fluorinate sulfinate SO_2CH_3 (5% and 6% yield, respectively). Finally, and unexpectedly, the Buchwald ligands (**7D-F**) were almost completely ineffective at promoting any of these C_{sp2}-SO_2R bond forming reductive elimination reactions (≤11% yield for all SO_2R groups). This is in stark contrast to Shekar's catalytic system, where RockPhos (**7D**) was a uniquely effective ligand for Pd-catalyzed coupling of aryl triflates with $NaSO_2CF_3$ and $NaSO_2CF_2H$.

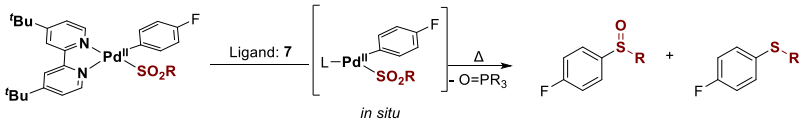
The byproducts of these reactions were investigated to better understand the mass balance. Firstly, **6-*p*tol** promoted desulfinylation of the sulfinate with all ligands, **Table 3.2**. This organic product was the major remainder of the mass balance for that ligand screen. The bidentate ligands **7B** and **7C** yielded **8b** in 61% and 77% yield, respectively. The bidentate ligands (**7A-C**) essentially gave quantitative yield of coupling products and only diverge in product distribution. The Buchwald ligands gave the lowest yields of **8b**, 16%, 20%, 9%, but there is no obvious trend. The non-bulky monodentate phosphines, **7G**, and **7J** gave very high yields of this product at 68% and 80% respectively, while the bulky monodentate phosphine ligands, **7H** and **7I**, gave moderate yields, 32% and 19%, respectively. This result is not anticipated based on precedent from de Gombert et al.[8] Surprisingly, **6-*p*tol** forms **8b** in 14% yield when stirred in toluene for 12 h at 120 °C with no ligand. The rest of the mass balance is 42% fluorobenzene and 41% (when calculated based on aryl group, instead of entire molecule) of 4,4'-difluorobiphenyl.



7X	A	B	C	D	E	F	G	H	I	J
Yield%	0	61	77	16	20	9	68	32	17	80

Table 3.2. Desulfinylation and coupling of **8-*p*tol**. Yields determined by ^{19}F NMR spectroscopy

Sulfoxide (Ar-SOR) and sulfide (Ar-SR) products derived from deoxygenation are the major observable byproducts. Separate control studies show that **8a-R** does not deoxygenate in the presence of phosphine with palladium, so the deoxygenation occurs before the coupling. The bidentate ligands **A-C** afford minimal (≤3%) deoxygenation for all of the sulfinate salts. The Buchwald ligands **D-F** yield minimal (≤1%) deoxygenation of the electron rich sulfinates; however, the SO_2CF_3 gives up to 5% deoxygenation, with JohnPhos giving the largest amount. In contrast, the monodentate phosphines afford significant quantities of deoxygenation products, particularly with electron deficient sulfinates. This issue is most prominent with P(*t*-Bu)$_2$Ph (which, for example, gives 68% combined yield of the deoxygenated products with $NaSO_2CF_3$) and PCy_3 (which gives 87% combined yield of the deoxygenated products with $NaSO_2CFH_2$). Other byproducts that are observed in all of the sulfinates are fluorobenzene and 4,4'-difluoro biphenyl. With **6-CF$_3$**, trifluormethylation of toluene is also a significant side reaction from competing desulfinylation of the SO_2CF_3. The 4-fluoro acyl fluoride is also detected in this system, likely through α-fluoride elimination and carbene insertion into the aryl group, which later hydrolyzes after exposure to ambient atmosphere



Ligand, 7	8a-CF_3	8a-CF_2H	8a-CFH_2	8a-CH_3	8a-*p*-tol
A	0	0	0	0	0
B	0	0	0	0	0
C	0	<1	<1	3	0
D	1	<1	<1	<1	0
E	3	<1	<1	0	0
F	5	<1	<1	0	2
G	68	21	46	<1	0
H	23	6	5	6	0
I	6	3	11	0	0
J	0	0	87	<1	5

Table 3.3. Total deoxygenation considers each oxygen removed in the product(2 * sulfide% + sulfoxide%) of sulfinate complexes. Yields determined by ^{19}F NMR spectroscopy.

Considering the reductive elimination results in Table 3.1, the data for RockPhos is particularly unexpected. This is a uniquely effective ligand in catalysis with both $NaSO_2CF_3$ and $NaSO_2CF_2H$ (*vida infra)*. However, in the stoichiometric studies, RockPhos yields only traces of the sulfone product. To explain this, we hypothesized that the RockPhos might need to be modified *in situ* in order to promote the key C_{sp2}–SO_2R_F coupling step. Buchwald has shown that this type of *in situ* modification is required for C_{sp2}–F bond-forming reductive elimination, where ^{t}BuBrettPhos and RockPhos undergoes initial arylation at the *meta* position of the pendant aryl group, **Figure 3.6**. This modified ligand is then competent in the catalysis and for promoting stoichiometric C_{sp2}–F coupling.[14,15] To preliminarily test whether a similar modification is occurring in the current transformation, high resolution electrospray ionization mass spectrometry analysis was performed at the completion of (1) the stoichiometric reductive elimination with RockPhos and (2) the Pd/RockPhos catalysis reaction using 4-fluorophenyl triflate and $NaSO_2CF_3$. As shown in **Figure 3.4**, a mass consistent with the 4-fluorophenyl arylated RockPhos (**7-K**, m/z = 563.3845) was detected.

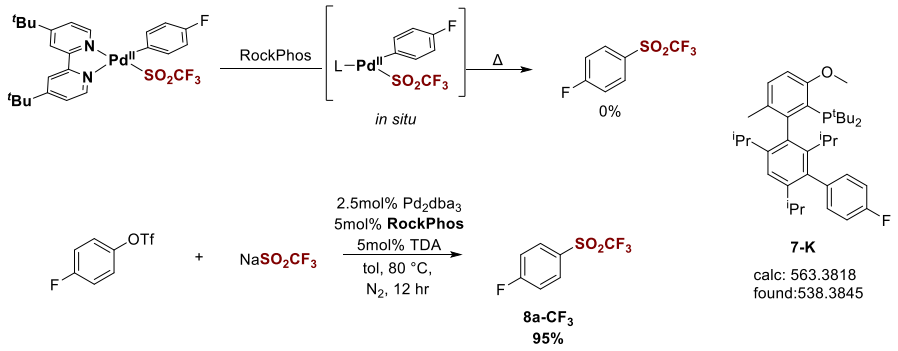


Figure 3.4. Identification of arylated RockPhos (**7-K)** from stoichiometric and catalytic reactions

We next designed a "cross-over" experiment aimed to test (i) whether the formation of **7-K** is the primary reactivity in the stoichiometric reaction as well as (ii) whether **7-K** is the key ligand involved in for catalysis. In this experiment, an aryl electrophile bearing a 4-trifluoromethyl substituent was added to the stoichiometric reductive elimination reaction. If the ligand is compatible with both reductive elimination and catalysis, we expect that two different $ArSO_2R$ products will be formed – 4-fluorophenyl–SO_2R (derived from the Pd(II) starting material) and 4-trifluoromethyl–SO_2R (derived from the electrophile). If the ligand is only effective for stoichiometric reductive elimination, then only 4-fluorophenyl–SO_2R will be generated. This

experiment was first validated by using **6-*p*-tol** with 2 equiv of XantPhos (**7A**), 1 equiv of 4-trifluoromethylphenyl iodide, and 1 equiv of $NaSO_2$*p*-tol, **Figure 3.5**. Importantly, the stoichiometric reductive elimination is facile in this system (see Table 3.1) and catalytic coupling of ArI with $NaSO_2$*p*-tol has been established by Cachi. Thus, as expected, "cross-over" was observed, with 4-fluorophenyl–SO_2*p*-tol (the initial reductive elimination product) formed in 92% yield and 4-trifluoromethylphenyl–SO_2*p*-tol (the catalytic coupling product) generated in 41% yield.

The same experiment was next conducted with **6-CF_3** and 2 equiv of RockPhos (**7D**), using 1 equiv of 4-trifluoromethylphenyl triflate and 1 equiv of $NaSO_2CF_3$. In this case, <1% of **8a-CF_3** was detected, consistent with our previous studies in Table 3.1. However, the "cross-over" product **8b-CF_3** was formed in 61% yield. Furthermore, masses indicative of RockPhos arylated with both a 4-fluorophenyl group (**7-K**) and a 4-trifluoromethyl group (**7-L**) were observed by ESI-MS. This same experiment was repeated with 4-trifluoromethyl-phenyl iodide, an electrophile that is not effective in the reported catalytic transformation. In this case, no **8a-CF_3** was formed. However, unexpectedly, **8c-CF_3** was generated in 4% yield. While this yield is low, it represents the first example of palladium-mediated cross-coupling between an aryl iodide and $NaSO_2CF_3$. Following the success of accessing a new electrophile, a modified version of this experment was conducted. **6-CF_3**, 2 equiv of RockPhos (**7D**), 1 equiv of 4-trifluoromethylphenyl triflate and 1 equiv of $NaSO_2CH_3$, a sulfinate that is ineffective in catalysis, were subjected to reaction conditions. Here, we again observe 0% **8a-CF_3,** but we observe 40% **8c-CH_3**. This is the first time a palladium reaction has coupled $NaSO_2CH_3$ with an aryl group!

This result informs us that **7** is not competent in reductive elimination under these conditions but instead becomes arylated. This arylated ligand is then activated for coupling with the exogenous aryl electrophile or sulfinate nucleophile. Following this result, we designed an experiment to test this hypothesis within the literature conditions. First, the RockPhos catalyzed reaction reported by Shekar and coworkers was conducted with 4-fluoro-phenyl triflate and $NaSO_2CF_3$. After the reaction was complete, the reaction vial was taken back into the glovebox and the entire contents were added to a vial containing 4-trifluoromethyl phenyl iodide and $NaSO_2CF_3$ and this mixture was subjected to the reaction conditions. In this case, **8a-CF_3** was formed in quantitative yields but **8c-CF_3** was not observed. We hypothesize that even with this activated ligand, transmetallation is still difficult with iodides and SO_2CF_3 anions, especially at on

80 °C. This experiment was repeated with $NaSO_2CH_3$ as the second nucleophile and 4-trifluoromethyl phenyl triflate as the second electrophile. Here we again observed **8a-CF₃** in quantitative yields, but this time there is 3% coupling with the previously ineffective $NaSO_2CH_3$ nucleophile. These results in totality show that arylation of RockPhos occurs before productive reactions and also that the modified ligand promotes the cross coupling of aryl electrophile partners with $NaSO_2CF_3$ and aryl triflates with $NaSO_2CH_3$. Certain aryl halides and certain nucleophiles are not capable of performing this arylation, thus are not competent in cross-coupling, but if the modified ligand is added, then the aryl halide becomes active. We hypothesis that the ionic character of the solution heavily influences the arylation, and that is the general reason why certain sulfinates and certain halides (after oxidative addition) are ineffective.

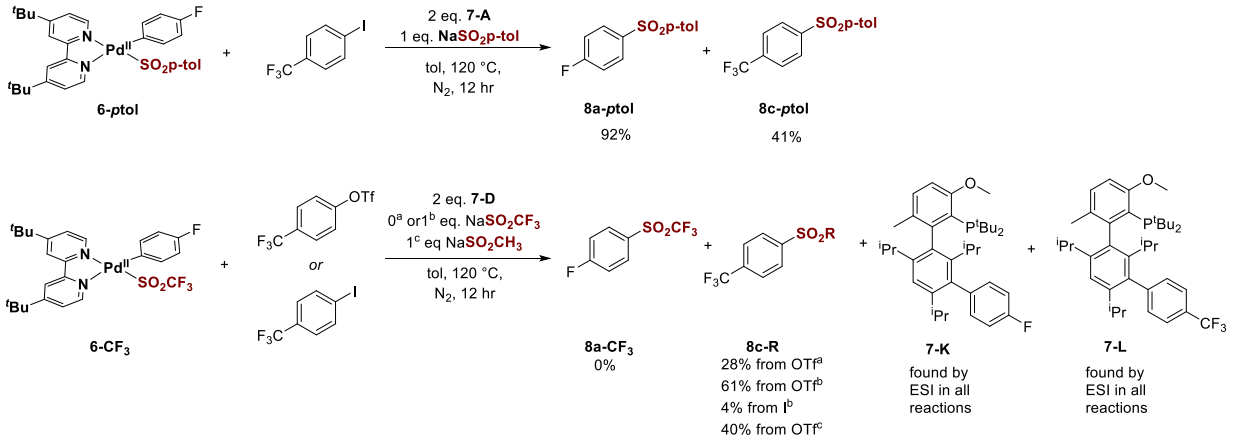


Figure 3.5. Crossover experiment of RockPhos catalysis and ligand assay. Yields determined by ^{19}F NMR spectroscopy. [a] 0 equiv of $NaSO_2CF_3$ was added. [b] 1 equiv of $NaSO_2CF_3$ was added. [c] 1 equivalent of $NaSO_2CH_3$ was added

3.4 Synthesis and Transmetallation of Phosphine-ligated Palladium(II) (*p*-fluorophenyl) Halide Complexes with Sulfinates

While the ligand exchange assay provides a rapid method of screening ligands for competency in reductive elimination, we sought to deepen our understanding of the privileged ligands identified from those assays. The ligand assay functions as a shuttle into the proposed catalytic cycle, giving us a view into **Int-3** and step **c**, **Figure 3.6**. We synthesized the Pd(II)(Ar)(psuedo)halide complexes of RockPhos andXantPhos, and PAd_3, **9-A**, **9-B**, **9-C** respectively, in order to investigate how transmetallation and reduction occurs with the ligand bound first, which is the direct comparison to the catalytic cycle steps **b** and **c**, and **int-2**.

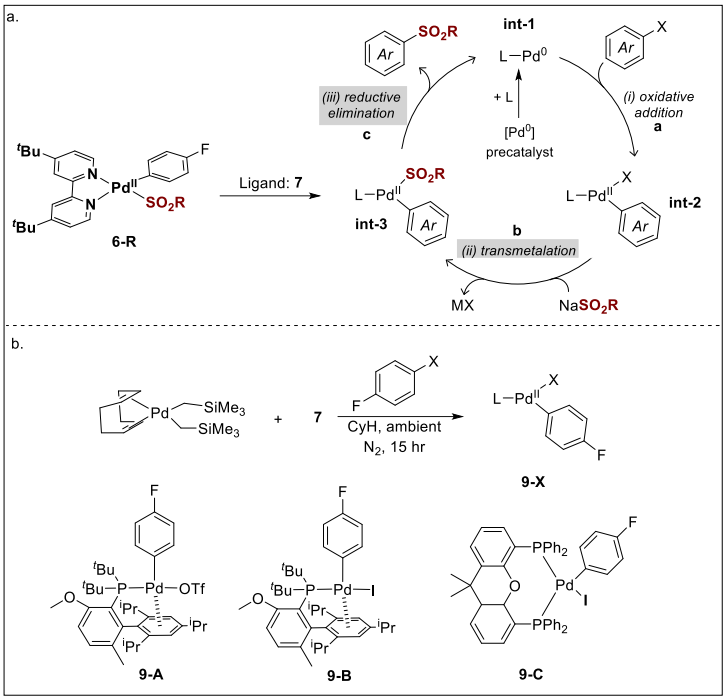
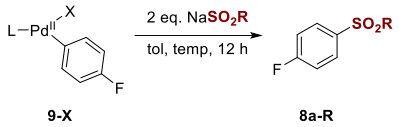


Figure 3.6. a. Proposed catalytic cycle with the pathways in which these two organometallic studies probe the elementary steps. b. Synthesis of Ligated complexes

These complexes were synthesized using (COD)Pd(CH_2SiMe_3)$_2$, which readily reductively eliminates 1,2-di-(trimethylsilyl)ethane at temperatures above 0 °C leaving a soluble Pd(0) source that is easily ligated and readily oxidatively adds into aryl (pseudo)halides. The iodide complexes were synthesized and isolated and subjected to the sulfinates at ambient temperature, 80 °C, and 120 °C.

Beginning with the iodide complexes, at 120 °C, nearly all of the complexes decompose. Around 60% of the mass balance from the reactions with **9-B** are 4-fluoro-phenyl iodide, meaning that the complex is able to reductively eliminate iodide onto the aryl substituent. Fluorobenzene and 4,4'-difluoro-biphenyl represent around 15% of the mass balance each. The byproducts of the **9-C** complex decomposition are largely unidentified, but there are trace fluorobenzene and 4,4'-difluoro-biphenyl. The sole productive chemistry from this study at 120 °C is the transmetallation of NaSO$_2$*p*-tol with **9-7AI**. This gives 36% of **8a-*p*tol**. In this way, these organometallic studies mirror catalysis, where XantPhos as a ligand is only able to couple aryl electrophiles with NaSO$_2$*p*-tol, as discussed in **Table 3.5**.



9-X 8a-R

	9-A		9-B	9-C
	22 °C	80 °C	120 °C	120 °C
$NaSO_2CF_3$	72%	73%	0%	0%
$NaSO_2CF_2H$	50%	36%	0%	0%
NaSO2CFH2	0%	53%	0%	0%
$NaSO_2CH_3$	13%	12%	0%	0%
$NaSO_2$*p*-tol	0%	8%	0%	36%

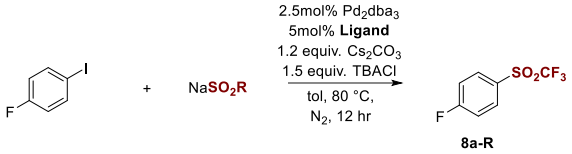
Table 3.4. Reaction of ligated Palladium aryl (psuedo)halide complexes with sulfinates at 120 °C. Yields determined by ^{19}F NMR spectroscopy.

In contrast to the iodide complex, the triflate complex of RockPhos is very reactive with these sulfinates. At room temperature and at 80 °C, **8a-CF3** was formed in 72% and 73% yield respectively. In fact, a shorter time point was obtained, and this result occurs in 1 hour. At room temperature, only $NaSO_2CF$, $NaSO_2CF_2H$, $NaSO_2CH_3$ were competent (72%, 50%, and 13% respectively). At 80 °C, all sulfinates are competent at transmetallation and reductive elimination. This is unexpected as these results do not reflect the catalytic behavior of RockPhos with aryl triflates. This shows that transmetallation of halide is much more pronounced than with **1-X** complexes. This supports the Shekar hypothesis that transmetallation is very difficult and is the rate-limiting step. This is in stark contrast to the ligand assay studies that show that just RockPhos is not competent for this reductive elimination. These conflicting results can be rationalized by considering that the complex **9-A** is not what appears *in situ* during catalysis. These results again inform us that some other form of RockPhos is relevant to catalysis, likely the arylated RockPhos

3.5 Catalytic Developments of Aryl Halide Cross-Coupling with Sodium Sulfinates

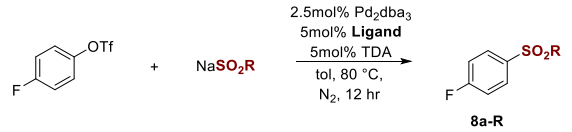
With this understanding of some of the elementary steps in this catalytic cycle, we moved to investigate the catalysis. As starting points, we investigated the generality of the conditions from the Cachi report, which used Cs_2CO_3 and TBACl along with XantPhos, Pd_2dba_3 and their coupling partners,[4] and the Shekar, which used a phase transfer reagent called TDA and a heated pre-stir of the RockPhos-Pd_2dba_3 catalytic system along with their coupling partners.[5] Our aim for this

catalytic investigation was to understand the limitations of these reported catalysis to better develop a general methodology.



Cachi Conditions

Sulfinate	7-A	7-I	7-D
R = CF_3	0%	0%	0%
CF_2H	0%	0%	0%
CFH_2	<1%	0%	0%
CH_3	<1%	0%	0%
p-tol	92%	12%	0%



Shekar Conditions

Sulfinate	7-A	7-I	7-D
R = CF_3	0%	0%	95%
CF_2H	0%	0%	92%
CFH_2	0%	0%	14%
CH_3	0%	0%	<1%
p-tol	81*%	0%	1%*

Table 3.5. Literature conditions applied to other sulfinates and ligands. Yields determined by ^{19}F NMR spectroscopy. Cachi conditions are 1.5 equiv. Cs_2CO_3, 1.2 equiv. TBACl, 1.2 equiv sulfinate, 5 mol% Ligand and 2.5%mol Pd_2dba_3 in toluene under N_2 at 80 °C for 12hr. Shekar conditions are 5 mol% TDA, 5 mol% Ligand, 2.5 mol% Pd_2dba_3, and 1.5 equiv. sulfinate in toluene under N_2 at 80 °C for 12hr. *Reaction at 120 °C

This study revealed that each of these conditions a greatly restricted in the nucleophile coupling partner. In the case of the Cachi conditions, the XantPhos catalytic system mirrors the reaction shown in **Figure 3.3**, where the XantPhos complex is only capable of transmetallating and reductive eliminating the SO_2*p*-tol moiety. Despite the decent yield of SO_2CH_3 and moderate yield of SO_2CFH_2 in the ligand assay study, catalysis does not reflect this result. Because the ligand assay skips into the catalytic cycle after the transmetallation, while the other study observes the transmetallation, we hypothesize that this discrepancy arises from the difficulty of transmetallation of $NaSO_2CH_3$ with the iodide. Increasing the temperature to 120 °C to encourage transmetallation is ineffective, and in fact reduced the yield of the literature reaction to 38% When, switching to

aryl triflates, at 120 °C, the XantPhos catalytic system is still unable to couple SO_2CH_3 with the electrophile partner, although $NaSO_2$*p*-tol still proceeds at 81% yield. We propose that the restricted electrophile scope of the XantPhos catalysis, which is simply that aryl chlorides perform poorly, is due to difficult oxidative addition into aryl chlorides, as is a common issue in palladium catalysis. The restricted nucleophile scope, then is related to the difficult transmetallation of the alkyl sulfinates with aryl iodides and bromides in tandem with the reduced efficacy of XantPhos promoted reductive elimination of the fluoroalkyl species.

The Shekar conditions were reported to for the coupling of SO_2CF_3, however, this study shows that it is also very capable of coupling SO_2CF_2H. However, simply replacing a fluorine for a hydrogen craters the yields to 14%, which only rise to 23% at 120 °C. The methyl substituent only gives trace product at both temperatures. More restrictive is the aryl electrophile scope, which was partially reported by Shekar and coworkers. Triflate electrophiles perform the best, followed by chloride, then bromide. Unreported, iodide are unreactive, which follows the trend and agrees with the hypothesis that transmetallation is the rate-limiting step and agrees with the transmetallation organometallic studies. We believe that this is indeed a sufficient explanation for the restricted electrophile scope. However, the fact that yield decreases with more nucleophillic sulfinates disagrees with that hypothesis as the explanation for the restricted nucleophile scope. Thus, we sought alternative explanations.

The arylation of the Buchwald ligand was an integral development for the catalytic methodologies of aryl fluoride cross-coupling[14] and it is possible that it plays a major role in this catalysis as well. We proposed that the initial form of the oxidative intermediate in the catalysis with RockPhos is not **9-A**, but more like ones shown in **Figure 3.6**. This complex must arylated on the initial turnover. After which, the Pd-**7-DAr** system is an effective catalytic system. However, the equilibrium between the pre-arylated species is very delicate and the ionic sphere of the sulfinates can change the equilibrium so that the arylation never fully occur. Thus, we proposed that the trend in the efficacy in sulfinate cross-coupling is due the trapping of the catalytic system in a dead-end due to the inability of the electron-rich sulfinate to encourage arylation.

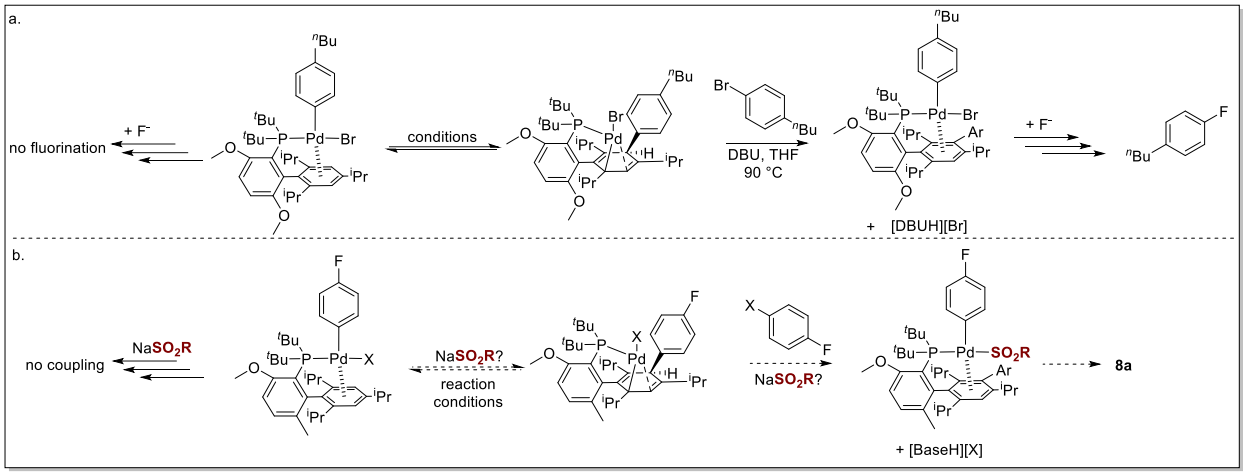
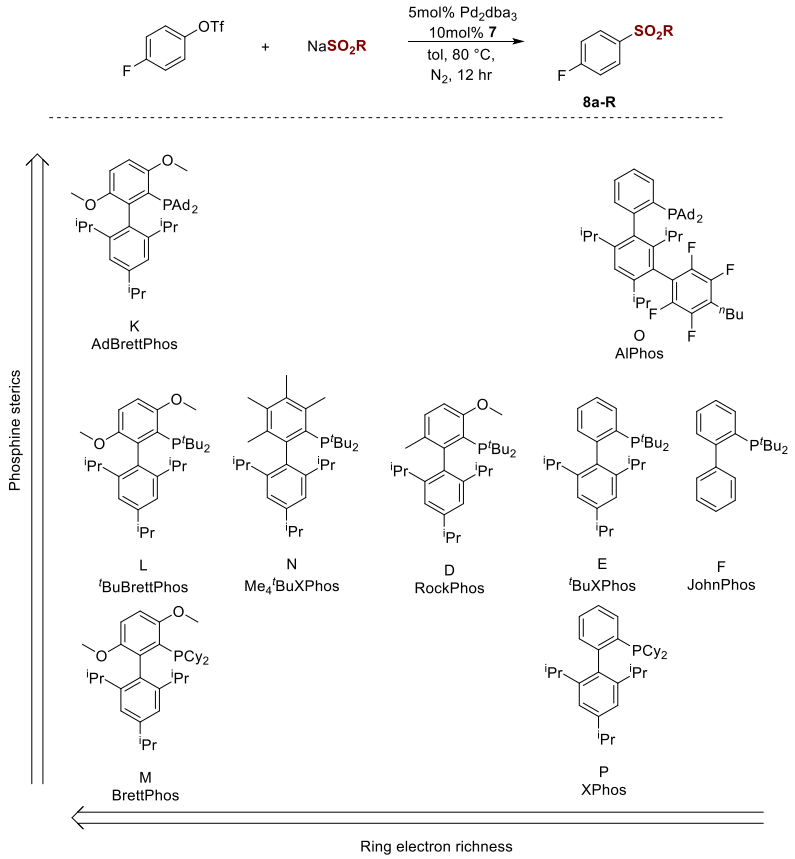


Figure 3.6. a. Demonstration of arylation of ^{t}BuBrettPhos and the stepwise equilibrium of pre-arylated intermediates as reported from the Buchwald lab. b. Analogy of RockPhos-catalyzed aryl-sulfone coupling and sulfinates' role in promoting the equilibrium

In all cases with $NaSO_2CF_3$, there is arylated ligand formed. To further probe this, we decided to investigate the steric and electronic effects of the Buchwald ligands. We carefully screened several Buchwald ligands to understand the effect of 1. ^{i}Pr groups on the pendant aryl ring, 2. Electron density of the main aryl ring, 3. steric bulk around the phosphorus atom, on the arylation of the ligand and the product formation of different sulfinates.



Ligand	$NaSO_2CF_3$ Product	$NaSO_2CF_3$ L-Ar?	$NaSO_2CF_2H$ Product	$NaSO_2CF_2H$ L-Ar?	$NaSO_2CFH_2$ Product	$NaSO_2CFH_2$ L-Ar?	$NaSO_2CH_3$ Product	$NaSO_2CH_3$ L-Ar?	$NaSO_2p$-tol Product	$NaSO_2p$-tol L-Ar?
AdBrettPhos	4	no	46	yes	16	yes	<1	no	0	no
AlPhos	3	n/a	16	n/a	<1	n/a	0	n/a	0	n/a
^{t}BuBrettPhos	4	no	42	yes	8	yes	<1	no	0	no
$Me_4{}^t$BuXPhos	5	no	61	yes	5	yes	<1	notbd	0	no
RockPhos	16	no	95	yes	29	no	1	no	0	no
^{t}BuXPhos	15	yes	88	yes	18	yes	<1	yes	0	no
JohnPhos	15	yes	15	yes	<1	yes	0	yes	<1	yes
BrettPhos	<1	no	13	no	4	no	<1	no	0	no
XPhos	3	yes	6	yes	<1	yes	0	yes	0	no

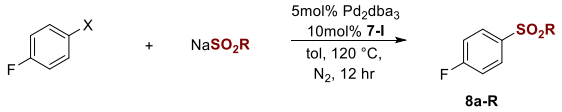
Table 3.5. Effect of Buchwald ligand identity on cross-coupling of aryl triflates with sodium sulfinates. Conditions are 2 equiv of sulfinate, 10mol% ligand, 5mol% Pd_2dba_3 with a 1 hour prestir at ambient temperature, no TDA, in toluene under N_2 at 80 °C for 12 hr. Yields determined by ^{19}F NMR spectroscopy.

Firstly, this experiment shows how essential the pre-stir and TDA are to the product formation of **8a-CF3**. In this reaction, RockPhos gives 16% yield, yet in the standard conditions, it gave 95% yield. In general, RockPhos (**7-D**) is the most productive ligand and the $NaSO_2CF_2H$ is the most active sulfinate. None of the ligands examined break the trend of R= CF_2H > CFH_2 >

CH_3 > *p*-tol in yield. There is no major increase in yield from ^{t}Bu to Ad on the phosphine, as seen by the comparison of **7-K** and **7-L**. There is a more pronounce increase from Cy to ^{t}Bu as seen in**7-P** to **7-E**. Interestingly, AlPhos (**7-O**) performed rather poorly, especially compared to **7-K** and **7-E**. AlPhos was designed in response to the Buchwald group's discovery of ligand arylation during fluorination reactions.[15] We hypothesized that AlPhos would be a more general ligand for the various nucleophiles, however this was not the case. This result encouraged us to look at the formation of the arylated ligand in all of these reactions to see if there was a discernable trend, however, none was observed. The electron deficient ligands (**7-E**, **7-F**, **7-P**) arylated with all sulfinates that they produce product with, however, yields are poor with $NaSO_2CFH_2$, $NaSO_2CH_3$, and $NaSO_2$*p*-tol. $NaSO_2CF_2H$ was the most productive sulfinate and produced arylated ligand with nearly all ligands screened. $NaSO_2$*p*-tol was the least productive and produced arylated ligand with a JohnPhos, the only ligand that affected product. In Shekar's conditions, RockPhos does form arylated ligand with $NaSO_2CF_3$, however not in these conditions. This may be related to why the yield is so poor comparatively. The relationship with ligand arylation and product formation is not direct.

Finally, we sought to employ PAd_3 in catalysis, given its productivity in the ligand assay. Unfortunately, the PAd_3 ligand appears to be caught in a confluence of several restrictive factors. Firstly, transmetallation of the sulfinates is very difficult, especially with the fluoroalkyl sulfinates. These sulfinates are the ones that perform the best in the assay. We see from the transmetallation organometallic study, that only the $NaSO_2$*p*-tol is able to give yield when transmetallating with the iodide, and that is reflected in the catalysis under the Cachi conditions, where only **8a-*p*tol** is formed, and only in 12% yield at both 80 °C and 120 °C. The next confounding issue is that oxidative addition with PAd_3 ligated palladium species is relatively difficult, especially with ArCl.[16] Most reports that contain aryl chlorides as productive electrophiles for PAd_3 catalysis utilize activated ArCl, and even then, are often in moderate yields. Curiously, it appears that oxidative addition into ArOTf with this ligand is not precedented at all. Attempts at synthesizing (PAd_3)Pd(*p*-F-Ph)(OTf) in the same manner as the RockPhos ligand failed. All triflate catalysis performed in this study returned starting material and reactions in the literature similarly show ArOTf as ineffective coupling partners for PAd_3-ligated catalytic systems.[17] The reason for this is unknown, but this does remove the most effective transmetallation partner from utilization in this

catalysis. These different reasons conspire to prove PAd_3 as an ineffective ligand for this catalytic transformation.



	Ar-OTf	Ar-I
SO_2CF_3	0%	0%
SO_2CH_3	0%	0%
SO_2*p*-tol	0%	12%

Table 3.5. Matrix of sulfinate and electrophile cross-coupling with PAd_3 catalytic system. Conditions are 2 equiv. of sulfinate, 10mol% PAd_3, 5mol% Pd_2dba_3, in toluene under N_2 at 80 °C for 12hr.

3.6 Conclusion

In summary, the palladium-catalyzed aryl-sulfone coupling has been investigated both catalytically and stoichiometrically using several organometallic complexes as model systems for proposed catalytic intermediates and reaction screening. With XantPhos as a ligand, we have identified the key restriction of poor reductive elimination with alkyl sulfinates in the nucleophile scope of catalytic reactions. We've identified a new ligand, **PAd_3**, for coupling of aryl groups and fluorinated sulfinates and explored its limitations in catalytic reactions. Finally, we have began to explore the varied reactivity with Buchwald ligands, specifically RockPhos, and their *in situ* behavior which may hold the key for further generalized aryl-sulfone coupling with both full electrophile and full nucleophile screen.

To this end, we are currently investigating this on three fronts. 1. We are exploring the use of **6-CF_3** as a precatalyst. Because of the results in condition D of **Figure 3.4**, we observed that Ar-SO_2CH_3 coupling from $NaSO_2CH_3$ is possible and enabled by ligand substitution from **6-CF_3**. 2. We are looking at methods of *in situ* halide exchange from the ineffective iodides and bromides to the triflate after oxidative addition as a way of circumventing the sluggish transmetallation that is observed with alkyl sulfinates in hopes of broadening the electrophile scope. 3. We are synthesing **7-K** to directly observe its use as a catalytic ligand.

3.7 Outlook

Looking forward, a primary objective is to elucidate the mechanism of the deoxygenation of sulfinates and harness this reactivity towards the catalytic methodology of synthesizing aryl sulfides, sulfoxides, and sulfones all from metal sulfinates and C_{sp2} halides, **Figure 3.7**.

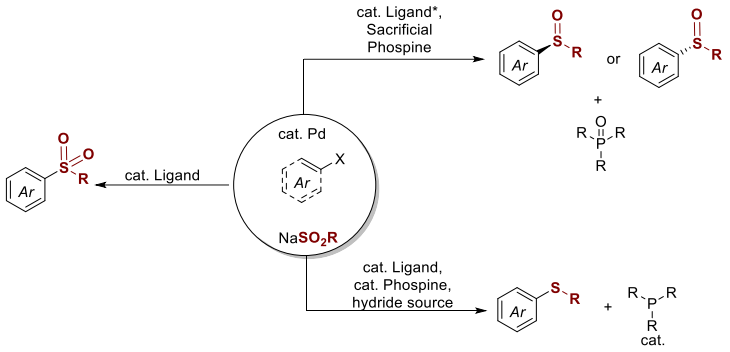


Figure 3.7. Proposed methodology of access to S^{II}, S^{IV}*, S^{VI} cross coupling of C_{sp2}-halides using palladium catalysis and phosphine deoxygenation

Preliminary results show that alkyl phosphine can deoxygenate palladium-sulfinate complexes and promote reductive elimination at elevated temperatures, as shown in **Table 3.2**. -PCy_3 is capable of fully deoxygenating and reductively eliminating SO_2CFH_2 from **6-CFH₂** to form *p*-monofluoromethyl-phenylfluoride in 44% yield. P^tBu_2Ph can perform the same reaction at **6-CFH₂**, **6-CF₂H**, and **6-CF₃** in 23%, 7%, and 33% yield, respectively.

Initial studies in harnessing this reactivity have led to the work of the Radosevich lab, where geometrically constrained phosphines are used to catalytically deoxygenate various compounds and are recharged *via* a hydride source like a silane.[18] Initial screening of silane sources shows that HSi^iPr_3 is both effective at turning over their phosphorus-substituted cyclobutane derivative, **7-Q,** and does not destroy **6-CF₃** at 80 °C in toluene. Using their phosphorus-substituted cyclobutane derivative on **6-CF₃** gives *in situ* **2** in 6% yield. **7-A** is added to this reaction mixture is and **4a** is formed in 13%. Using this phosphine with $NaSO_2CF_3$ and XantPhos gives the **4a** in low yields, depending on the aryl source. Even more excitingly, this can be applied to the other alkyl sulfinates to give the sulfide product, albeit in poor yields. Despite these initial poor yields, these results provide a starting point for exploration into this idea.

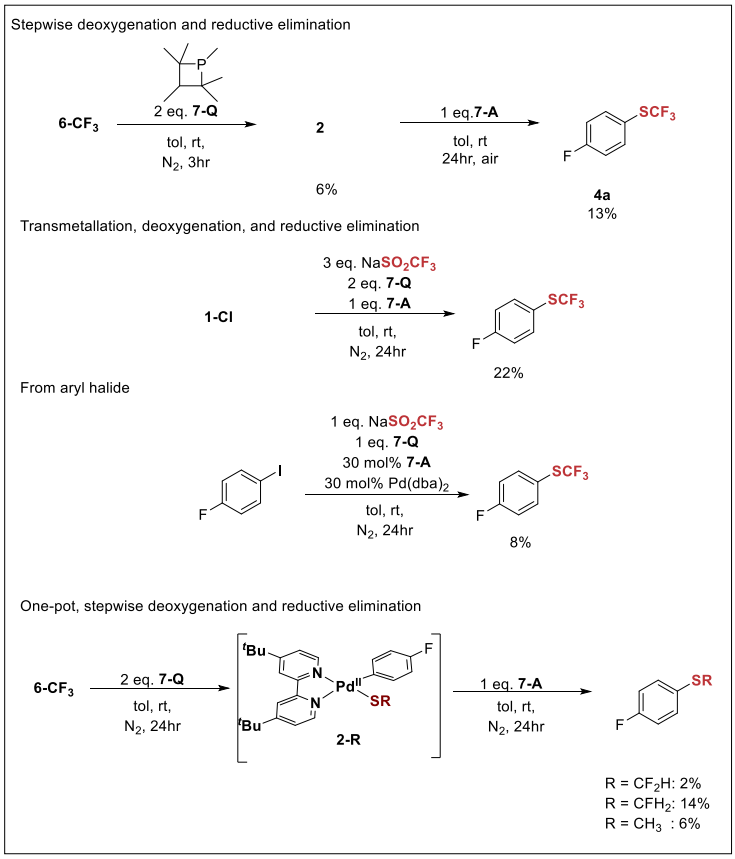


Figure 3.8. Summary of coupled sulfinate deoxygenation-reductive elimination attempts using Radosevich phosphine **7-Q** and XantPhos from various starting materials

3.8 Experimental

3.8.1 Synthesis of Palladium Complexes

Complexes **9-A,B,C** were synthesized via modified literature procedure[19].

General Synthesis of 6-R: In air, a 20 mL vial was charged with 1 mmol **1-Cl**, 2 mmol $NaSO_2R$, 5mL dichloromethane, and a stir bar. The reaction was stirred 15 h at ambient temperature. After the reaction was done, a celite filter was used to remove the salts and the filtrate was evaporated. Most reactions are pure product, but if there are impurities, column chromatography on silica gel at ~15% ethyl acetate in hexanes was used to further purify the complex.

R =CF_3: White solid, 84% yield. ^{1}H NMR (500 MHz, CD_2Cl_2) δ 9.55 (d, *J* = 5.8 Hz, 1H), 7.97 (dd, *J* = 5.6, 1.9 Hz, 2H), 7.59 (dd, *J* = 5.9, 1.9 Hz, 1H), 7.37 (dd, *J* = 8.3, 6.2 Hz, 2H), 7.31 – 7.14 (m, 3H), 6.93 – 6.76 (m, 2H), 1.36 (s, 9H), 1.29 (s, 9H). ^{13}C NMR (126 MHz, CD_2Cl_2) δ 164.94 (d, *J* = 75.8 Hz), 160.61, 154.84 (d, *J* = 263.2 Hz), 151.86, 150.62, 135.29 (d, *J* = 5.9 Hz), 124.07, 123.70, 118.86, 118.69, 114.44, 114.28, 35.52, 35.48, 30.01, 29.89. The trifluoromethyl carbon was not observed due to complex splitting. ^{19}F NMR (564 MHz, CD_2Cl_2) δ -83.25, -121.00 (m).

R = CF_2H: White solid, 93% yield. ^{1}H NMR (500 MHz, CD_2Cl_2) δ 9.62 (d, *J* = 5.8 Hz, 1H), 7.97 (dd, *J* = 4.4, 2.0 Hz, 2H), 7.59 (dd, *J* = 5.9, 2.0 Hz, 1H), 7.48 – 7.41 (m, 2H), 7.33 (d, *J* = 5.9 Hz, 1H), 7.22 (dd, *J* = 6.0, 2.0 Hz, 1H), 6.91 – 6.83 (m, 2H), 4.81 (t, *J* = 55.6 Hz, 1H), 1.36 (s, 9H), 1.29 (s, 9H). ^{13}C NMR (126 MHz, CD_2Cl_2) δ 165.05, 164.54, 155.75, 153.92, 151.24 (d, *J* = 225.1 Hz), 136.17 (d, *J* = 5.9 Hz), 123.87 (d, *J* = 51.8 Hz), 118.79, 118.61, 116.87, 114.60, 114.54, 114.39, 35.51, 35.47, 30.01, 29.91. The difluoromethyl carbon was not observed due to complex splitting. ^{19}F NMR (564 MHz, CD_2Cl_2) δ -120.60 (m), -129.11 (d, *J* = 55.6 Hz).

R = CFH_2: White solid, 97% yield. ^{1}H NMR (500 MHz, CD_2Cl_2) δ 9.66 (d, *J* = 5.9 Hz, 1H), 7.96 (t, *J* = 2.6 Hz, 2H), 7.58 (dd, *J* = 5.8, 2.0 Hz, 1H), 7.51 – 7.44 (m, 2H), 7.38 (d, *J* = 5.9 Hz, 1H), 7.21 (dd, *J* = 6.0, 2.0 Hz, 1H), 6.91 – 6.82 (m, 2H), 3.98 (d, *J* = 47.9 Hz, 2H), 1.36 (s, 9H), 1.29 (s, 9H). ^{13}C NMR (126 MHz, CD_2Cl_2) δ 164.81, 164.34, 162.46, 160.54, 154.82 (d, *J* = 223.1 Hz), 152.19, 150.46, 145.91, 135.78 (d, *J* = 5.9 Hz), 123.97, 123.56, 118.60 (d, *J* = 28.3 Hz), 114.43, 114.28, 97.06 (d, *J* = 214.2 Hz), 35.48, 35.44, 30.02, 29.92. ^{19}F NMR (564 MHz, CD_2Cl_2) δ -126.9 (m), -208.75 (m).

R = CH_3: White solid, 81% yield after column chromatography. ^{1}H NMR (500 MHz, CD_2Cl_2) δ 9.65 (d, *J* = 5.8 Hz, 1H), 7.95 (t, *J* = 1.8 Hz, 2H), 7.56 (dd, *J* = 5.9, 1.9 Hz, 1H), 7.49 (td, *J* = 6.5, 1.8 Hz, 2H), 7.45 (d, *J* = 5.9 Hz, 1H), 7.20 (dd, *J* = 6.0, 1.9 Hz, 1H), 6.90 – 6.81 (m, 2H), 2.15 (d, *J* = 1.3 Hz, 3H), 1.35 (d, *J* = 1.2 Hz, 9H), 1.29 (d, *J* = 1.3 Hz, 9H). ^{13}C NMR (126 MHz, CD_2Cl_2) δ 164.32 (d, *J* = 54.4 Hz), 160.37, 154.80 (d, *J* = 216.5 Hz), 152.23, 150.49, 148.05 (d, *J* = 2.8 Hz), 136.05 (d, *J* = 5.6 Hz), 123.89, 123.46, 118.62, 118.34, 114.22, 114.07, 52.65, 35.44, 35.40, 30.03, 29.94. ^{19}F NMR (564 MHz, CD_2Cl_2)) δ -121.42 (app. ddt).

R = *p*-tol: White solid: 91% yield. ^{1}H NMR (500 MHz, CD_2Cl_2) δ 9.95 (d, *J* = 5.8 Hz, 1H), 7.96 (dd, *J* = 12.5, 2.0 Hz, 2H), 7.62 (dd, *J* = 5.9, 1.9 Hz, 1H), 7.31 (d, *J* = 5.9 Hz, 1H), 7.17 – 7.10 (m, 3H), 7.04 – 6.98 (m, 2H), 6.91 (d, *J* = 7.9 Hz, 2H), 6.60 – 6.51 (m, 2H), 2.22 (s, 3H), 1.38 (s, 9H), 1.27 (s, 9H). ^{13}C NMR (126 MHz, CD_2Cl_2) δ 164.27 (d, *J* = 47.0 Hz), 159.91, 154.79 (d, *J* = 207.5 Hz), 152.32, 150.75, 149.47, 139.39, 135.39 (d, *J* = 5.8 Hz), 127.99, 125.63, 123.85, 123.37, 118.53, 118.37, 113.47, 113.32, 35.41, 30.06, 29.92, 20.92. ^{19}F NMR (564 MHz, cd_2cl_2) δ -122.61 (app. ddd).

General Procedure for Synthesis of Phosphine-Ligated Palladium Aryl Halides Complexes: In a N_2-filled glovebox, a 4 mL vial is charged with 0.1 mmol of (COD)Pd(CH_2SiMe_3)$_3$ and dissolved in 1 mL of cyclohexane. In a separate 4 mL vial, 0.1 mmol of ligand and aryl halide are added and dissolved in 1 mL of cyclohexane. A stir bar is added. While stirring vigorously, the (COD)Pd(CH_2SiMe_3)$_2$ solution was pippetted into the ligand and aryl halide solution. This reaction was capped and stirred vigorously at ambient temperatures for 18 hours. Add this time, 1 mL of pentane is added and the vial was placed in a -35 °C freezer for 1 hour. The solid were collected on a glass frit and washed with cyclohexane and pentane.

3.8.2 Organometallic Studies

General Procedure for Ligand Substitution Study: In a 4 mL vial, 0.01 mmol of **6—R** was weighed, along with a stir bar. This vial was brought into the glovebox. In the glovebox, 2 equiv of ligand, 1 equiv of $PhOCF_3$ (^{19}F NMR standard), and 1mL of toluene was added to the vial. The vial was capped, sealed, and placed on a 120 °C hot plate for 24 h. The reaction was then cooled to ambient temperatures and a ^{19}F NMR spectrum was obtained.

General Procedure for Transmetallation of Palladium Complexes with Sodium Sulfinates: In a N_2-filled glovebox, charge a 20 mL vial with 0.06 mmol of palladium complex, 9.7 mg (0.06 mmol, 1 equiv) of trifluoromethoxybenzene, 6 mL of toluene, and a stir bar. Stir the solution at ambient temperature until homogenous. In five 4 mL vials with a stir bar, add 0.02 mmol of $NaSO_2R$ (R = CF_3, CF_2H, CFH_2, CH_3, *p*-tol). Add 1 mL of the palladium complex solution to each vial, capped, seal and stir at desired temperature. With the remaining 1 mL of palladium

stock solution, take ^{19}F NMR to get the exact ratio of starting palladium complex to trifluoromethoxybenzene standard.

3.8.3 Reaction Conditions

General Procedure for catalysis with Cachi Conditions: In a N_2-filled glovebox, a 4 mL vial is charged with 0.1 mmol (1 equiv) of 4-fluoro-phenyl halide, 16.2 mg (0.1 mmol, 1 equiv) of trifluoromethoxybenzene, 2.3 mg (0.0025 mmol, 0.025 equiv) of Pd_2dba_3, 0.005 mmol (0.05 equiv) ligand, 0.12 mmol (1.2 equiv) of selected sodium sulfinate, 48.9 mg (0.15 mmol, 1.5 equiv) Cs_2CO_3, 33.4 mg (0.12 mmol, 1.2 equiv) of TBACl, 0.6 mL of toluene, and a stir bar. Cap, seal, and stir at 80 °C for 12 hr.

General Procedure for catalysis with Shekar Conditions In, a N_2-filled glovebox, a 4 mL vial is charged with 2.3 mg (0.0025 mmol, 0.025 equiv) of Pd_2dba_3, 0.005 mmol (0.05 equiv) ligand, 1 mL of toluene, and a stir bar. This vial is capped, sealed, and stirred at 80 °C for thirty minutes. A separate vial is charged with 0.1 mmol (1 equiv) of 4-fluoro-phenyl halide, 16.2 mg (0.1 mmol, 1 equiv) of trifluoromethoxybenzene, 0.15 mmol (1.5 equiv) of selected sodium sulfinate, 1.2 mg (0.005 mmol, 0.05 equiv) of tris(2-(2-methoxyethoxy)ethyl)amine (TDA), and a stir bar. The catalyst mixture is brought back into the glovebox and transferred to the reaction vial. This vial is capped, sealed, and stirred of 80 °C for 12 hr.

3.9 References

1. Feng, M.; Tang, B.; Liang, S.; Jiang, X. "Sulfur Containing Scaffolds in Drugs: Synthesis and Application in Medicinal Chemistry", *Curr Top Med Chem*, **2016**, 16, 1200-1216
2. Regueiro-Ren, A. "Chapter One – Cyclic sulfoxides and sulfones in drug design", *Adv Het Chem.*, **2021**, 134, 1-30
3. Xu, L.; Cheng, J.; Trudell, M. L. "Chromium(VI) Oxide Catalyzed Oxidation of Sulfides to Sulfones with Periodic Acid", *J. Org. Chem.*, **2003**, 68, 5388-5391
4. (a) Cachi, S.; Fabrizi, G.; Goggiamani, A.; Parisi, L. M. "Unsymmetrical Diaryl Sulfones through Palladium-Catalyzed Coupling of Aryl Iodides and Arenesulfinates", *Org. Lett.*, **2002**, 4, 4719–4721; (b) Cachi, S.; Fabrizi, G.; Goggiamani, A.; Parisi, L. M.; Bernini, R.; "Unsymmetrical Diaryl Sulfones and Aryl Vinyl Sulfones through Palladium-

Catalyzed Coupling of Aryl and Vinyl Halides or Triflates with Sulfinic Acid Salts", *J. Org. Chem.*, **2004**, 69, 5608–5614

5. Smyth, L. A.; Phillips, E. M.; Chan, V. S.; Napolitano, J. G.; Henry, R.; Shekar, S. "Pd-Catalyzed Synthesis of Aryl and Heteroaryl Triflones from Reactions of Sodium Triflinate with Aryl (Heteroaryl) Triflate", *J. Org. Chem.*, **2016**, 81, 3, 1285–1294
6. Zhu. W; Ma. D. "Synthesis of Aryl Sulfones via L-Proline-Promoted CuI-Catalyzed Coupling Reaction of Aryl Halides with Sulfinic Acid Salts", *J. Org. Chem.*, **2005**, 70, 2696-2700
7. Zhang, L.; Du. W.; Wu, J.; Yang, R.; E. X.; Wang, J.; Xia, Z. " Au(I)/Au(III)-Catalyzed Sulfonylation of Aryl Iodides for the Synthesis of Various Functionalized Aryl Sulfones", *Org. Lett.*, **2024**, 26, 9413-9418
8. de Gombert, A.: McKay, A. I.; Davis, C. J.; Wheelhouse, K. M.; Willis, M. C. "Mechanistic Studies of the Palladium-Catalyzed Desulfinative Cross-Coupling of Aryl Bromides and (Hetero)Aryl Sulfinate Salts", *J. Am. Chem. Soc., **2020**, 142, 3564-3576*
9. Villalba, F.; Albeniz, C. A. "Palladium hydrazonato complexes and their role in the Pd-catalyzed cross-coupling reactions of hydroazones as carbene precursors", *Dalton Trans,* **2022**, 51, 17733-17737
10. Scattolin, T.; Santo, C.; Demitri, N.; Canovese, L.; Visentin, F. "Chemoselective oxidation addition of vinyl sulfones mediated by palladium complexes bearing picolyl-N-heterocyclic carbnene ligands" *Dalton Trans*, **2020**, 49, 5684-5694
11. Zhao, X.; Dong, V. M. "Carbon-Sulfur Reductive Elimination from Palladium(IV) Sulfinate Complexes" *Angew. Chem. Int. Ed.*, **2011**, 50, 932-934
12. Chatelain, P.; Sau, A.; Rowley, C. N. "Suzuki-Miyaura Coupling of (Hetero)Aryl Sulfones: Complementary Reactivity Enables Iterative Polyaryl Synthesis", *Angew. Chem. Int. Ed., **2019**, 58, 14959-14963*
13. Ferguson, D. M.; Bour, J. R.; Canty, A. J.; Kampf, J. W.; Sanford, M. S. "Aryl-CF_3 Coupling from Phosphinoferrocene-Ligated Palladium(II) Complexes", *Organometallics*, **2019**, 38, 519-526
14. Lee, H. G.; Miner, P. J.; Buchwald, S. L. " Pd-Catalyzed Nucleophilic Fluoroination of Aryl Bromides", *J. Am. Chem. Soc*. **2014**, 136, 3792–3795

15. Sather, A. C.; Lee, H. G.; De La Rosa, V.; Yang, Y.; Muller, P.; Buchwald S. L. "A Fluorinated Ligand Enables Room-Temperature and Regioselective Pd-Catalyzed Fluorination of Aryl Triflates and Bromides", *J. Am. Chem. Soc.* **2015**, 137, 13433–13438
16. Lau, S.; Yu, P.; Chen, L.; Madsen-Duggan, C. B.; Williams, M. J.; Carrow, B. P. "Lau, S.; Yu, P.; Chen, L.; Madsen-Duggan, C. B.; Williams, M. J.; Carrow, B. P." *J. Am. Chem. Soc.* **2020**,*142*, 20030-20039
17. Ostrowska, M.; I.; Morris, J. A.; Ball, L. T.; "Pd-Catalyzed O-Arylation of Phenols Mediated by a Weak, Soluble Organic Base: Methodology, Mechanism, and Compatibility with Enabling Technologies", *J. Am. Chem. Soc*. **2025,** 147, 40, 36870–36881
18. Li, G.; Lavagnino, M. N.; Ali, S. Z.; Hu, S.; Radosevich, A. T. "Tandem C/N-Difunctionalization of Nitroarenes: Reductive Amination and Annulation by a Ring Expansion/Contraction Sequence", *J. Am. Chem. Soc*. **2023**, 145, 1, 41–46
19. Mamimone, T. J.; Milner P. J.; Kinzel, T.; Zhang, Y.; Takase, M. K.; Buchwald, S. L. "Evidence for in Situ Catalyst Modification during the Pd-Catalyzed Conversion of Aryl Triflates to Aryl Fluorides", *J. Am. Chem. Soc*. **2011**, 133, 45, 18106–18109

Chapter 4 Mechanistic Elucidation of Copper-Mediated C-C and C-S Coupling of Directed Aryl Iodides and Sulfinates Salts

4.1 **Background**

(Hetero)aryl sulfones are valuable components of bioactive molecules; however, there are few general methods for accessing these functional groups with diverse substituents on the sulfone moiety. Transition metal catalyzed coupling of aryl halides with sulfinate salts would offer an attractive solution to this limitation. However, to date, there are only four methods available to achieve this transformation, three of which are limited to one specific subclass of sulfinate coupling partners. With the goal of expanding the canon of methodologies for general aryl–sulfinate cross coupling, we pursued the identification of novel copper-based catalysts **(Figure 4.1**).

One of the first methods for Ar–SO_2R coupling was from Ma and coworkers,[1] who used a copper proline catalyst to couple aryl bromides and iodides with $NaSO_2R$, where R = methyl or *p*-tolyl (**Figure 4.1**). This 2005 report was the first example of a group 11 metal catalyzing this transformation. While the method required high temperatures >100 °C and DMSO as a solvent, it offered the advantages of commercially available and inexpensive reagents along with just 10 mol % catalyst loading. The main limitation was a lack of generality with respect to the R substituent on the sulfinate salt. While the coupling of ArI with $NaSO_2CFH_2$ afforded modest yields (42 and 49% for Ar = *p*-$MeOC_6H_4$ and *p*-FC_6H_4, respectively), more electron deficient (and less nucleophilic) $NaSO_2CF_2H$ and $NaSO_2CF_3$ gave <1% yield under the standard reaction conditions. Most recently, Zhang and coworkers demonstrated the directed-C4-H sulfinylation of indoles using a copper(II) source and $NaSO_2R$ (R = alkyl, aryl). This method suffers the same limitation with respect to fluoroalkyl sulfinates.[2]

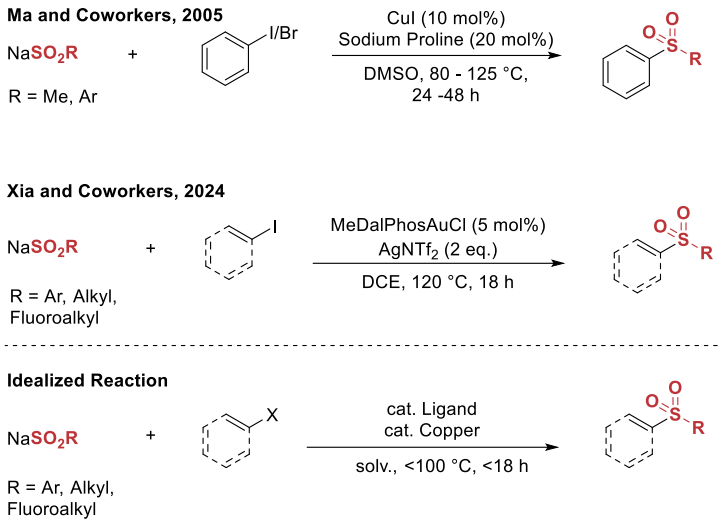
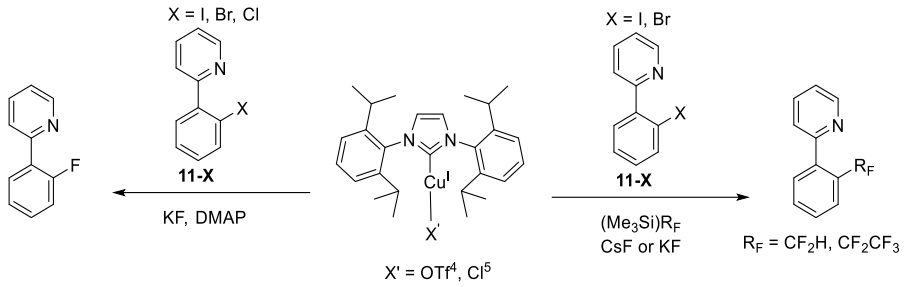


Figure 4.1. Group 11 catalyzed aryl-sulfone cross coupling reactions from the literature and the target reaction

Two decades after Ma's work, Xia and coworkers[3] reported that gold-MeDalPhos complexes are effective catalysts for coupling aryl iodides with a diverse set of sulfinate salts, using superstoichiometric silver ($AgNTf_2$) as a transmetallating reagent. This represented the first reported example of a *general* cross-coupling methodology for $NaSO_2R$. However, this method still has several limitations, including the need for an expensive Au-catalyst in conjunction with 2 equiv of Ag(I), the requirement for high temperature (120 ºC), and the restrictions to aryl iodides as coupling partners. Since copper is the 1st-row congener of gold, we hypothesized that it would be possible to identify a Cu(I) based catalyst that mirrored this general reactivity.

Copper(I) is well-known to perform cross-coupling reactions with other electron-deficient nucleophiles, including fluoride,[4] pentafluoroethyl, and difluoromethyl.[5] In many of these cases, the Cu(I) is ligated with an N-heterocyclic carbene [(1,3-bis-(2,6-diisoproylphenyl)-imidazolinium (IPr)]. The strongly electron-donating carbene facilitates oxidative addition, while the steric bulk of this ligand effectively promotes the challenging reductive elimination. Two reports from the Sanford lab have isolated and characterized IPrCuX (X = F, CF_2H, CF_2CF_3) complexes that undergo cross-coupling with ArX (**Scheme 4.1**). These linear Cu(I) complexes react with directed aryl halides to form reactive copper(III) intermediates that participate in the challenging reductive eliminations.



Scheme 4.1. Stoichiometric fluorination[4] and fluoroalkylation[5] of directed aryl halides from IPrCu (pseudo)halide complexes.

We hypothesized that this IPrCu system would mediate analogous couplings of directed aryl halides with $NaSO_2R_F$ (R_F = fluoroalkyl) via the Cu(I/III) pathway outlined in **Figure 4.3**. Direct coupling of fluoroalkyl sulfinate salts and electrophiles has a limited precedent, as discussed above. The primary use of $NaSO_2CF_3$, also known as Langlois's Reagent, is as a $F_3C\bullet$ source. When this salt is oxidized, the resulting S-based radical undergoes homolysis, releasing SO_2 and $F_3C\bullet$.[6] In many reactions, this $F_3C\bullet$ is captured by copper *in situ*, which goes on to perform productive coupling with aryl groups. While $NaSO_2CF_2H$ does not participate in this oxidatively induced desulfinylation, the analogous zinc salt does.[7] Based on these precedents, we anticipated that the Cu(III) intermediates formed via oxidative addition might be sufficiently oxidizing to promote desulfinylation of SO_2R_F ligands. This would provide a potential bifurcation of reactivity that could lead to either be aryl-SO_2R_F coupling or aryl–R_F coupling, **Figure 4.2**.

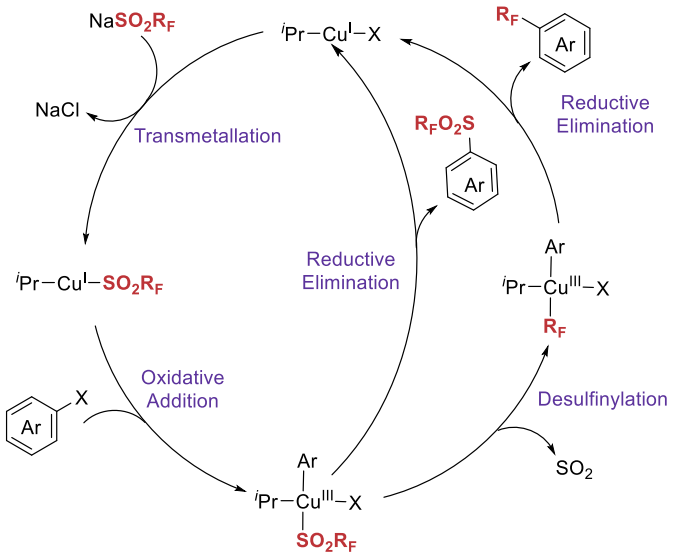
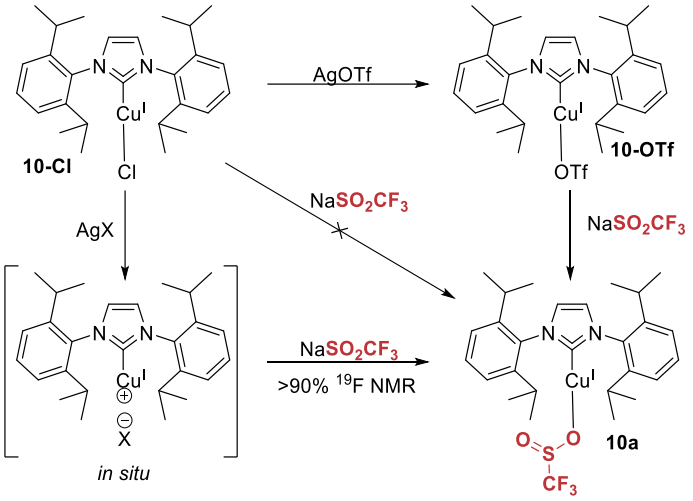


Figure 4.2. Proposed catalytic cycles of copper(I/III)-catalyzed cross-coupling between aryl halides and metal sulfinate salts and desulfinylation pathway.

4.2 Synthesis of (1,3-bis-(2,6-diisopropylphenyl)imidazolinium) Copper (sulfinate) Complexes

By analogy to the work in Chapters 2 and 3, we first sought to synthesize and isolate a series of (1,3-bis-(2,6-diisopropylphenyl)imidazolinium)copper(sulfinate) (IPrCuSO$_2$R (R = CF$_3$, CF$_2$H, CFH$_2$, CH$_3$, *p*-tol)) complexes and investigate their reactivity. To start, IPrCuCl (**10-Cl**), a stable commercial compound, was treated with 2 equiv of NaSO$_2$CF$_3$ (**Scheme 4.2**). No reaction was observed, even at elevated temperatures (up to 60 ºC). This represents a stark contrast with the Pd^{II} systems in Chapter 3, where transmetallation between NaSO$_2$CF$_3$ and the [Pd(II)]-Cl was extremely fast at room temperature. We next converted **10-Cl** to the more labile triflate analogue by reaction with 1.1 equiv of AgOTf in THF.[8] **10-OTf** was isolated in 98% yield after filtration and removal of solvent *in vacuo*. The treatment of **10-OTf** with 2 equiv of NaSO$_2$CF$_3$ at 25 ºC for 18 h afforded the target trifluoromethylsulfinate complex **10a** in quantitative yield as determined by ^{19}F NMR spectroscopy.



Scheme 4.2. Transmetallation of **10-X** with NaSO$_2$CF$_3$ to form **10a**

Following the success of this 2-step procedure, we sought to telescope the first step. A screen of silver salts was conducted, where **10-Cl** was combined in a vial with 1 equiv of AgX (X = OTf, BF$_4$, PF$_6$, or NTf$_2$). A stir bar and THF were added, the reaction was stirred overnight after which , 2 equiv of NaSO$_2$CF$_3$ were added, and the reaction was stirred for an additional 18 h. ^{19}F NMR spectroscopic analysis revealed that all of the Ag salts afforded similar and nearly

quantitative yield of **10a**. As such, $AgBF_4$ was chosen as the salt moving forward due to availability. **10-Cl** was added to a vial with 1 equiv of $AgBF_4$ with a stirbar and THF were added, and the reaction was stirred for 15 min. The AgCl was then removed by filtration using a 0.45-micron syringe filter, with the filtrate solution directly transferred into a vial containing 2 equiv of $NaSO_2CF_3$. The reaction was stirred at 25 ºC for 15 h, concentrated *in vacuo*, and then the resulting white solid was redissolved in dichloromethane This heterogenous mixture was filtered to remove NaCl as well as any remaining sulfinate salt. The product was then recrystallized at –35 ºC from a 1:1 solution of CH_2Cl_2 and pentane to afford **10a** in 64% yield following recrystallization, **Figure 4.3**.

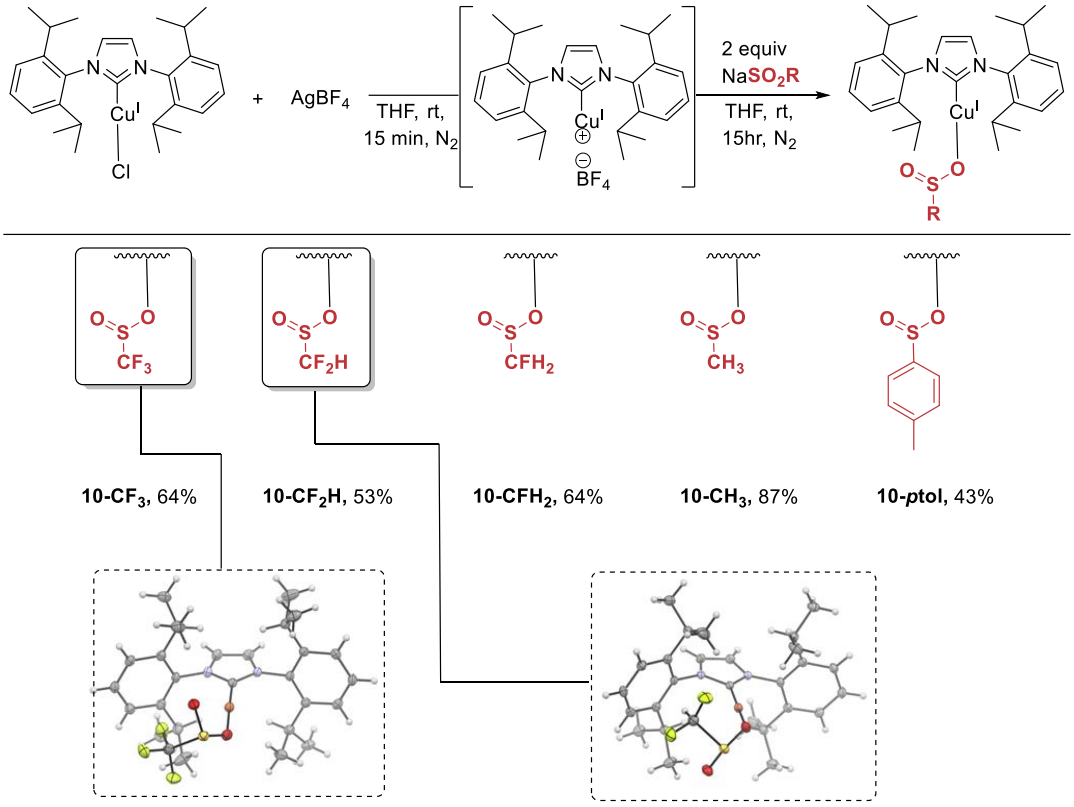


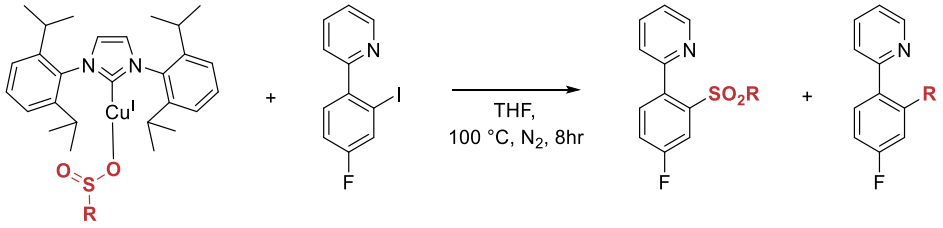
Figure 4.3. Optimized reaction conditions to form IPrCu(SO_2R). Single crystal X-ray structures of **10-CF_3** and **10-CF_2H** show that the sulfinate is bound through the oxygen. Yields are isolated after one recrystallization; additional product can be obtained through further recrystallizations of the mother liquor.

The full series of methyl-substituted sulfinates (CF_3, CF_2H, CFH_2, CH_3) as well as the *para*-tolyl analogue were synthesized using this same procedure. Single crystal x-ray structures of **10-CF_3** and **10-CF_2H** reveal that the sulfinate ligands are O-bound to Cu(I). This stands in contrast

to the Pd^{II} complexes described in Chapter 3, where the sulfinate is bound through the sulfur. This difference may be due to the smaller size and harder nature of first-row metal Cu versus second-row metal Pd. A search of the Cambridge Crystallographic Data Centre reveals that there are no copper complexes submitted to the database that contains a sulfinate bound to a copper center through the sulfur.

4.3 Stoichiometric Cross-Coupling of (1,3-bis-(2,6-Diisopropylphenyl)imidazolinium) Copper (sulfinate) with Aryl Iodides

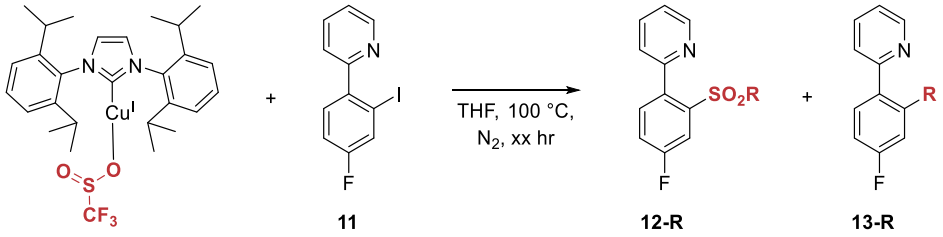
With these complexes in hand, we sought to investigate the ability of IPrCu(SO_2R) complexes (**10-R**) to participate in Ar–SO_2R coupling reactions. These complexes are expected to undergo oxidative addition into aryl halide bonds to form square planar Cu^{III} aryl intermediates. Notably, most Cu^{III} intermediates of this type are highly reactive towards reductive eliminaton and thus not detectable or isolable. As such, Ar–SO_2R coupling reductive elimination is expected to occur rapidly to release the product. The reactivity of **10-R** with aryl iodides was evaluated using ^{19}F NMR spectroscopy to monitor the formation of the target reductive elimination product as well as any side products. The 2-pyridyl aryl iodide **11** was used as a substrate, since previous studies from Sharninghausen[4] and Hall[5] showed that this undergoes facile oxidative addition at related IPrCuX complexes (X = F or CF_2H). At 100 ºC, all of the complexes reacted completely with 2 equiv of **11** over 8 h (**Table 4.1**). With R = CF_2H, CFH_2, CH_3, and tolyl, the aryl–SO_2R coupled product was formed in >90% yield. Notably, this represents a significant advance over Ma's Cu/proline system, which gave moderate yields with $NaSO_2CFH_2$ and did not afford productive coupling with $NaSO_2CF_2H$.



entry	R =	12-R	13-R
1	CF_3	3%	28%
2	CF_2H	92%	0%
3	CFH_2	>99%	0%
4	CH_3	>99%	0%
5	*p*-tol	>99%	0%

Table 4.1. Reaction of 2-(2-pyridyl)-5-fluoro-phenyl iodide (**11**; 2 equiv) with IPrCu(SO_2R) complexes at 100 °C in THF with $PhOCF_3$ as a ^{19}F NMR standard.

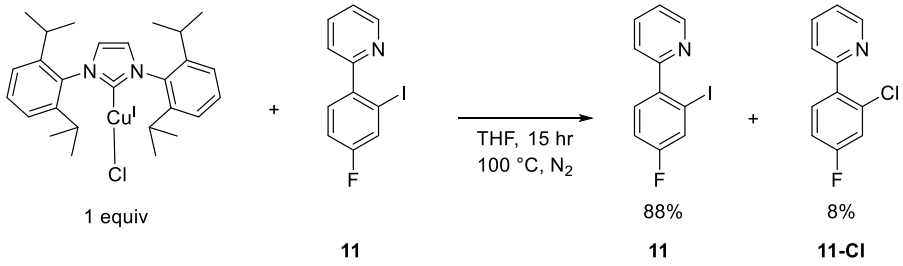
In contrast to the other complexes, **10-**CF_3 afforded only traces (3%) of the Ar–SO_2CF_3 product. Instead, desulfinylation occurred prior to reductive elimination to afford **13-CF₃** in 28% yield. This reactivity was investigated further, since significant quantities of starting material (both **10-CF₃** and **11**) remained under the conditions in **Table 4.1**, suggesting that oxidative addition at **10-CF₃** is slower than with the other complexes. This is likely because -SO_2CF_3 is the most electron-withdrawing of the sulfinate ligands. As shown in **Table 4.2**, increasing the equiv of **10-CF₃** (to 3 equiv) and conducting the reaction for longer times resulted in higher yields of **13-CF₃** (up to 68%). Only traces (3%) of **12-SO₂CF₃** were formed under these conditions. Notably, **10-CF₃** was largely consumed after 15 h (3% remaining), despite being in excess compared to the aryl iodide. A separate study revealed that in the absence of ArI, **10-CF₃** shows minimal decomposition over 48 h at 100 °C in THF. This indicates that **10-CF₃** decomposition in the presence of aryl iodide is not merely a thermal process; furthermore, desulfinylation does not occur at Cu^{I} and is instead related to (or induced by) the oxidative addition step.



entry	Cu	11	12-R	13-R
0 min	100%	100%	0%	0%
15 hr	3%	18%	3%	68%
48 hr	0%	11%	4%	75%

Table 4.2. Flipped stoichiometry of reactions between **10-CF₃** and **11** as a function of reaction time.

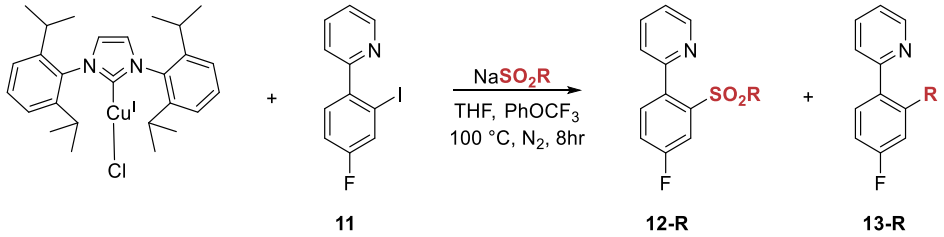
We next probed analogous reactions starting from the IPrCu^{I}Cl, $NaSO_2R$, and aryl iodide **11**, **Scheme 4.3**. Here, *in situ* transmetallation to form **10-R** could be followed by the oxidative addition/reductive elimination sequence to yield **12-SO₂R**. The control reaction with no sulfinate added returned predominantly the starting material **11** (88%) but formed 8% yield of **11-Cl**. The **11-Cl** is believed to form via oxidative addition of **11** at IPrCu^{I}Cl followed by Ar–Cl bond-forming reductive elimination. Since **11-Cl** is expected to be unreactive towards a subsequent oxidative addition, it acts as a thermodynamic sink.



Scheme 4.3. Reaction of IPrCu^{I}Cl with 2 equiv of **11** in THF at 100 °C for 15 h

We next explored this reaction in the presence of each sulfinate salt (**Table 4.3**). All of the fluoroalkyl sulfinates afforded low (<20%) yield of the Ar-SO_2R coupled product **10-R** under these conditions. This is likely due to slow transmetallation with these poorly nucleophilic salts. In contrast, the methyl and tolyl derivatives both afforded good yield (68% and 67%, respectively), demonstrating the feasibility of the transmetallation/oxidative addition/reductive elimination

sequence in these systems. The aryl mass balance in all of these reactions was predominantly **11-Cl**. While the formation of **11-Cl** is not surprising based on the results from **Scheme 4.3**, the amount of this side product (up to 90% yield with $NaSO_2CF_3$) was unexpected. The added sulfinate salts may promote faster reactivity, thus increasing the amount of **11-Cl** that is formed. Alternatively, added $NaSO_2R$ may encourage Cl reductive elimination from the Cu(III) intermediate described above.

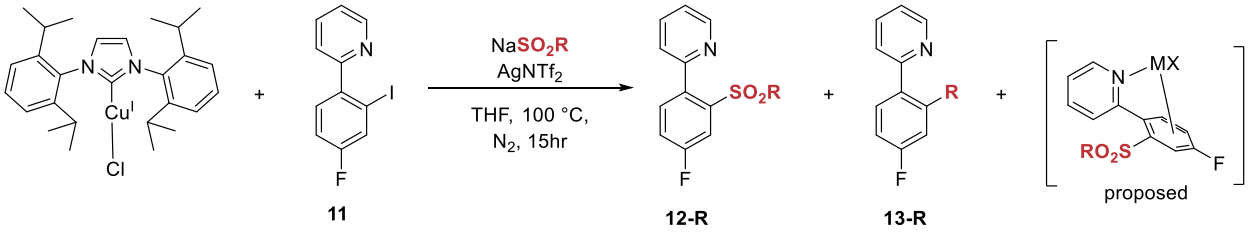


11 **12-R** **13-R**

entry	R =	12-R	13-R	11-Cl
1	CF_3	0%	trace	90%
2	CF_2H	3%	0%	77%
3	CFH_2	17%	0%	30%
4	CH_3	68%	0%	5%
5	*p*-tol	67%	0%	7%

Table 4.3. Stoichiometric reactions of **10** with 1 equiv of **11** in the presence of 2 equiv of $NaSO_2R$ in THF at 100 ºC. Yields determined by ^{19}F NMR spectroscopy using trifluoromethoxybenzene as a standard.

Since that transmetallation appears to be difficult for the fluoroalkyl sulfinates, $AgNTf_2$ was explored as an additive to promote this step. Taking inspiration from Xia and coworkers,[2] $AgNTf_2$ was tried first in the stoichiometric reaction of IPrCuCl with $NaSO_2CF_3$/$NaSO_2CF_2H$ and substrate **11**. As shown in Table 4.4 entry 2, 2 equiv of the Ag additive turned on reactivity, such that **12-SO_2CF_2H** was produced in 81% yield (compared to 3% without Ag under otherwise analogous conditions). Doubling the amount of silver to 4 equiv resulted in an unidentified set of broad resonances in the ^{19}F NMR spectrum with nearly the same shifts as the organic product and an approximate integration matching the product. We propose that these peaks are associated with a complex between the **12-CF_2H** product and Ag(I).



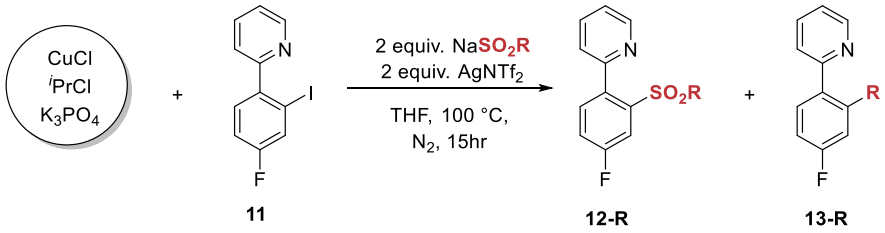
entry	R =	Ag eq.	12-R	13-R	complex
1	CF_3	2	0%	0%*	15%
2	CF_2H	2	81%	0%	0%
3	CF_3	4	0%	0%	17%
4	CF_2H	4	0%	0%	59%
5	CH_3	2	12%*	0%	30%

Table 4.4. Reaction of **10** with **11** with $NaSO_2R$ in the presence of $AgNTf_2$. Yields determined by ^{19}F NMR spectroscopy. *Isolated yield after workup (liquid/liquid extraction with dichloromethane and saturated aqueous sodium bicarbonate).

When $AgNTf_2$ was added to the reaction with $NaSO_2CF_3$ (Table **4.4**, entries 1 and 3), the sole detectable product had a broad ^{19}F NMR signal at -75.49 ppm, consistent with the formation of a Ag(I) complex of **12-SO_2CF_3** rather than **13-CF_3**. The yield was relatively low (15%), and increasing from 2 to 4 equiv of $AgNTf_2$ had minimal impact (17% yield with this change). With $NaSO_2CH_3$, a putative Ag(I)-**12-SO_2CH_3** complex was formed in 30% yield. Treatment of the crude reaction mixture to liquid/liquid extraction with dichloromethane and saturated aqueous $NaHCO_3$ released **12-SO_2CH_3** in 12% yield.

In the literature, it common to form Cu(I) complex **10** *in situ* from the combination of CuCl, IPrHCl, and a base.[9] We hypothesized that analogous Ar–SO_2R coupling reactions could proceed with this *in situ* formed complex, and further that the added base could play a dual role of activating the IPrHCl to IPrand also liberating the organic product from the metal. As shown in **Table 4.5**, a stock solution of **11**, a ^{19}F NMR standard, and IPrHCl was prepared in THF. In a vial with a stir bar, CuCl, K_3PO_4, $AgNTf_2$, and $NaSO_2R$ were combined. A portion of stock was added to each vial, which was immediately placed on a 100 °C hot plate for 15 h. With $NaSO_2CF_3$, **12-SO_2CF_3** was formed in 85% yield as a putative Ag(I) adduct. Again, no desulfinylation was observed in this reaction, suggesting that the silver facilitates a different reactivity manifold than what occurs in **Table 4.1** and **Table 4.2**. The other sulfinate salts also showed reactivity under these conditions,

and **12-SO_2R** was formed in yields ranging from 17-91%. Similar to the methodologies reported by Ma and by Shekar, the CF_3/CF_2H and CFH_2/CH_3 salts behave fundamentally differently. Thus, we hypothesized that the difference in reactivity from entries 1 and 2 from 3-5 may reflect a difference in mechanism. The trend of increasing yield across entries 3-5 is related to an increase of electron density, facilitating transmetallation and reductive elimination at the Cu center. In contrast, we hypothesized that the success of entries 1 and 2 implicate a silver-promoted pathway, based on the poor or modest yields of **12-SO_2CF_3/SO_2CF_2H** in the previous copper-only reactions. Indeed, results in section 4.4 below confirm that the $AgTf_2$ mediates Ar–SO_2CF_3 and Ar–SO_2CF_2H coupling *in the absence of Cu(I)* (*vide infra*).



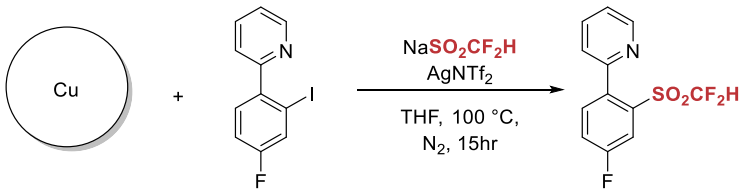
entry	R =	12-R	13-R
1	CF_3	85%*	0%
2	CF_2H	91%	0%
3	CFH_2	17%	0%
4	CH_3	37%	0%
5	*p*-tol	77%	0%

Table 4.5. Reaction **11** with 1 equiv of CuCl, 1 equiv of IPrCl, and 1 equiv of K_3PO_4 in the presence of 2 equiv of $NaSO_2R$ and 2 equiv of $AgNTf_2$. Yields determined by ^{19}F NMR spectroscopy. *Yield of putative Ag(I) complex.

4.4 **Catalytic Development of Aryl-Sulfinate Cross-Coupling with IPrCuCl**

Preliminary studies were conducted to translate this reactivity to copper catalysis by lowering the equiv of Cu from 1 to 0.1 using $NaSO_2CF_2H$ as the sulfinate source (Table 4.6, entries 1-3). Decreasing the Cu loading to 0.1 equiv resulted in a boost in yield from 55% to >99%. This led us to run the control reaction without Cu (entry 4), which gave >99% yield of **12-SO_2CF_2H**. This result shows that $AgNTf_2$ also mediates the target transformation, a finding that will be followed up in future work. Further studies revealed that the $AgNTf_2$ reaction affords comparable

yield of in the dark (entry 5), indicating that the Ag(I) reactivity is not photoinduced. However, the dark reaction mixture looked different from that in the light, with heterogenous silver particles stuck to the sides of the vial and not evenly dispersed in the solution. Furthermore, prior to the workup, the ^{19}F NMR peaks of the product were broad and slightly shifted compared to those for the reaction under ambient light. This result suggests that light may be playing a role in deligating the product from the Ag. Finally, when **10** was used as the copper source without any base, the Ag was still required to achieve high yields of product (entries 6-9).



entry	Cu source	Cu equiv	Ag equiv	%
1	CuCl	1	2	58%
2	CuCl	0.5	2	85%
3	CuCl	0.1	2	>99%
4	--	--	2	>99%
5	--	--	2*	>99%*
6	^{i}PrCuCl	0.1	1	88%
7	^{i}PrCuCl	0.1	0.5	69%
8	^{i}PrCuCl	0.1	0.1	10%
9	^{i}PrCuCl	0.1	0	0%

Table 4.6. Equivalents screen of copper and silver in cross-coupling of **11** with $NaSO_2CF_2H$. For entries 1-3, IPrHCl and K_3PO_4 were added in 1:1 ratio of the CuCl. *In dark. **Yield of putative silver complex

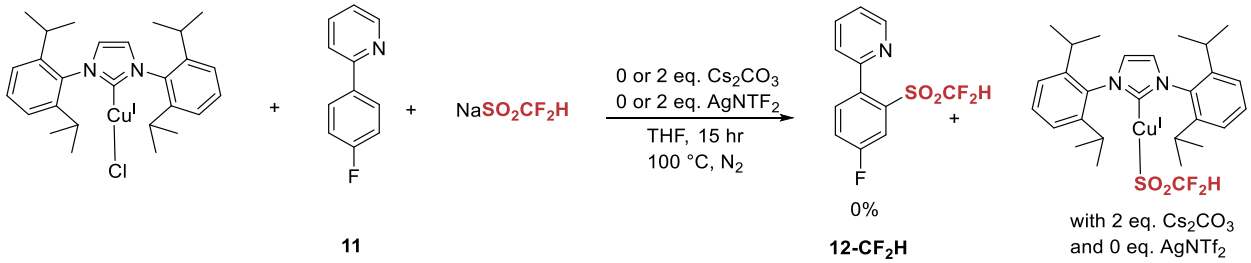
4.5 **Conclusion**

Organometallic studies were used to investigate cross-couplings between sulfinate salts and aryl iodides using N-heterocyclic carbene Cu(I) complexes as well as Ag(I) salts. A series of novel IPrCu(SO_2R) complexes were synthesized and crystallographically characterized. In all cases, the sulfinate binds Cu through the oxygen, as opposed to the sulfur. These complexes show divergent reactivity based on the sulfinate substituent. The SO_2CF_3 complex undergoes desulfinylation upon oxidative addition of the aryl iodide, ultimately resulting in Ar–CF_3 coupling.

In contrast, all of the other sulfinate complexes react with ArI to afford Ar–SO_2R coupling products. The reactivity was expanded to using CuCl as a starting material, demonstrating that N-heterocyclic carbene ligation, $NaSO_2R$ transmetallation, ArI oxidative addition, and Ar–SO_2R reductive elimination can all occur productively in a single pot, especially if the sulfinate nucleophile is electron rich. Finally, control studies uncovered that silver, the 2nd row congener of copper, is competent for the cross-coupling of ArI with $NaSO_2CF_2H$ and $NaSO_2CF_3$. instead of IPrCuCl or CuCl. In the Ag system, desulfinylation is not detected with $NaSO_2CF_3$.

4.6 **Outlook**

Moving forward, several key details about the stoichiometric reactions will be investigated in further detail. Optimization of solvent, temperature, and stoichiometry of the reagents will be pursued. Rate studies of the reactions in **Tables 4.1** and **4.2** will provide further insights into sulfinate electronic effects on the slow step of the sequence (proposed to be oxidative addition). These stoichiometric investigations will be leveraged to inform the identification of catalysis conditions. One promising direction in this regard will be to use Cs_2CO_3 to promote transmetalation, since preliminary results show that this base is effective in promoting transmetallation between **10** and $NaSO_2CF_2H$ (**Scheme 4.4**). The carbonate base may generate a Cu(I)-ate complex that is primed for transmetallation.



11 **12-CF$_2$H**

Scheme 4.4. Attempts at C-H activation using **10** and a combination of Cs_2CO_3 and $AgNTf_2$. Formation of **10-CF$_2$H** identified from ^{19}F NMR

Studying the role of the silver is also of high interest for several reasons. First, the proposed coordination complexes between Ag^I and product complicate the analysis of these reactions, since their broad peaks shift based on concentration and silver equivalents. Confirming the identity of these species will be essential to understanding these systems. Second, silver has been known to participate is several modes of reactivity. Homogenous silver species, including those bearing NHC ligands, can perform cross-coupling reactions.[10] Recently, Dr. Taylor Spiller in the Sanford

showed that silver nanoparticles in the presence of visible light can mediate the transfer of aryl group from ArX to a copper species. The Ar–SO_2R coupling reactivity is maintained in the absence of light, but there is a major difference in the behavior in the presence of silver. Next, silver salts are known as halogen-abstractors, which was the intended purpose of them in this reaction. Finally, silver salts can be oxidants, and their oxidation potential can vary greatly depending on the solvent.[11] Many of the reactions described above ended with a blue reaction color. Blue is a color commonly associated with Cu(II), implying that some of the silver oxidized Cu(I) to Cu(II). The competency of Cu(II) species in this reaction has not been investigated.

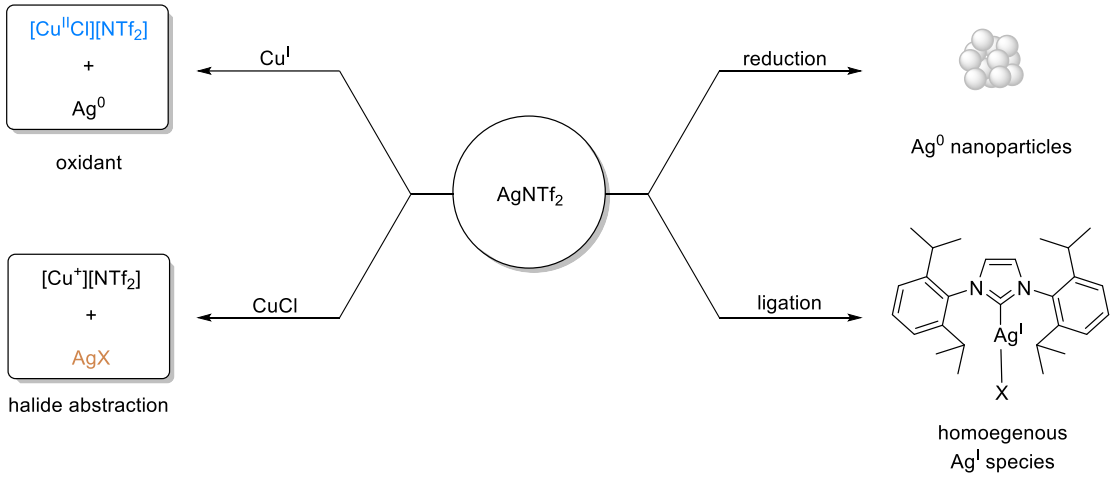


Figure 4.4. Different proposed roles of silver in the cross-coupling of aryl iodides with sulfinates. The left side demonstrates the most commonly implicated roles of silver in catalytic reactions, while the right side shows the less studied and more reactive roles that sivler can play. The upper half demonstrates Ag(0) pathways while the bottom half shows Ag(I) pathways.

The observation of desulfinylation is exciting; however, it is currently limited to the $NaSO_2CF_3$ salt. This is still a very important result, as typical CF_3 sources in transition-metal mediated trifluoromethylation are relatively expensive liquids like $TMSCF_3$, which has poor stability under typical cross coupling conditions.[12] In contrast, $NaSO_2CF_3$ is an air stable, inexpensive solid. Traditional methods for using $NaSO_2CF_3$ as a CF_3 source require peroxide oxidants and form radical species that give rise to poor chemoselectivity and regioselectivity. Harnessing this desulfinylation at Cu for cross-coupling could address these issues. Expanding the desulfinylation to less electron-withdrawing substituents would expand the R groups that could be coupled. A possible method for achieving this would be the use of Lewis acids to coordinate to the SO_2 and promote SO_2 extrusion.

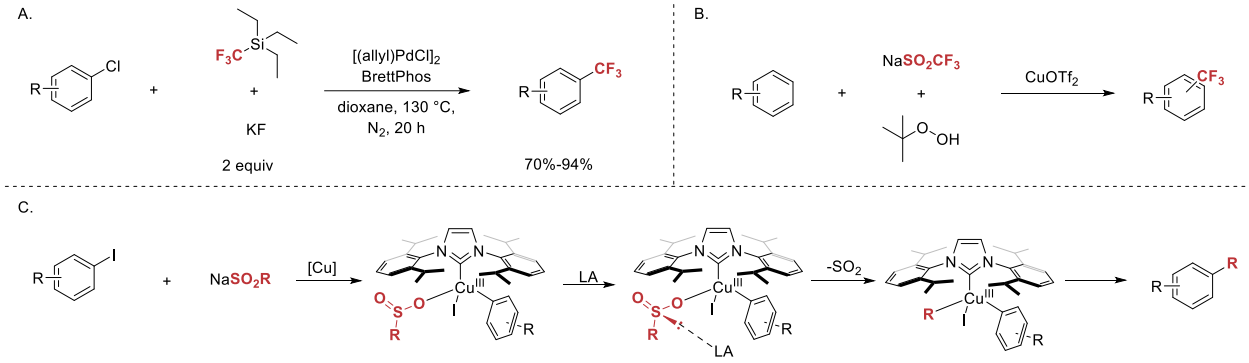
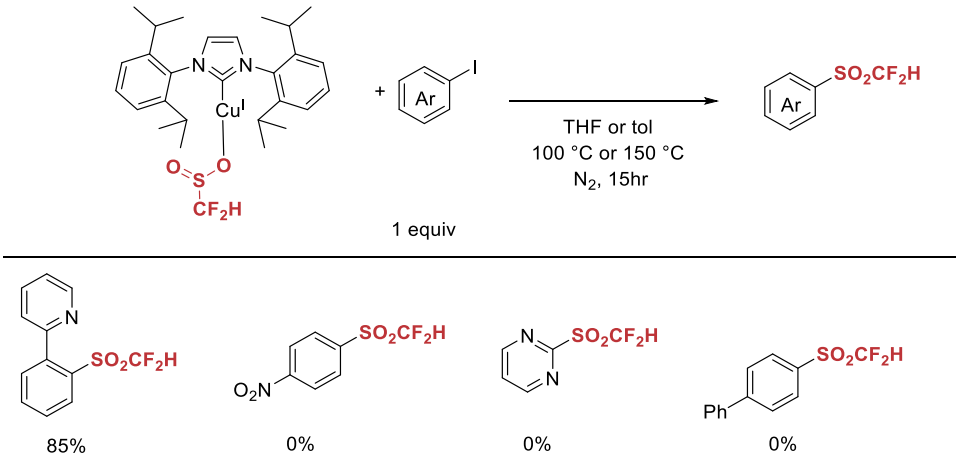


Figure 4.5. A. Pd-catalyzed trifluoromethylation of aryl chlorides from the Buchwald lab using silyl sources of CF_3. B. General scheme of Langlois radical CF_3 production from $NaSO_2CF_3$ for trifluoromethylation of arenes. C. Proposed Lewis acid activation of copper-bound sulfinates to promote desulfinylation.

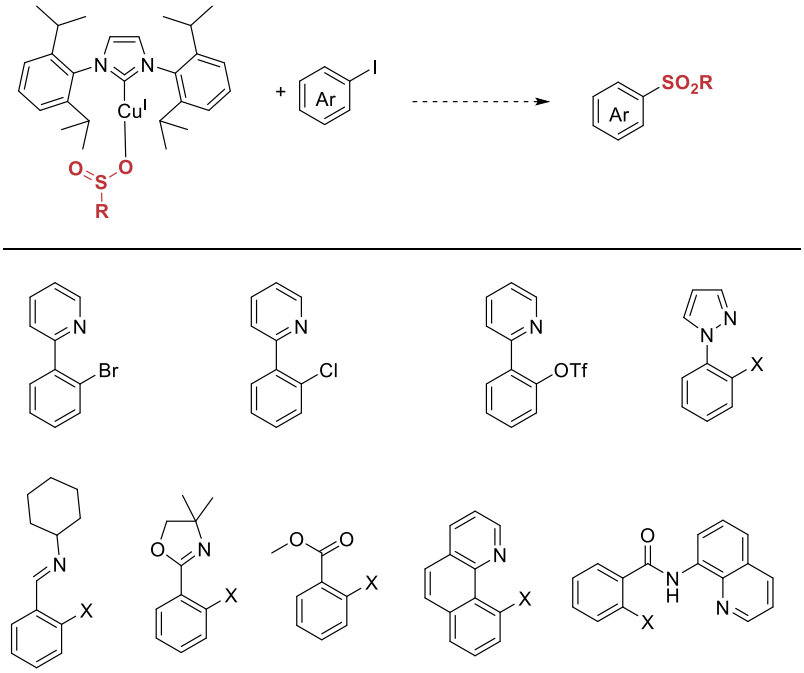
Finally, an expansion of the electrophile scope would be highly desirable. Thus far, only 2-(2-pyridyl)-5-fluoro iodobenzene and 2-(2-pyridyl)-iodobenzene have proven competent in these reactions. 2-Iodopyrimidine, 4-nitroiodobenzene, and 4-phenyliodobenzene have been preliminarily explored and returned no product.



Scheme 4.6. Scope of attempted electrophiles with stoichiometric reactivity with **10b**. Yields determined by ^{19}F NMR spectroscopic analysis

These studies should start by examining the bromide and chloride analogues of **11** to evaluate the efficacy of directed oxidative addition with less reactive halides. Notably, aryl chlorides and bromides were viable substrates for directed fluorination and fluoroalkylation reactions using IPrCuX complexes. Next, other directed aryl iodides, including iodobenzoquinoline and 1-iodo-

2,3,4,5-tetrafluoro-N-(8-quinoline)benzamide, should be explored to assess the breadth of directed IPrCu(SO_2R) complex reactivity. Accessing Cu^I–aryl intermediates via directed C-H activation would represent another synthetically useful step forward for this chemistry.



Scheme 4.7. Substrate scope with candidates for expanded scope of directed aryl halides.

4.7 Experimental

4.7.1 Synthesis of Copper Species

General Synthesis of 10-R: **10-Cl** was added to a vial with 1 equiv of $AgBF_4$ with a stirbar and THF were added, and the reaction was stirred for 15 min. The AgCl was then removed by filtration using a 0.45-micron syringe filter, with the filtrate solution directly transferred into a vial containing 2 equiv of $NaSO_2CF_3$. The reaction was stirred at 25 ºC for 15 h, concentrated *in vacuo*, and then the resulting white solid was redissolved in dichloromethane This heterogenous mixture was filtered to remove NaCl as well as any remaining sulfinate salt. The product was then recrystallized at –35 ºC from a solution of CH_2Cl_2 and pentane to afford **10-R** as clear crystals suitable for SC-XRD. Yields are isolated after one recrystallization; additional product can be obtained through further recrystallizations of the mother liquor.

R= CF_3: ~1 : 1 solution of DCM to pentane was used. 64% yield. ^{1}H NMR (500 MHz, $CDCl_3$) δ 7.44 (t, *J* = 7.8 Hz, 2H), 7.25 (d, *J* = 7.7 Hz, 4H), 7.10 (s, 2H), 2.46 (hept, *J* = 7.0 Hz, 4H), 1.21 (d, *J* = 6.8 Hz, 12H), 1.16 (d, *J* = 6.9 Hz, 12H). ^{13}C NMR (126 MHz, $CDCl_3$) δ 145.50, 134.17, 130.69, 124.27, 123.38, 28.78, 24.54, 24.00. Carbene carbon peak was not observed in any spectra. Isopropyl methyl carbon peaks appear as one signal, despite chemical differences. The trifluoromethyl carbon was not observed due to complex splitting. ^{19}F NMR (564 MHz, CD_2Cl_2) δ -88.00

R= CF_2H: ~1 : 1 solution of DCM to pentane was used. 53% yield. ^{1}H NMR (500 MHz, $CDCl_3$) δ 7.45 (t, *J* = 7.8 Hz, 2H), 7.25 (d, *J* = 7.8 Hz, 4H), 7.11 (d, *J* = 1.4 Hz, 2H), 4.25 (t, *J* = 55.7 Hz, 1H), 2.46 (hept, *J* = 6.9 Hz, 4H), 1.19 (dd, *J* = 31.1, 6.9 Hz, 24H). ^{13}C NMR (126 MHz, $CDCl_3$) δ 145.60, 134.24, 130.71, 124.30, 123.36, 28.80, 24.62, 24.03. Carbene carbon peak was not observed in any spectra. Isopropyl methyl carbon peaks appear as one signal, despite chemical differences. The difluoromethyl carbon was not observed due to complex splitting.^{19}F NMR (564 MHz, CD_2Cl_2) δ -125.86 (d, *J* = 56.1 Hz).

R= CFH_2: ~1 : 1.5 solution of DCM to pentane was used. 64% yield. ^{1}H NMR (500 MHz, $CDCl_3$) δ 7.44 (t, *J* = 7.8 Hz, 2H), 7.25 (d, *J* = 7.8 Hz, 4H), 7.10 (s, 2H), 3.69 (d, *J* = 48.8 Hz, 2H), 2.47 (hept, *J* = 6.9 Hz, 4H), 1.20 (dd, *J* = 35.0, 6.9 Hz, 24H). ^{13}C NMR (126 MHz, $CDCl_3$) δ 145.63, 134.32, 130.67, 124.28, 123.31, 100.40 (d, *J* = 212.4 Hz), 28.79, 24.68, 24.02. Carbene carbon peak was not observed in any spectra. Isopropyl methyl carbon peaks appear as one signal, despite chemical differences. ^{19}F NMR (564 MHz, CD_2Cl_2) δ -212.45 (t, *J* = 48.8 Hz).

R= CH_3: ~1 : 3 solution of DCM to pentane was used. 87% yield. ^{1}H NMR (500 MHz, $CDCl_3$) δ 7.42 (t, *J* = 7.8 Hz, 2H), 7.23 (d, *J* = 7.8 Hz, 4H), 7.12 (s, 2H), 2.46 (hept, *J* = 6.9 Hz, 4H), 1.62 (s, 2H), 1.18 (dd, *J* = 21.0, 7.0 Hz, 24H). ^{13}C NMR (126 MHz, $CDCl_3$) δ 145.63, 134.37, 130.62, 124.25, 123.42, 50.93, 28.76, 24.77, 23.97. Carbene carbon peak was not observed in any spectra. Isopropyl methyl carbon peaks appear as one signal, despite chemical differences

R= CH_3: ~1 : 3 solution of DCM to pentane was used. 43% yield. ^{1}H NMR (500 MHz, $CDCl_3$) δ 7.45 (t, *J* = 7.8 Hz, 2H), 7.23 (d, *J* = 7.8 Hz, 4H), 7.05 (s, 2H), 7.03 (d, *J* = 7.8 Hz, 2H), 6.89 (d, *J*

= 7.7 Hz, 2H), 2.45 (hept, *J* = 7.0 Hz, 4H), 2.24 (s, 3H), 1.15 (dd, *J* = 15.2, 6.9 Hz, 24H). ^{13}C NMR (126 MHz, $CDCl_3$) δ 145.59, 134.37, 130.53, 128.78, 124.21, 123.77, 123.19, 28.76, 24.66, 23.96, 21.32. Carbene carbon peak was not observed in any spectra. Isopropyl methyl carbon peaks appear as one signal, despite chemical differences

4.7.2 Stoichiometric Oxidative Addition Reactions

General Procedure for stoichiometric cross-coupling screen of 10-R with 11: In a N_2-filled glovebox, a 4 mL vial was charged with 1 equiv of **10-R** and a stir bar. A 20 mL vial was charged with 2x equiv of **11**, x equiv of ^{19}F NMR standard ($PhOCF_3$), and x mL of THF to make a stock solution of substrate and standard where x = 1+ the number of reactions to run. 1mL of this stock solution was added to each 4 mL containing **10-R**. The remaining portion of the stock was placed in an NMR tube to determine the ratio of **11** to standard. The reaction vials were capped, wrapped in electrical tape inside the glovebox, removed from the glovebox and wrapped again for additional security. These vials were placed on a 100 °C hot plate and stirred for 8 h. Products of each reaction was determined by ^{19}F NMR analysis, ESI-MS and GC-MS. **13-CF_3** was synthesized independently and spiked to confirm.

4.7.3 10-CF_3 Time Study

In a N_2-filled glovebox, a 4 mL vial was charged with 3 equiv. **10-CF_3**, 5 mg (0.0167 mmol, 1 equiv) **11**, 1 equiv $PhOCF_3$ and 1mL of THF. This homogenous mixture was transferred to an NMR tube, with was capped, carefully wrapped in electrical tape. An initial ^{19}F NMR was taken, then the tube was placed in a 100 °C NMR tube heating mantle for the time study

4.7.4 10-Cl Control Reaction

In a N_2-filled glovebox, a 4mL vial was charged with 1 equiv of **10-Cl**, 5 mg (0.0167 mmol, 1 equiv) of **11** and 1 mL of THF. This vial was capped, wrapped in electrical tape inside the glovebox, removed from the glovebox and wrapped again for additional security. This vial was placed on an 100 °C hot plate and stirred for 15 h

4.7.5 Stoichiometric Transmetallation and Oxidative Addition Reactions

General Procedure for stoichiometric transmetallation and oxidative addition screen of 10-Cl with sulfinate salts 11 and $AgNTf_2$: In a N_2-filled glovebox, 4mL vials were charged with 2 equiv $AgNTf_2$, 2 equiv appropriate sodium sulfinate, and a stir bar. A 20mL vial was charged with x equiv of **10-Cl**, x equiv of **11**, x equiv of ^{19}F NMR standard ($PhOCF_3$), and x mL of THF to make a stock solution of substrate and standard where x = 1+ the number of reactions to run. 1mL of this stock solution was added to each 4mL containing the other reagents. The remaining portion of the stock was placed in an NMR tube to determine the ratio of **11** to standard. The reaction vials were capped, wrapped in electrical tape inside the glovebox, removed from the glovebox and wrapped again for additional security. These vials were placed on a 100 °C hot plate and stirred for 8 h. Products of each reaction were determined by ^{19}F NMR analysis, ESI-MS and GC-MS.

General Procedure for stoichiometric transmetallation and oxidative addition screen of CuCl, IPrHCl, and K_3PO_4, with sulfinate salts, 11 and $AgNTf_2$: In a N_2-filled glovebox, 4 mL vials were charged with 2 equiv $AgNTf_2$, 2 equiv appropriate sodium sulfinate, 1 equiv K_3PO_4, 1 equiv CuCl and a stir bar. A 20mL vial was charged with x equiv of IPrHCl, x equiv of **11**, x equiv of ^{19}F NMR standard ($PhOCF_3$), and x mL of THF to make a stock solution of substrate and standard where x = 1+ the number of reactions to run. 1mL of this stock solution was added to each 4 mL containing the other reagents. The remaining portion of the stock was placed in an NMR tube to determine the ratio of **11** to standard. The reaction vials were capped, wrapped in electrical tape inside the glovebox, removed from the glovebox and wrapped again for additional security. These vials were placed on a 100 °C hot plate and stirred for 8 h. Products of each reaction were determined by ^{19}F NMR analysis, ESI-MS and GC-MS.

4.7.6 Silver-mediated Aryl-Sulfone Coupling

General Procedure for Silver-mediated coupling reactions: In a N_2-filled glovebox, a 4 mL vial was charged with 1 equiv of **11**, 2 equiv of $AgNTf_2$, 2 equiv of $NaSO_2R$, 1 equiv of $PhOCF_3$ standard, and appropriate equiv of **10-Cl** or CuCl/IPrHCl/K_3PO_4. The reaction vials were capped, wrapped in electrical tape inside the glovebox, removed from the glovebox and wrapped again for

additional security. These vials were placed on a 100 °C hot plate and stirred for 15 h. Products of each reaction were determined by ^{19}F NMR analysis, ESI-MS and GC-MS.

4.8 References

1. Zhu. W; Ma. D. "Synthesis of Aryl Sulfones via L-Proline-Promoted CuI-Catalyzed Coupling Reaction of Aryl Halides with Sulfinic Acid Salts", *J. Org. Chem.*, **2005**, 70, 2696-2700
2. Mei, M-S.; Meng, F.; Tang, J.; Yi, D.; Zhang, Y. "Copper-Mediated C4-H Sulfonylation of Indoles via a Transient Directing Group Strategy" *Org. Lett.*, **2025**, 27, 9710–9715
3. Zhang, L.; Du. W.; Wu, J.; Yang, R.; E. X.; Wang, J.; Xia, Z. " Au(I)/Au(III)-Catalyzed Sulfonylation of Aryl Iodides for the Synthesis of Various Functionalized Aryl Sulfones", *Org. Lett.*, **2024**, 26, 9413-9418
4. Sharninghausen, L. S.; Brooks, A. F.; Winton, W. P.; Makaravage, K. J.; Scott, P. J. H.; Sanford, M. S. "NHC-Copper Mediated Ligand-Directed Radiofluorination of Aryl Halides", *J. Am. Chem. Soc.*, **2020**, 142, 16, 7362–7367
5. Hall, J. R.; Blythe, I. M.; Sharninghausen, L. S.; Sanford, M. S. "Copper-Mediated Fluoroalkylation of Aryl Bromides and Chlorides Enabled by Directing Groups", *Organometallics*, **2023**, 42, 7, 543–546
6. Langlois, B. R.; Laurent, E.; Roidot, N. "Trifluoromethylation of aromatic compounds with sodium trifluoromethanesulfinate under oxidative conditions", *Tet. Lett.*, **1991**, 32, 7525-7528
7. Fujiwara, Y.; Dixon, J. A.; Rodriguez, R. A.; Baxter, R. D.;, Dixon, D. D.; Collins, M. R., Blackmond, D. G., Baran, P. S. "A New Reagent for Directo Difluorimethyltion" J. *Am. Chem. Soc*. **2012**, 134, 3, 1494–1497
8. Dang, H.; Mailig, M.; Lalic, G. "Mild COpper-Catalyzed Fluorination of Alkyl Triflates with Potassium Fluroide", *Angew. Chem. Int. Ed.* **2014**, 53, 6473–6476
9. Voloshkin, V. A.; Zorba, L. P. Nolan, S. P. "The influential ^{I}Pr: 25 years after its discovery
10. Anand, N. S.; Philip, R. M.; Anilkumar, G. "Silver-catalyzed decarboxylative cross-couplings" *Tetrahedron,* **2023**, 133715

11. Connelly, N. G.; Geiger, W. E. “Chemical Redox Agents for Organometallic Chemistry: *Chem. Rev.* **1996**, 96, 877-910
12. Cho, E. J.; Senecal, T. D.; Kinzel. T.; Zhang, Y.; Watson, D. A.; Buchwald, S. L. “The Palladium-Catalyzed Trifluoromethylation of Aryl Clorides”, *Science*, **2010**, 328, 1679-1681

Chapter 5 Formation and Electrochemical Study of Fe(0) Phosphine Complexes from Bench-Stable Fe(II) Precatalysts

5.1 **Background**

Iron(0) phosphine complexes – (P-P)Fe^0 – have been known to promote activation of E-H bonds for the past 50 years. E-H bonds (E = B,[1] Si[2], C_{sp}, C_{sp2}, and C_{sp3}[3-5]) can all react stoichiometrically with bis-(1,2-disubstituted-phosphinoethane)Fe^0 complexes, forming Fe^{II}(H)(E) oxidative addition complexes, **Figure 5.1a** Recently, Holland has shown that this reactivity is not limited to phosphine complexes and that Fe complexes bearing anionic 1,2-diketiminide ligands also facilitate C-H activation[6] with the assistance of alkali metal cations.[7]

Despite this long history of stoichiometric E-H bond activation, subsequent functionalization of the Fe organometallic intermediates has been sparse. To date, there are only four reports that have succeeded in capturing these to achieve downstream reactivity. In the first example, Jesson and coworkers[4] coupled CO_2 to C-H activated acetonitrile complexes. Holland[6] coupled benzene with a dinitrogen derivative in a stoichiometric, stepwise fashion. In 2015, Darcel[1] showed the first catalytic methodology by coupling pinacol borane with electron-rich arenes using di-(1,2-bis-dimethylphosphinoethane)-iron(II)-dimethyl (**A1**) as a precatalyst. Finally, and most recently, Ackermann performed alkenylation of ketimines, using di-(1,2-bis-diphenylphosphinoethane)-iron(II)-hydride (**B1**)[8] or (1,2-bis-diphenylphosphinoethane)-iron(0)-η^6-tolyl (**B2**)[9] as a precatalyst, **Figure 5.1b**.

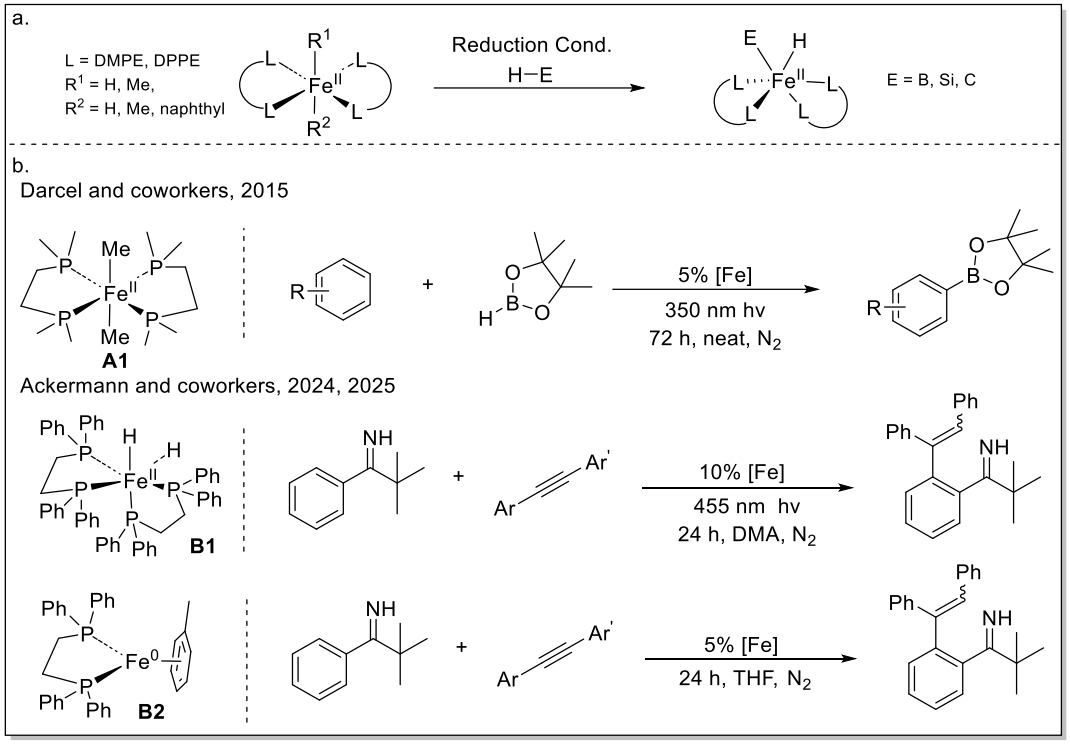


Figure 5.1. (a) E–H bond activation at bis-ligated Fe(0) complexes. (b) Catalytic methods involving bis-ligated Fe(0) complexes.

A major reason for the lack of methodologies stemming from this reactivity is that accessing the reactive iron(0) intermediates is very challenging and studying these complexes is even more difficult. For example, the starting Fe complexes for the Darcel and Ackermann methodologies (**A-1** and **B-1**) are highly air-sensitive neutral Fe(II) species that require several pyrophoric reagents to synthesize. Even after the successful synthesis and isolation of these complexes, the subsequent reduction to Fe(0) is uncontrolled and hard to investigate.

Some of the earliest reductions of Fe(II) to Fe(0) in the literature were chemical or thermal reductions. In 1968, Miyake and coworkers used ethoxydiethylaluminum to reduce of $Fe(acac)_3$ in the presence of DPPE.[10] This was proposed to yield the Fe(0) complex **B1a**, which underwent rapid intramolecular C–H activation to generate **B3**. In 1977, Jesson and coworkers leveraged the reversible reductive elimination of naphthalene from $(DMPE)_2Fe(H)(naphthyl)$ (**A3)** to access a proposed $(DMPE)_2Fe^0$ analogous to **B1a**.[4] This complex underwent intermolecular activation of solvent to yield C_{sp}, C_{sp2}, and C_{sp3}-H activation products. A decade later in 1986, Field and Baker showed that (DEPE)Fe(II) complex **C1** undergoes a thermal reductive elimination of methane,

followed by an analogous intermolecular solvent activation.[5] Using ^{31}P NMR, they observed a transient species, which they proposed as **C2**, a strained intramolecular C–H activation product analogous to the more stable complex **B3**. Finally, Ackermann has used ^{t}BuMgCl to reduce the (DPPE)Fe(Br)$_2$ (**B4**) in the presence of electron-rich arenes to form (DPPE)Fe^0(η^6-arene) species.[9]

In 1983, Morris and Azizian showed that the reduction of Fe(II) complex **B1** to **B3** proceeds under irradiation at 366 nm.[11] This work was followed up in 1993 by George and coworkers with the reduction of (DMPE)$_2$Fe(H)$_2$ (**A2**) via rapid photo-reduction with pulsed lasers at low temperatures.[3] This sequence yielded solvent C-H activated iron(II) complexes. Darcel and coworkers[1] harnessed an analogous pathway using (DMPE)$_2$Fe(Me)$_2$ as a pre-catalyst in combination with 350 nm irradiation to yield catalytically active Fe(0) for C–H borylation. Finally, Ackermann harnessed a photochemical activation approach using pre-catalyst **B1** and 445 nm irradiation to achieve the coupling of C_{sp2}–H substrates with alkynes.[8]

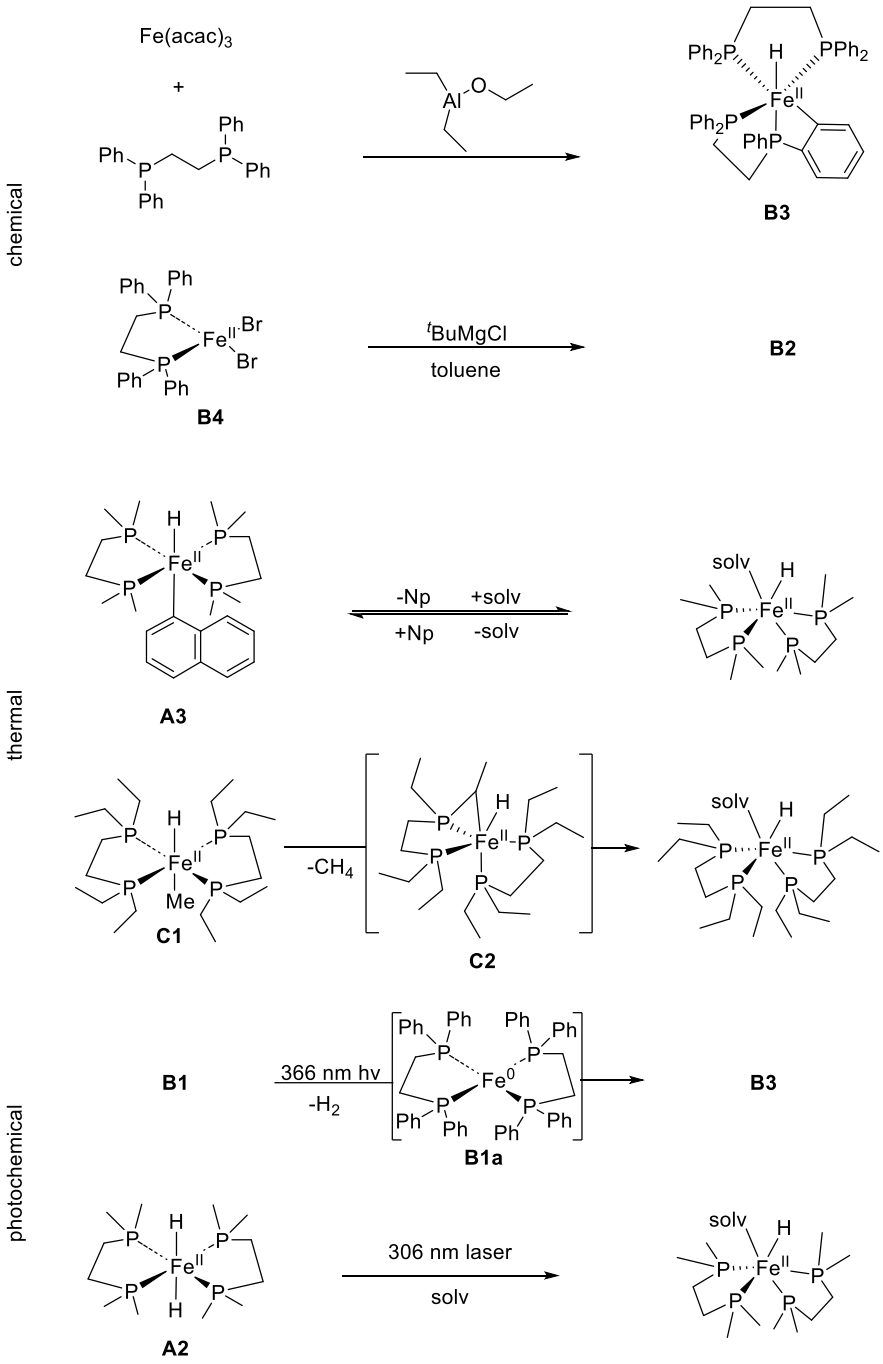


Figure 5.2. Chemical, thermal, and photochemical methods to access Fe(0) phosphine complexes.

While the reduction methods in Figure **5.2** have various benefits, one obvious omission is electrochemical reduction. We anticipated that electrochemical reduction could proceed with a more diverse array of Fe(II) precursors than the literature methods, thus potentially enabling the

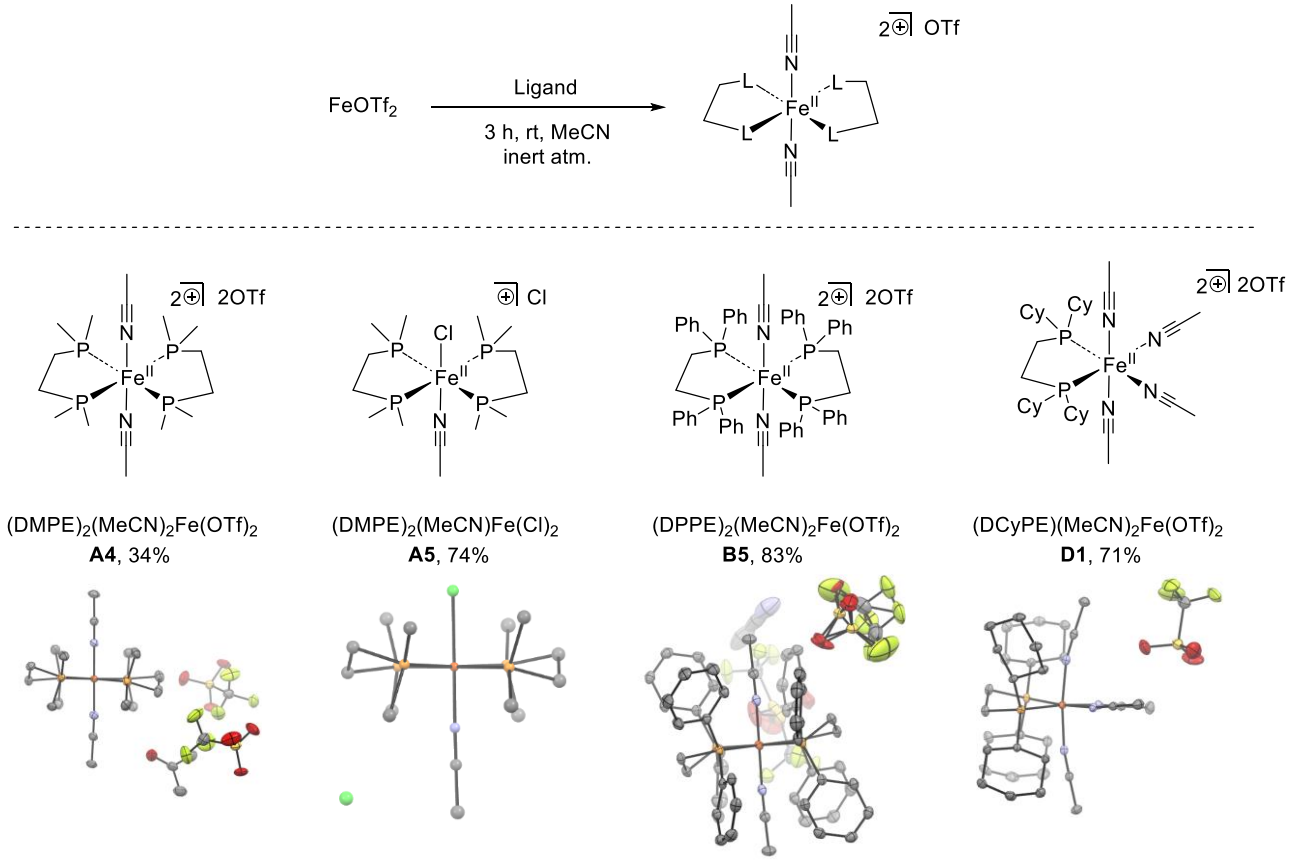
use of bench-stable precatalysts. Additionally, electrochemistry enables much more controlled pathways for the reduction Fe(II) species, thus offering the potential for higher yields and or different structures of the Fe(0) products. Finally, the use of reference electrodes, along with the potentiostat, should allow us to gather *in situ* mechanistic data about these reduction processes, such as the number of electrons passed at a given potential. Overall, the goals of these studies were two-fold. First, we sought to develop readily accessible, bench-stable Fe(II) precursors that could serve as precursors to catalytically relevant Fe(0) species. Second, we sought to use electrochemistry to reduce these compounds and study to corresponding pathways.

5.2 **Synthesis and Characterization of Dicationic Bidentate Phophosine Iron(II) Complexes**

The general structure of the precursors used in the literature for thermal or photochemical activation are Fe(II) bisphosphine complexes bearing two anionic ligands, most commonly hydride or methyl. These anionic ligands are highly electron-donating and are the source of the general instability of these complexes. For instance, every iron precursor described in **Figure 5.2** is air sensitive. For the current work, we sought cationic iron phosphine complexes with outer-sphere anions. Our initial investigations led us to the work of DuBois who developed the synthesis of $(PPh_3)(MeCN)_2Fe(BF_4)_2$ and $(DPPE)_2(MeCN)_2Fe(BF_4)_2$ and studied these complexes electrochemically.[12]

The synthesis of $(DPPE)_2(MeCN)_2Fe(BF_4)_2$ proved to be highly modular, and proved applicable to three different phosphine ligands (DPPE, DCyPE, DMPE) and three different iron sources ($Fe(OTf)_2$, $Fe(BF_4)_2$, and $FeCl_2$), **Scheme 5.1**. $Fe(BF_4)_2$ and $Fe(OTf)_2$ formed isolable monomeric complexes with all of the ligands. However, $FeCl_2$ afforded infinite (and insoluble) polymers with DPPE and DCyPE.[13] The OTf counteranion was found to be the most soluble in organic solvents and was thus chosen to move forward. The BF_4 and OTf salts of each complex behaved very similarly. **A4** and the BF_4 analogue were isolated in ~30-40% yield as blocky yellow crystals due to formation of an deep orange byproduct which is likely a DMPE-bridged **A4** dimer where one DMPE phosphorus coordinates to the apical site instead of an MeCN ligand, although the structure has not been elucidated. Comparatively, the synthesis with $FeCl_2$ forms exclusively the light pink **A5** in 74% isolated yield, likely because the inner sphere Cl prevents adventitious DMPE from binding. **B5** and **D1** and their BF_4 analogues form deep pink and blood red crystals,

respectively, in >70% as well. These complexes are all diamagnetic, low-spin Fe(II) species.



Scheme 5.1. General synthesis of dicationic phosphine-ligated Fe(II) complexes. BF_4 complexes were synthesized but excluded from presentation for brevity.

The $(P\sim P)_2Fe(MeCN)_2(OTf)_2$ complexes (**A4**, **B5**, and **D1**) are completely bench-stable. They show no degradation after months stored on the bench either as a solid or in MeCN solution. This indicates stability to both O_2 and adventitious water. The DMPE chloride complex **A5** has one chloride bound inner-sphere and one outer-sphere. **A5** is stable on the bench for roughly a week before it decomposes, demonstrating the effect of inner-sphere anions on the bench-stability of these complexes.

The acetonitrile ligand appears to be important for the stability, especially with the DCyPE ligand. When dissolved in tetrahydrofuran, this red complex bleaches and precipitates a white solid that may be free DCyPE. However, when additional MeCN is added to this mixture, the solid redissolves and the red color returns.

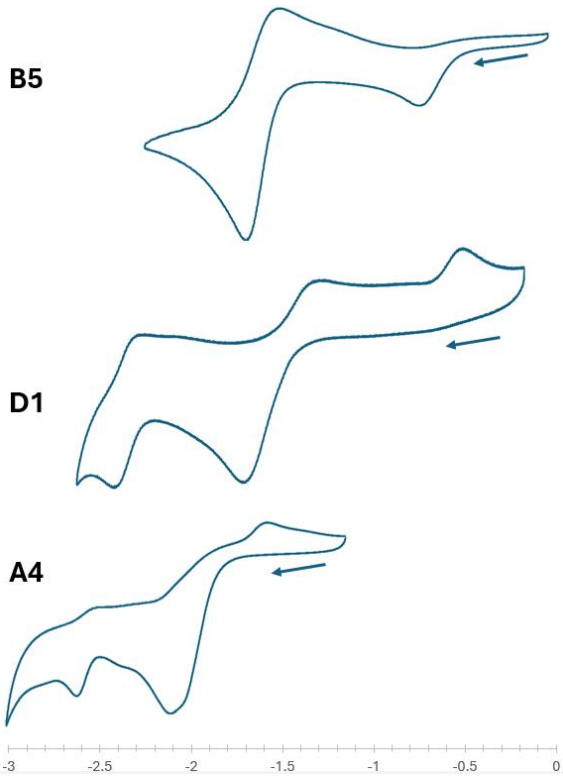


Figure 5.3. Cyclic voltammograms of **A4**, **B4**, and **D1** at 100mV dissolved in at 100 mV/s 0.1M $TBAPF_6$ in MeCN with 1mm glassy carbon disc working electrode, graphite rod counter electrode, and silver wire psuedo-reference electrode in a glass compartment connected with VyCor frit containing 0.1M $TBAPF_6$ in MeCN. Voltammograms were referenced to Fc/Fc^+

These complexes exhibit reduction potentials that are accessible within the reduction window of acetonitrile. Additionally, **B5** has a reduction potentials around 800 mV more positive than the alkyl-substituted phosphine complexes. Even though DCyPE is more electron-donating than DMPE, the reduction potentials of the corresponding complex are 17mV more positive. This is likely due to the fact that it is mono-ligated and two DMPEs and two acetonitriles provide more electron density to the metal center than one DCyPE and four acetonitriles. The 2^{nd} reduction of **A4** and **D1** are lower intensity than the first. We propose that their second reduction involves a structural rearrangement that is slower than the time scale of the CV, so the current measured is lower.

5.3 **Comparison of Reactivity Modes of Iron(II) Complexes**

The Fe precursors synthesized in this chapter did not undergo photoreduction when irradiated with UV light **(Figure 5.4).** Because of the outer-sphere anions, there is no thermodynamic product that could be released via reductive elimination. Instead, we are using these complexes to investigate the novel electrochemical pathways and benchmarking them against a chemical reduction for accessing Fe^0. Ackermann's chemical reduction with *tert*-butyl magnesium bromide[9] was used as the chemical pathway, since it is a versatile procedure that can be applied to any Fe^{II} species.

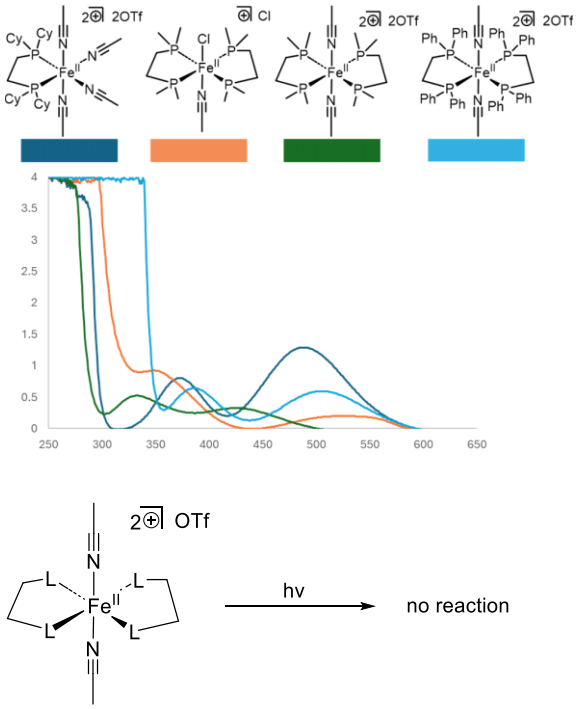


Figure 5.4. UV-Vis spectra. Photochemical irradiation of iron(II) complexes at their most energetic UV-Vis feature (**D1**: 370nm, **A5**: 370nm, **A4**: UVB, **B5**: 390nm) for 24 h in MeCN showed no change.

Reactivity of Fe Complexes

$(P\sim P)_2Fe^{II}$ complexes are the most common starting materials for chemical reduction to Fe^0. The first reported and most straightforward transformation of this class is the formation of **B3** from the reduction of $(DPPE)_2Fe^{II}$ complexes. The transient $(DPPE)_2Fe^0$ immediately undergoes intramolecular C-H activation at the ortho position of one of the phenyl groups. This forms a stable

5-membered ferrocycle, which is readily kinetically accessible and thermodynamically stable. Thus, this complex is readily formed whenever $(DPPE)_2Fe^0$ is accessed.

Treatment of a MeCN solution of **B5** with 2.1 equiv of ^{t}BuMgCl under N_2 resulted in an immediate color change from pink to dark red. ^{31}P and ^1H NMR spectroscopic analysis of the filtered solution showed the formation of **B3** in 77% yield, along with free DPPE, likely from decomposition of some of the starting complex. This result confirms that chemical reduction is a viable route from **B5** to **B3**.

Subjecting this **B5** to constant potential bulk electrolysis in a divided cell using RVC as a working electrode at -2.3V (20 mV more reducing than the 2nd cathodic peak observed during the cyclic voltammetry studies) led to complex **B3** in 86% yield along with some free DPPE. Various supporting electrolytes, including TBAOTf, $TBAPF_6$, KOTf, NaOTf, and LiOTf, afforded comparable yields and product distributions. LiOTf caused the electrolysis to take longer than the other electrolytes but still reaches the same product and product distribution.

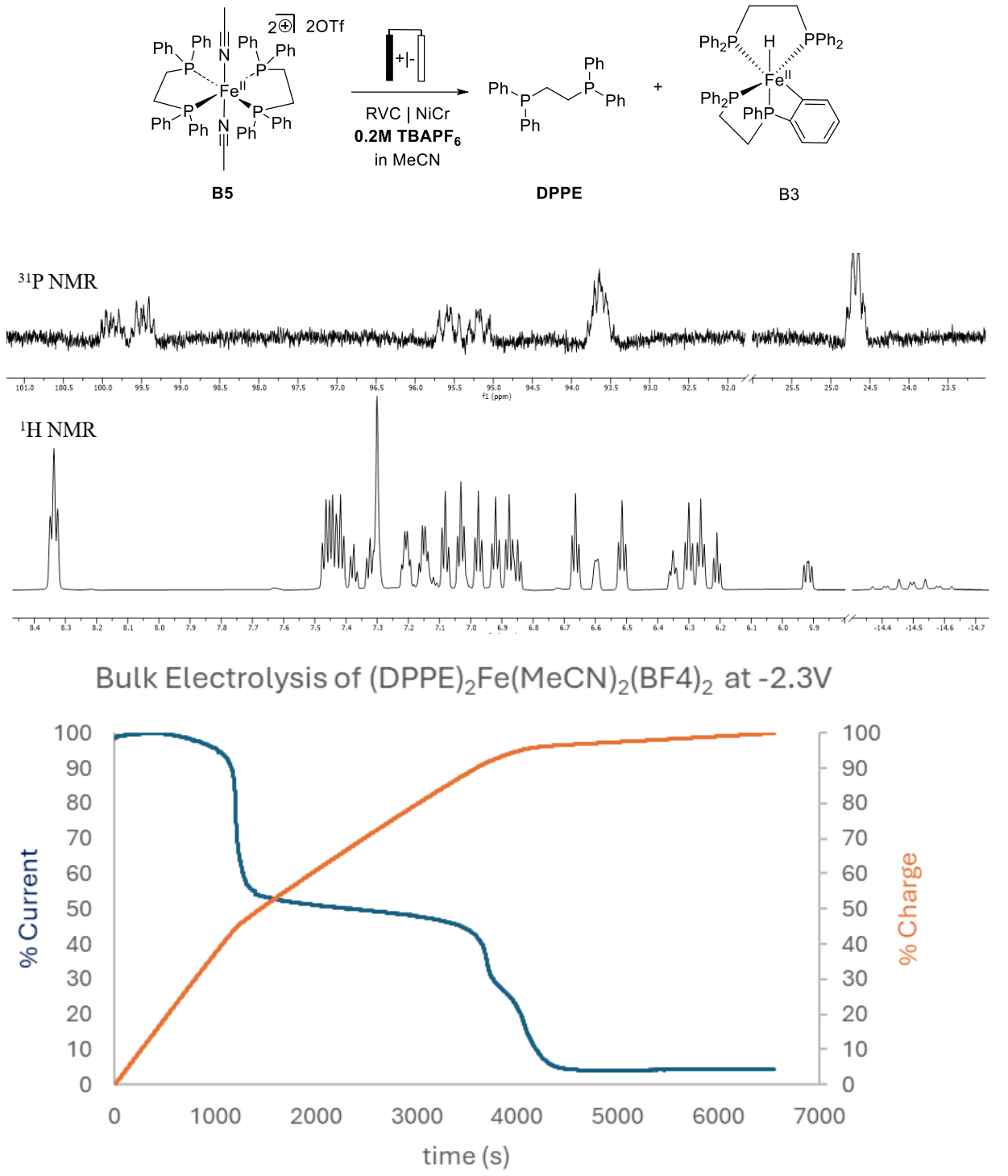


Figure 5.5. ^{1}H and ^{31}P NMR spectra of electrochemical reductions of complex **B5**. Bulk electrolysis trace of constant potential electroreduction of 0.05 mmol of **B5** where on y-axis1, the proportion of current measured based on the initial current is plotted and on y-axis2, the amount of charged passed as a proportion of theoretical charge needed to reduce the amount of complex in the reaction is plotted.

The corresponding electrochemical reduction of $(DMPE)_2Fe(OTf)_2$, **A4**, is much more complex. In 0.2 M LiOTf, different reductive behavior is observed compared to **B5**, **Figure 5.6**. Here, there are no longer 2 distinct reduction events, and instead just one is observed when the appropriate amount of charge has been passed. Additionally, the current never reaches zero, staying at ~50% of the initial current even after enough electrons for complete reduction of the complex are passed. This may be because the potentials required to reduce the DMPE complex are close to the reduction potential of acetonitrile, and this background reactivity is maintaining the current even after all of the iron species have been reduced.

The product distribution from the electrochemical reduction of **A4** was similar to that from the DPPE complex; however, the yields were significantly lower (*vide infra*). The intramolecular C-H activation complex (**A6**) is formed in 13% yield and shows a hydride signal at -11.2 ppm by ^{1}H NMR spectroscopy. Notably, an analogue of **A6** was proposed in the literature in reduction reactions of with **C1**, **Figure 5.2**[5]. We do not observe the *cis*-$(DMPE)_2Fe(H)(CH_2CN)$ species that Miyake and coworkers obtained from reduction of their $(DMPE)_2Fe(H)$(napthyl) in acetonitrile.[10] Unexpectedly, we also observe a pentet at -24.5 ppm. The coupling of this hydride corresponds to a doublet in the coupled ^{31}P NMR, suggesting a $(DMPE)_2Fe^{II}(H)(R)$ species. Miyake and coworkers previously reported this pentet to be the *trans*-$(DMPE)_2Fe^{II}(H)(CH_2CN)$ species. However, they suggested that it was the slow-forming thermodynamic product that could only be accessed through rearrangement of the *cis* complex. Since we did not observe the *cis* complex, even when taking time points during the electrolysis, we conclude that this species is instead $[(DMPE)_2Fe(H)][OTf]$, **A7**. Additionally, when a solution of this species is exposed to air, it decomposes slowly after a few days. This inconsistent with an Fe^{II} complex like *trans*-$(DMPE)_2Fe^{II}(H)(CH_2CN)$, which contains two strongly donating anionic ligands and thus should be highly oxygen sensitive.

As the post-electrolysis reaction mixture is allowed to stand at ambient temperature, the NMR signals associated with **A6** decay while those for **A7** increase. Several crystal structures containing multiply deprotonated acetonitrile species have been obtained of these reaction mixtures. Due to this, we propose that the intramolecular C-H activation product **A6** is formed initially. The Fe–C bond of **A6** is then protonated by solvent, releasing $[(DMPE)_2Fe(H)][X]$ (**A7**) and deprotonated acetonitrile that promotes further reactivity to form **A9** and **A10**.

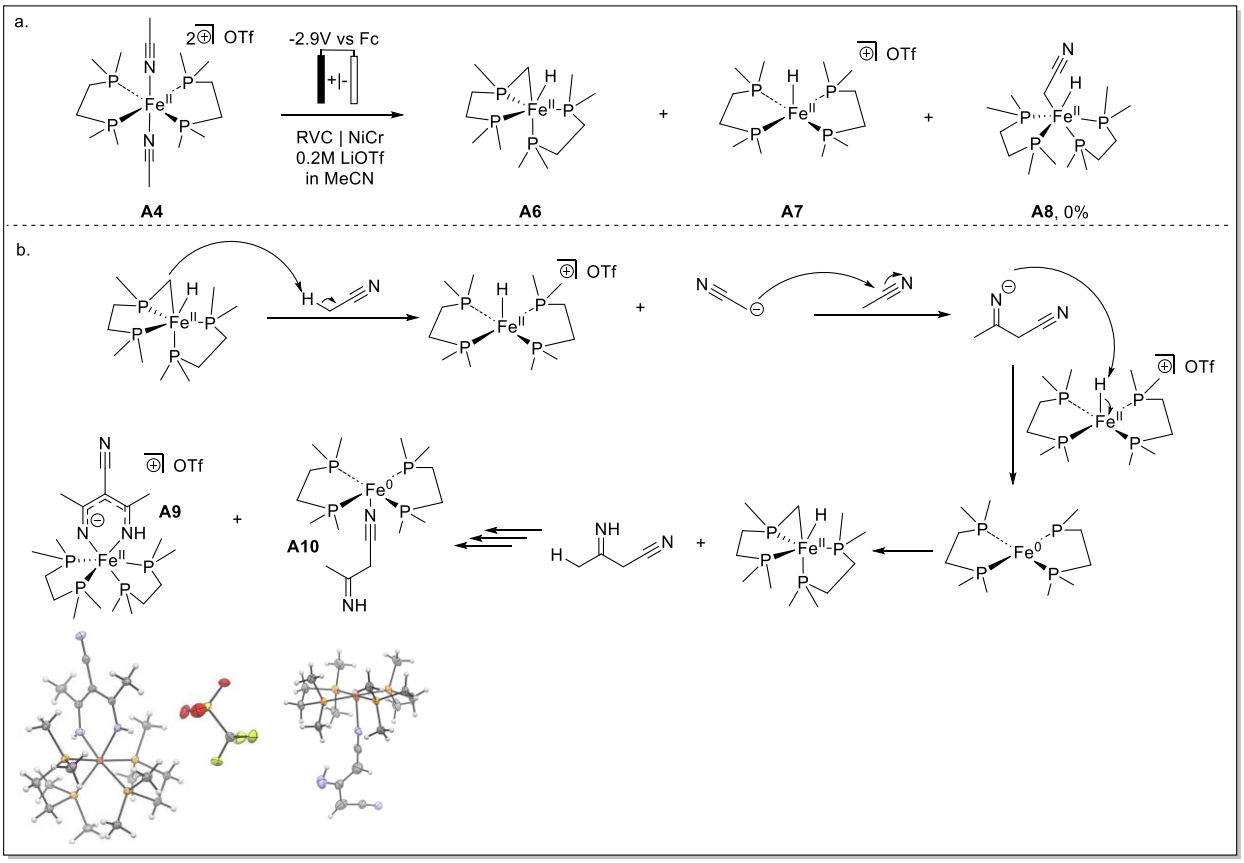


Figure 5.6. (a) Electrochemical reduction of **A4** in 0.2 M LiOTf forming **A6** and **A7** but not *cis*-(DMPE)$_2$Fe(H)(CH$_2$CN). (b) Proposed mechanism for formation of **A7**, resulting in deprotonated MeCN and downstream products. Some atoms show in the XRD structure of A9 and A10 have partial occupancies that are removed for clarity.

With (DMPE)$_2$Fe(OTf)$_2$, the supporting electrolyte plays a central role in the product distribution from electrochemical reduction. Upon moving to NaOTf, KOTf, and TBAOTf, a new species – the *cis*-(DMPE)$_2$Fe(H)(CH$_2$CN) (**A8**) – appears and **A7** diminishes until it is not present at all in TBA electrolyte, **Figure 5.7**. The overall mass balance also increases as the size of the cation increases. Focusing on TBAOTf as an electrolyte, the reduction is completely selective for intermolecular C-H activation, forming **A8** in 31% yield and **A7** is formed in 18% yield. This effect may be due to the Lewis acidity of the cations or another solvent packing effect. Recent work from the Holland group has shown that cations can play a large role in the rate of C-H activation.[7]

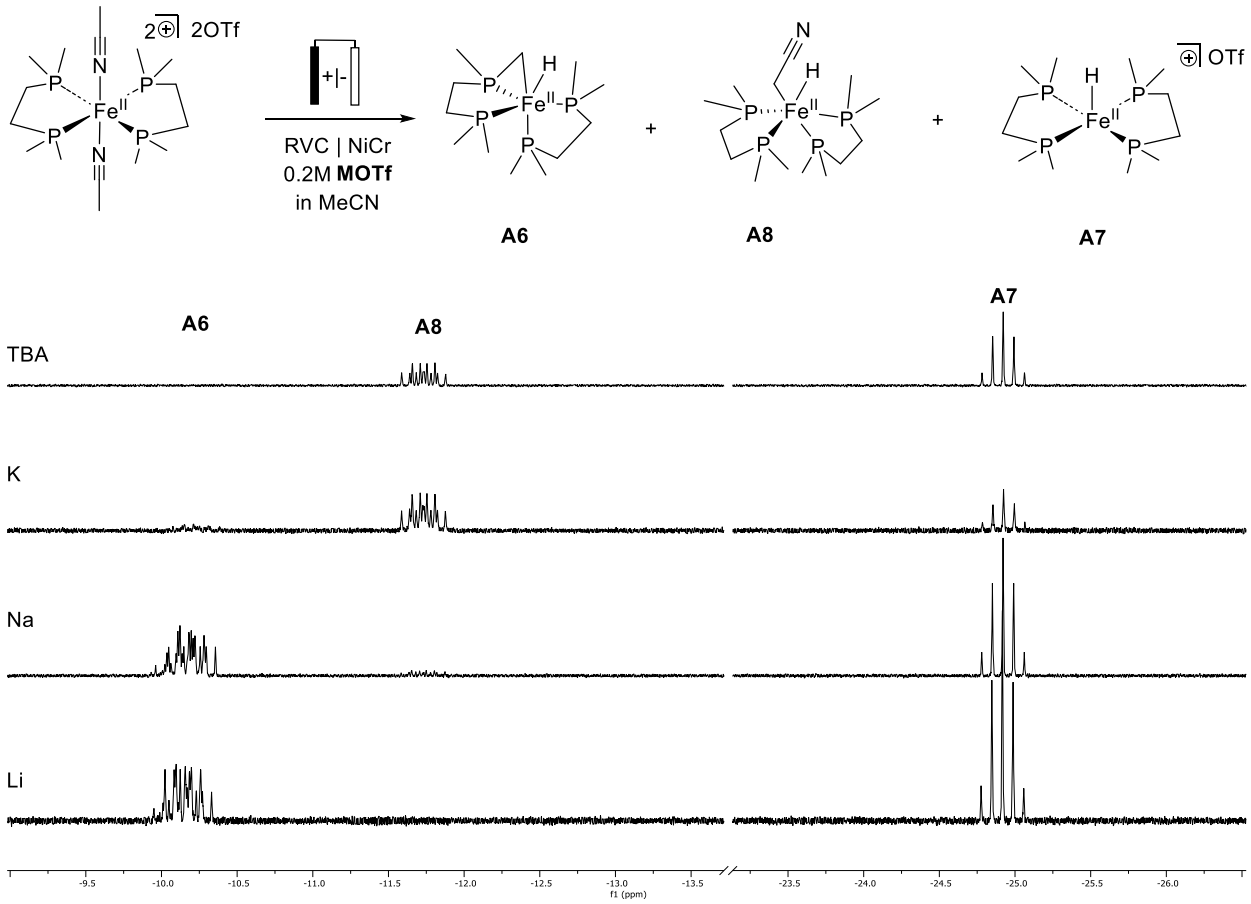


Figure 5.7.[1]H NMR spectra showing the hydride region of the electrolyte screen of the electroreduction of **A5.**

Electroreductions of **A4** in MeCN-d_3 with LiOTf or TBAOTf as the supporting electrolyte were performed under identical conditions. With TBA electrolyte, none of **A8** or **A7** was observed by ^{1}H NMR spectroscopy, **Figure 5.8, left side**. In the ^{31}P NMR spectra, the **A7D** peak is now coupled to a spin = 1 nuclei. In contrast, with Li, both **A6** and **A7** are observed, **Figure 5.8, right side**. The ratio of **A6** : **A7** in proteo solvent is 1 : 0.6, while in deuterated solvent, the ratio is now 1:0.4. In the ^{31}P NMR spectrum, both the proton coupled and deuterium coupled peaks are present. These results suggest that there are multiple pathways to access **A7**, one of them being from C-H activation of the DMPE ligand (the only source of protons) and other from solvent activation. **A7** is likely a thermodynamic sink for many of the hydride species formed. This study also provides support for the proposal that Li promotes intramolecular C-H activation while TBA promotes intermolecular C-H activation.

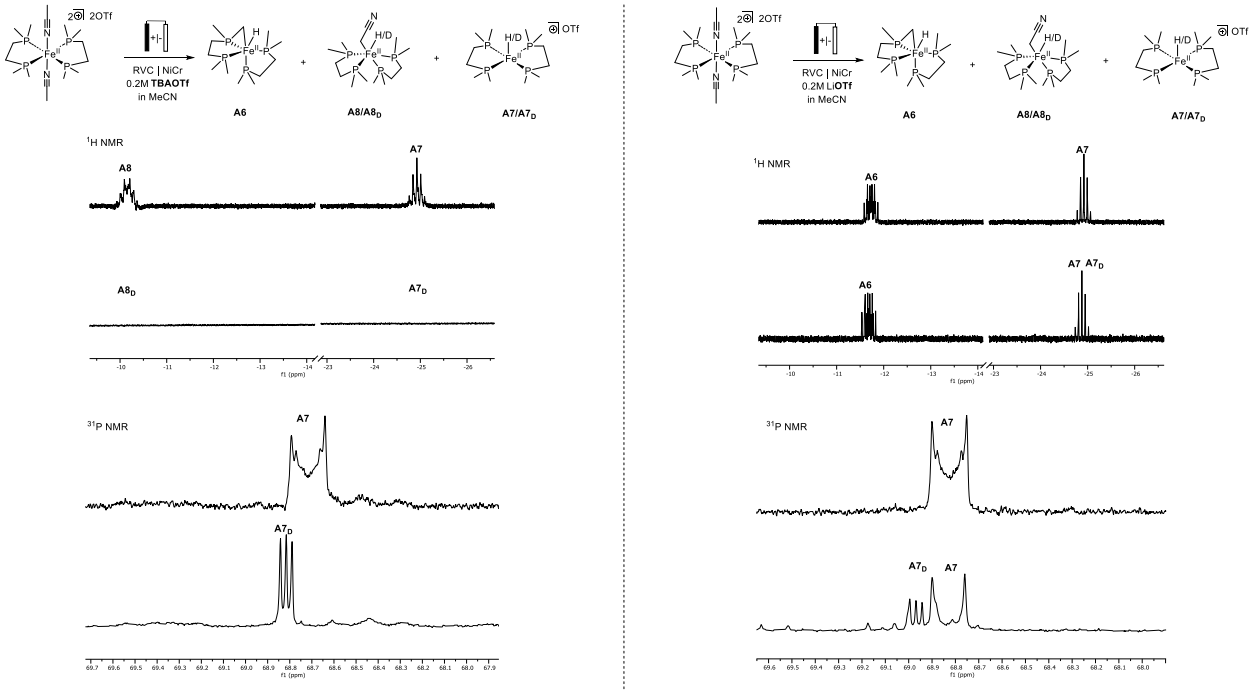


Figure 5.8. Deuterated solvent study with **A5**. Left side depicts the ^{1}H NMR (top) and ^{31}P NMR (bottom) constant potential bulk electrolysis of **A5** with TBAOTf electrolyte in MeCN-h_3 (1st) and MeCN-d_3 (2nd). Right side depicts the same data with bulk electrolysis using LiOTF electrolyte.

Chemical reduction of $(DMPE)_2Fe(OTf)_2$ with *t*-BuMgCl in MeCN yields the -25 ppm hydride (assigned as complex **A7**), the intramolecular C-H activation product **A6**, and the acetonitrile activation product **A8** in a 8 : 2 : 1 ratio. This highlights a key advantage of electrochemical reduction. The varying chemoselectivity afforded by the supporting electrolyte is another benefit of electrochemical reduction.

In comparison to bis-ligated bidentate iron phosphine complexes, studies of mono-ligated bidentate iron phosphine species for Fe^0 access are comparatively rare. The only reported example is (DPPE)Fe(η^6-arene). The Ackermann group showed that reduction of $(DPPE)FeBr_2$ (**B4**) with ^{t}BuMgCl in of toluene forms (DPPE)Fe(η^6-toluene) abduct, **B2.** However, when **B4** was reduced under constant potential bulk electrolysis at -2.3V in 0.2 M TBAOTf in MeCN in the presence of 100 equivalents of toluene, a different product was observed. The reaction changed color from pale green to a light pink and then deep orange. At the end of the reaction, the ^{1}H NMR spectrum showed majority conversion to **B3** along with some free DPPE, **Figure 5.9**. None of the η^6 toluene

complex **B2** was detected by ^{31}P NMR spectroscopy. This suggests that some of the complex decomposes under the electrochemical conditions, releasing free DPPE. This free DPPE then binds to a mono-ligated Fe species in solution, and intramolecular C–H activation occurs to form the bis-ligated species **B3**. The chemical reaction is performed in neat toluene, while the electrochemical is performed with MeCN as the solvent. The MeCN could encourage release of free DPPE that leads to the differing reactivity.

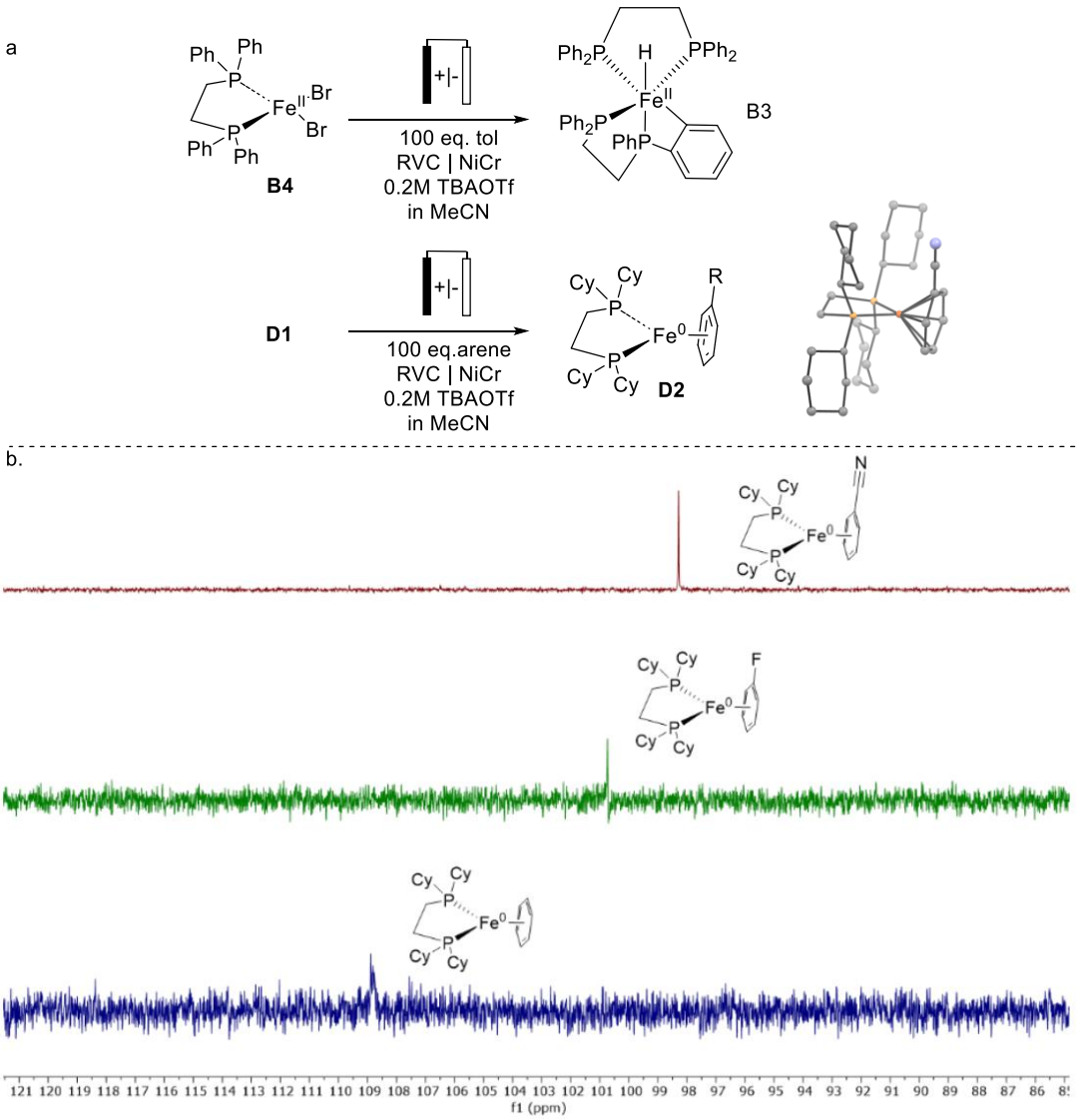


Figure 5.9. a. Electrochemical reduction of **B4** and **D1** in the presence of arene. b. ^{31}P NMR of benzonitrile, fluorobenzene, and benzene η^6- abducts with (DCyPE)Fe^0

In contrast, the mono-ligated DCyPE complex **D1** exhibits different reactivity. When reduced in the presence of MOTf (M = TBA, K, Na, or Li) in MeCN, the reaction mixture bleaches,

and the only peak observed in the ^{31}P NMR spectrum is free DCyPE. However, in the presence of 100 equiv of arene under an Ar atmosphere, the η^6 complexes were formed as the major species. The benzonitrile complex, **D2**, readily crystalized from solution after ~24 h at ambient conditions and was isolated in 64% yield and characterized by X-ray crstalllography. Interestingly, the stability of this complex is exclusive to Ar atmosphere. Under N_2, the complex forms and then slowly decomposes to form green and brown colored products. These may be the result of a N_2-adduct that performs deleterious reactivity which yields a ^{31}P NMR silent species for a yet-to-be-known reason.

For comparison, chemical reduction of **D1** with 2 equiv of ^{t}BuMgCl in MeCN with 100 equivalents of benzonitrile under N_2 leads to the formation of **D2** as a minor product in 6% yield. However, the major product (74% yield) was an Fe(II) species with a single hydride bound axial to a single DCyPE, based on the doublet in the ^{31}P NMR spectrum and triplet in the ^1H NMR spectrum with matching coupling constants. This is the first hydride observed from this complex. We propose that the Grignard reagent attacks the benzonitrile and forms ^{t}Bu-phenylketimine. This species can coordinate to the Fe(0) species and perform directed-C-H activation to generate product **D3**. We propose that the mono-ligated bidentate phosphine sets the Fe(0) species to an electronic configuration that prefers η^6 coordination over C-H activation. However, once the ketimine coordinates, the geometry allows C-H activation. This result provides evidence that these complexes can act as precatalysts for the chemistry reported by Ackermann in 2024[8] and 2025, in which ^{t}Bu-phenylketimine acts as a directed-C-H substrate for *ortho*-alkenylation catalyzed by bidentate-phosphine bound Fe(0) catalysts.

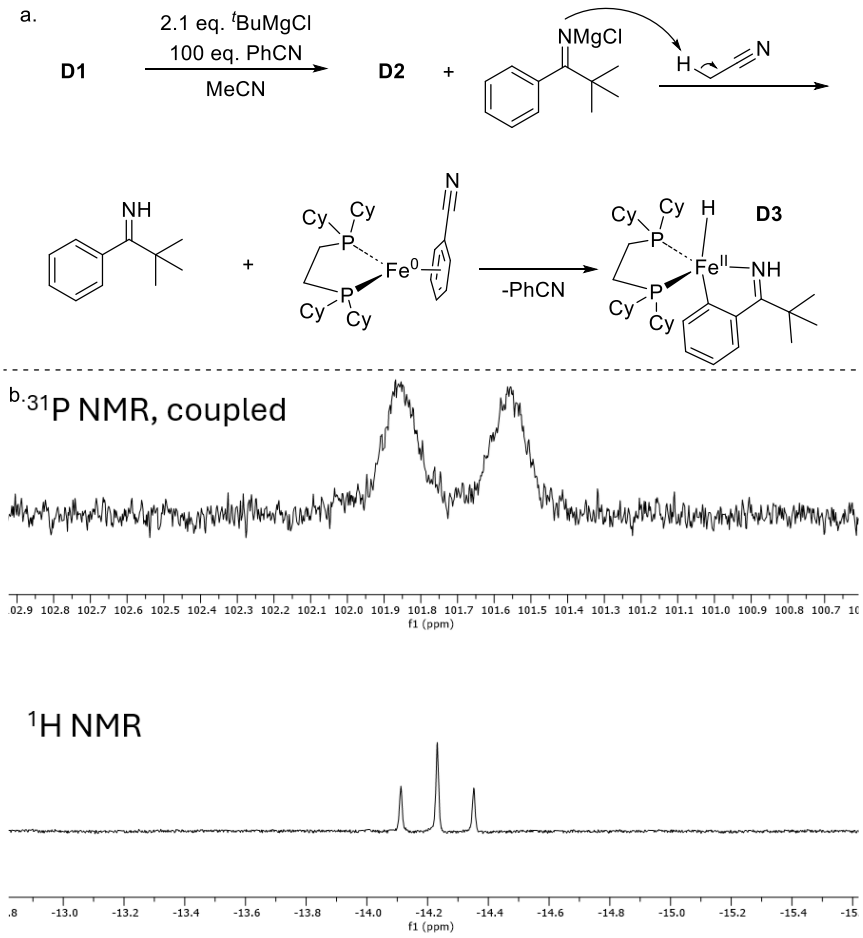


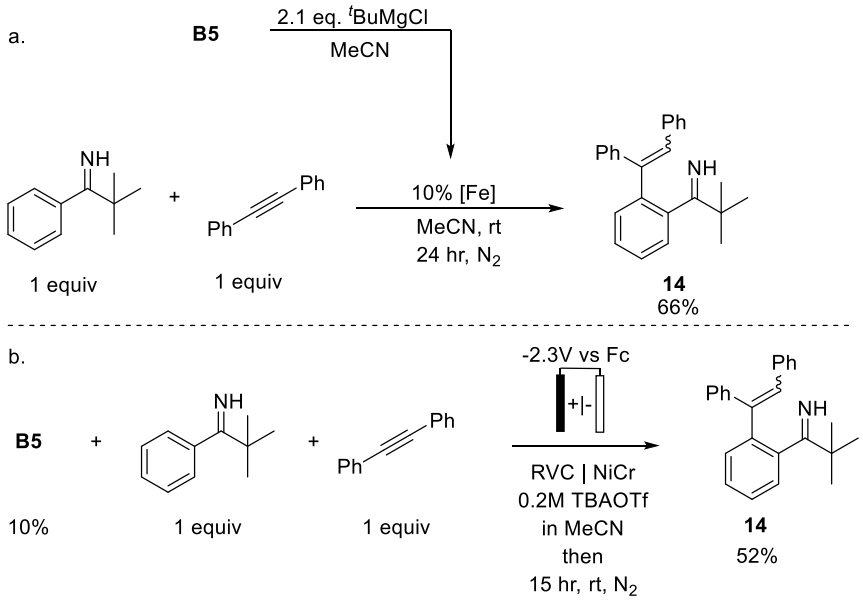
Figure 5.10. (a) Reaction of ^{t}BuMgCl with benzonitrile, forming a directed C-H activated substrate. (b) ^{1}H and ^{31}P NMR spectra of proposed C-H activated species. Coupling constant of 84.1 Hz.

5.4 **Electrocatalysis with Iron(II) Precatalysts**

The Ackermann group reported ^{t}Bu-phenylketimine as a competent substrate for *ortho*-C-H alkenylation *via* $(DPPE)_2Fe(0)$ species, **Figure 5.1**. In this method, the ketimine captures this Fe(0) species, avoiding the thermodynamic trap of **B3** and progressing towards productive C–H functionalization chemistry.[8] The following year, they reported **B2** as a competent, next generation catalyst for these transformations.

First, we investigated the ability **B5** to act as a catalyst in this transformation using a chemical reductant in MeCN, as described in Ackermann 2024, **Scheme 5.2a**. A 4mL vial was charged with 0.1 mmol ^{t}Bu-phenylketimine, 0.1 mmol diphenylacetylene, and a stir bar, and capped with a septa cap and taken out of the glovebox. A separate 4mL vial was charged with 0.01

mmol **B5** and 1 mL MeCN and capped with a septa cap, taken out of the glovebox, and charged with 2.1 equiv of ^{t}BuMgCl via syringe. The solution immediately turned from dark pink to nearly black. This mixture was drawn up via syringe and injected into the 4mL vial with the organic reagents. The mixture was stirred at ambient temperature for 24 h. This reaction gave 66% yield of **14** as determined by ^{1}H NMR spectroscopic analysis of the crude reaction mixture. In the photocatalysis from Ackermann, **Figure 5.1**, optimized conditions gives 75% yield. We next explored electroreduction as a means of activating the precatalyst **B5**, **Scheme 5.2b**. The reaction mixture was electrolyzed until the complex was fully reduced (~1.5 h), as monitored by the current versus time plot. Electrolysis was then stopped, and the reaction was stirred at ambient temperature for additional 15 h. Excitingly, this reaction gave **14** in 52% ^{1}H NMR yield, validating electrochemistry as a method for activating an iron precatalyst.



Scheme 5.2. (a) Chemical reduction to activate **B5** for catalysis. 0.1 M reaction concentration. (b) Electrochemical reduction to activate **B5** for catalysis. Electrochemical portion was monitored by live constant potential electrolysis trace. When the appropriate amount of charge to reduce 0.01 mmol of **B5** was passed, and the trace showed two reduction events, the electrolysis was stopped, electrodes removed, and the reaction was transferred to a new 20 mL vial to stir overnight. 0.1 mmol of substrate was used for both reactions.

5.5 **Conclusion**

This Chapter demonstrates the synthesis of a series of new bench stable Fe(II) complexes ligated with bidentate phosphines. Electrochemical reduction of these complexes provides access

to many of the same reactive Fe(0) intermediates reported in the literature from photochemical and chemical reductions of air sensitive Fe precursors. We show that tuning of the supporting electrolyte identity can be used to modulate product distributions. Finally, we demonstrated $(DPPE)_2(MeCN)_2Fe(OTf)_2$ to be a viable precatalyst for C-H cross-coupling reactions in both chemical and electrochemical manifolds.

5.6 **Outlook**

Moving forward, the DCyPE complex will be investigated as a precatalyst for the Ackermann directed alkenylation. Although the dinitrogen sensitivity of the free (DCyPE)Fe(0) complex lowers the stability of the η^6 Fe(0) complex, *in situ* reduction of the Fe(II) precatalyst is still an attractive avenue. The greater bulk of the cyclohexyl substituents could facilitate reductive elimination during catalysis.

In this vein, other directing groups will be investigated for this reaction. In Ackermann's report, the ^{t}Bu-phenylketmine was uniquely effective as a substrate. Changing the phosphine ligand and/or reductive pathway could potentially open up a greater scope of substrate. Along these lines, mono-substituted alkynes were largely ineffective in this Ackermann's chemistry. While the exact reason is not understood, the bulky DCyPE ligand might expand the alkyne scope of this transformation. Finally, other coupling partners would also be of interest for these transformations. For instance, B_2Pin_2 or boronic acids could be also couple in this system to generate C-C and C-B bonds, respectively.

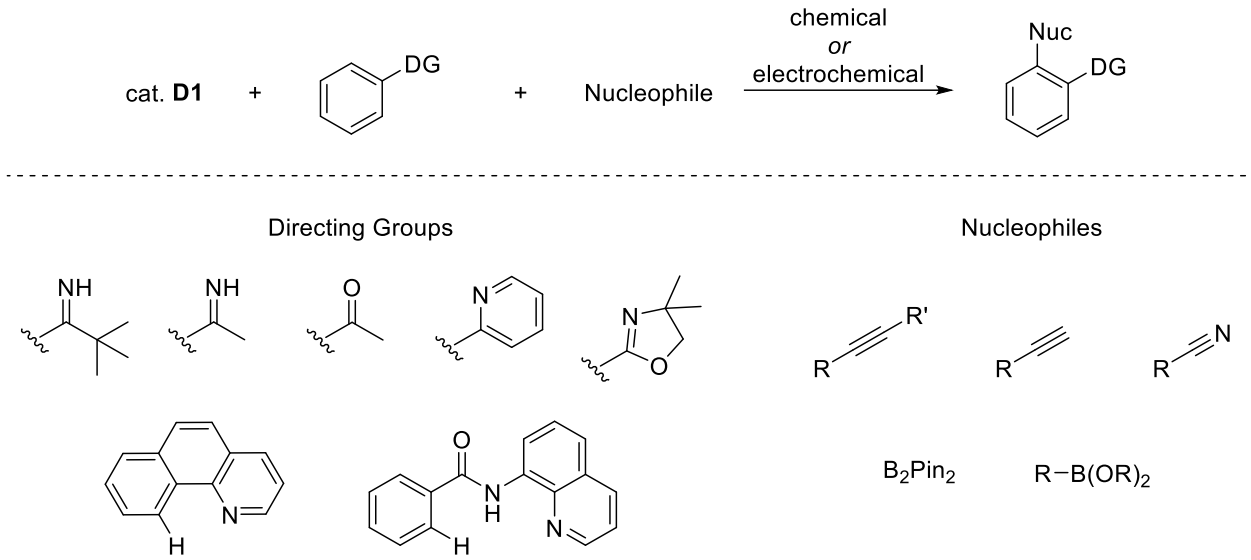
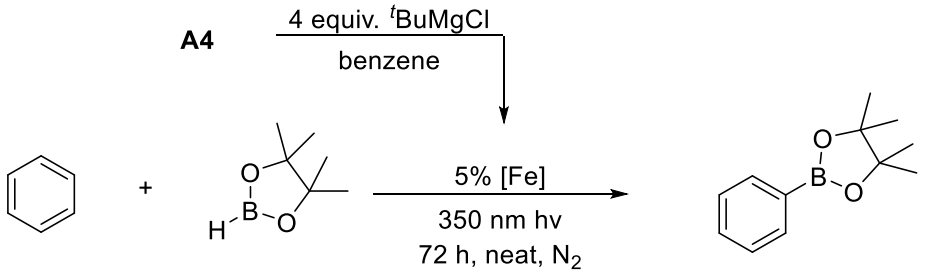


Figure 5.11. (a) Scheme of DCyPE as chemical and electrochemical precatalysts. (b) Extended directing group scope and coupling partner scope

Another next avenue for catalytic investigation is with the $(DMPE)_2$ complex **A4**. We were unable to transfer the photochemistry from Darcel and coworkers to electrochemistry precisely because electroreduction is so precise. This catalysis likely relies on the repeated photoreduction of would-be deleterious hydride species back to the active Fe(0) species, which eventually funnels to the observed reactivity. Because constant potential reduction in locked into the relatively weak reduction potential the cationic iron species, the neutral hydride species would have far too reducing cathodic potentials to be accessible. Thus, the deleterious species persist and there is no productive chemistry. For the chemical reductant, even though the Grignard would likely promote the reduction of the hydride species, it is not a continuous reductant so after the Grignard is exhausted, the reaction stalls.

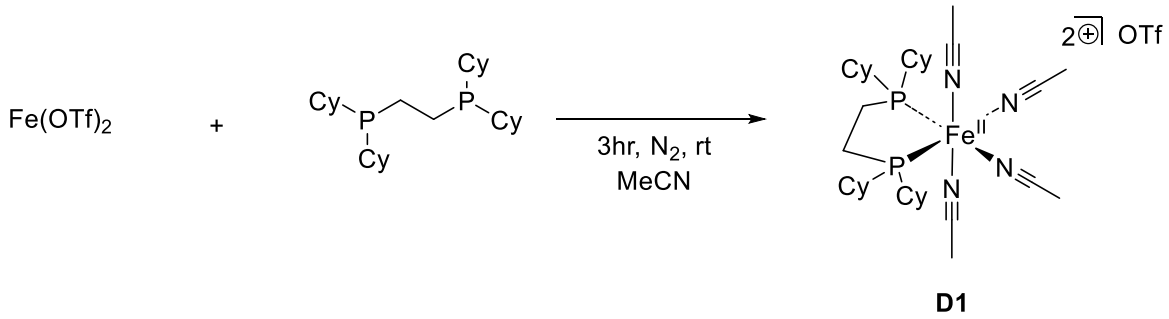
To circumvent this, we propose an initial chemical reduction to generate the Fe(0) and subsequently the dead-end Fe hydride species, followed by continual photoreduction would provide access to the C-H borylation reported by Darcel using our precatalysts.



Scheme 5.5. Cooperative chemical and photochemical proposal to access C-H borylation from bench-stable precatalysts.

5.7 Experimental

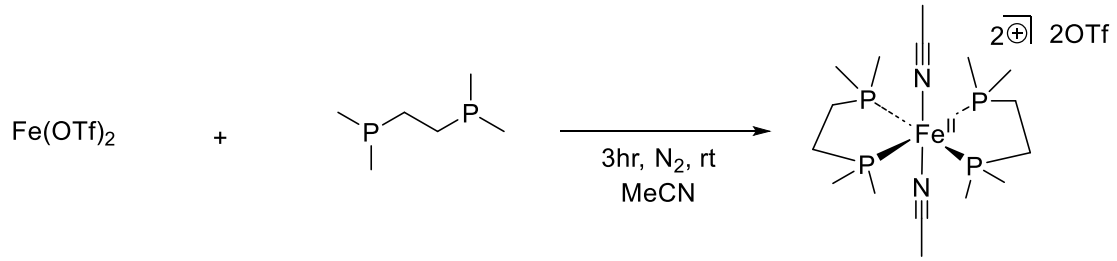
5.7.1 Synthesis of Iron(II) Triflate Phosphine Species



D1

In an Argon or N_2-filled glovebox, charge a 20mL vial will 355mg (1mmol, 1 equiv) of anhydrous $Fe(OTf)_2$, 844mg (2mmol, 2 equiv), of 1,2-bis-dicyclohexylphosphinoethane (DCyPE), 10mL of acetonitrile, and a stir bar. The reaction instantly turns red and is homogenous. This reaction was stirred for 3 hours at ambient temperatures. After this time, the reaction was filtered through celite or a syringe filter into a massed 20mL vial. The reaction vial was taken outside of the box at this point. The filtered solution was concentrated under vacuum or N_2 flow to about 3mL. To this solution, diethyl ether was added to the solution slowly until the upper layer forms a precipitate layer that does not immediately redissolve (~10mL). The vial was homogenized, ~5mL of Et_2O was added and the vial was placed in the -35 °C freezer overnight. Dark red suitable for SC-XRD crystals formed almost immediately, the mother liquor was decanted into another vial (which can be resubjected to recrystallization conditions). The remaining solids were dried under vacuum and powdered to yield dark red solids (669mg, 71% from two recrystallizations of the mother liquor).

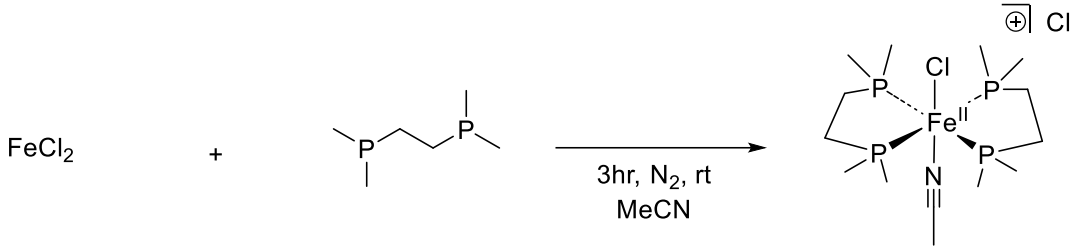
^{1}H NMR (500 MHz, CD_3CN) 1.84 (m, 16H), 1.72 (app. d, J = 11.4 Hz, 4H), 1.59 (qd, J = 11.3, 9.8, 6.7 Hz, 4H), 1.35(m, 8H), 1.25(m, 8H) The MeCN peaks exchange rapidly with solvent. ^{13}C NMR (126 MHz, CD_3CN) δ 36.24 – 35.71 (m), 29.33, 28.06 (t, *J* = 5.6 Hz), 27.45 (d, *J* = 4.6 Hz), 26.47. ^{31}P NMR (203 MHz, CD_3CN) δ 72.70.



A4

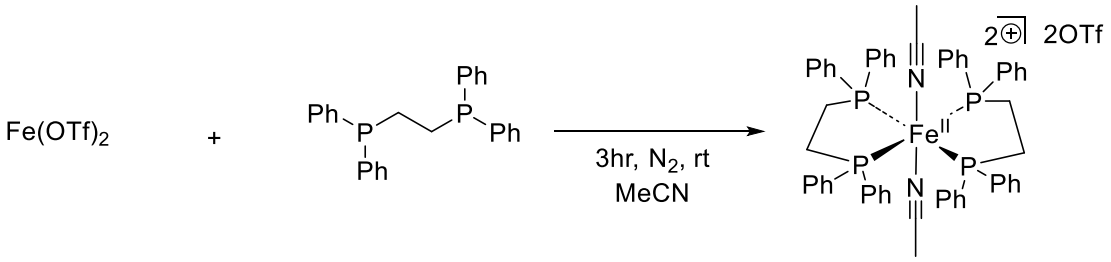
In an Argon or N_2-filled glovebox, charge a 20mL vial will 355mg (1mmol, 1 equiv) of anhydrous $Fe(OTf)_2$, 300mg (2mmol, 2 equiv), of 1,2-bis-dimethylphosphinoethane (DMPE), 10mL of acetonitrile, and a stir bar. The reaction instantly turns red and is homogenous. This reaction was stirred for 3 hours at ambient temperatures, during which it turns a lighter shade of red. After this time, the reaction was filtered through celite or a syringe filter into a 20mL vial. To this solution, diethyl ether was added to the solution slowly until the upper layer forms a precipitate layer that does not immediately redissolve (~10mL). The vial was homogenized, ~5mL of Et_2O was added and the vial was placed in the -35 °C freezer overnight. Dark orange solids (impurity) formed overnight, the mother liquor was decanted into another vial. The mother liquor was dried completely, dissolved in acetone, and recrystallized with pentane. Yellow crystals suitable for SC-XRD formed overnight, which are product. The process may need to be repeated several times. The crystals were dried under vacuum and powdered to yield bright yellow solids (250mg, 34% yield).

^{1}H NMR (500 MHz, CD_3CN) δ 2.14 (s, 8H), 1.49 (p, *J* = 1.9 Hz, 24H). The MeCN peaks exchange rapidly with solvent. ^{13}C NMR (126 MHz, CH_3CN) δ 66.54 (d, *J* = 4.8 Hz), 15.88 (d, *J* = 13.0 Hz). ^{31}P NMR (203 MHz, CD_3CN) δ 59.65 (d, *J* = 4.3 Hz).



A5

In an Argon or N_2-filled glovebox, charge a 20mL vial will 128mg (1mmol, 1 equiv) of anhydrous $FeCl_2$, 300mg (2mmol, 2 equiv), of 1,2-bis-dimethylphosphinoethane (DMPE), 10mL of acetonitrile, and a stir bar. The addition of DMPE to $FeCl_2$ is green. The reaction instantly turns purple and is homogenous when the MeCN is added. This reaction was stirred for 3 hours at ambient temperatures. After this time, the reaction was filtered through celite or a syringe filter into a 20mL vial. To this solution, diethyl ether was added to the solution slowly until the upper layer forms a precipitate layer that does not immediately redissolve (~5mL). The vial was homogenized, ~3mL of Et_2O was added and the vial was placed in the -35 °C freezer overnight. Dark pink suitable for SC-XRD crystals form, which are product. The mother liquor was decanted into another vial (which can be resubjected to recrystallization conditions). The crystals were dried under vacuum and powdered to yield light purple solids (346mg, 74% yield).



B4

In an Argon or N_2-filled glovebox, charge a 20mL vial will 355mg (1mmol, 1 equiv) of anhydrous $Fe(OTf)_2$, 797mg (2mmol, 2 equiv), of 1,2-bis-diphenylphosphinoethane (DPPE), 10mL of acetonitrile, and a stir bar. The reaction instantly turns red and is homogenous. This reaction was stirred for 3 hours at ambient temperatures. After this time, the reaction was filtered through celite or a syringe filter into a massed 20mL vial. The reaction vial was taken outside of the box at this point. To this solution, diethyl ether was added to the solution slowly until the upper layer forms a precipitate layer that does not immediately redissolve (~5mL). The vial was

homogenized, ~3mL of Et_2O was added and the vial was placed in the -35 °C freezer overnight. Dark red crystals suitable for SC-XRD formed overnight, the mother liquor was decanted into another vial (which can be resubjected to recrystallization conditions). The remaining solids were dried under vacuum and powdered to yield magenta solids (1024mg, 83% from two recrystallizations of the mother liquor).
^{1}H NMR (500 MHz, CD_3CN) δ 7.55 (t, *J* = 7.5 Hz, 1H), 7.31 (t, *J* = 7.6 Hz, 2H), 7.06 – 6.80 (m, 2H), 2.96 (q, *J* = 5.3 Hz, 2H). The MeCN peaks exchange rapidly with solvent ^{13}C NMR (126 MHz, CD_3CN) δ 133.19, 132.31, 132.09, 131.65. ^{31}P NMR (202 MHz, CD_3CN) δ 50.85.

5.7.2 Cyclic Voltammetry of Iron Species

Initial cyclic voltammograms for characterization were collected in 0.1M $TBAPF_6$ in MeCN at 100mV scan rate with 0.005 mmol complex dissolved in a 20mL vial. Our working electrode was a 1mm disc glassy carbon electrode, graphite rod as the counter electrode, and the reference electrode consisted of a silver wire inside a glass tube filled with electrolyte solution separated from the main solution with a VyCor glass frit. After the CV was taken, ferrocene was added to the solution and the CV was conducted again. Potentials listed are referenced to ferrocene.

Before each constant potential bulk electrolysis, a CV was taken of the complex with the reference electrode. Because our reference electrode does not contain a Ag/Ag^+ ion buffer, this pseudo-reference may “drift”. The CV was taken right before the electrolysis and the potential of the electrolysis was set to 20mV more negative than the approximate cathodic peak measured at that time with that reference.

5.7.3 Bulk Electrolysis of Iron Species

Constant potential bulk electrolyses were performed in an H-Cell divided by a glass frit. On the working side, reticulated vitreous carbon foam was used as the electrode material. Care was taken to ensure that the copper wire that connected the electrode material to the lead from the potentiostat did not come in direct contact with the reaction solution. On the counter side, a coil a NiCr wire was used as the counter. An equal height of electrolyte solution was added to each side

of the H-Cell. The cells were not sealed from the glovebox atmosphere. Any reaction that included an additive, the additive was added to the working side at the time of the reaction setup.

5.7.4 Chemical Reduction of Iron Species

General Procedure for Grignard-reduction of iron species: In a N_2-filled glovebox, a 4 mL vial was charged with a stir bar, 0.05 mmol of iron complex, solvent of choice, then capped with a septa cap, wrapped in electrical tape and removed from the glovebox. This vial was cooled to 0 °C for 30 minutes, then 2.1 equiv of ^{t}BuMgCl in Et_2O was added via syringe while stirring. This reaction stayed at 0 °C for 30 minutes and then was allowed to warm to ambient temperature for 4 h. After which, the vial was brought back into the glovebox and an NMR was taken.

5.7.5 Catalytic Reactions

Chemical

General Procedure for Grignard-reduced catalytic reaction: A 4 mL vial was charged with 0.1 mmol ^{t}Bu-phenylketimine, 0.1 mmol diphenylacetylene, a stir bar, and capped with a septa cap and taken out of the glovebox. A separate 4mL vial was charged with 0.01 mmol of precatalyst and 1 mL MeCN and capped with a septa cap, taken out of the glovebox, and charged with 2.1 equiv of ^{t}BuMgCl via syringe. This mixture was drawn up via syringe and injected into the 4 mL vial with the organic reagents. The mixture was stirred at ambient temperature for 24 h. 0.1mmol of 1,3,5-trimoethoxy benzene is added and a crude ^{1}H NMR was taken was of this reaction mixture. The alkenyl proton is observed and integrated. Isolation of organic product follows procedure from Ackermann[8,9]

Electrochemical

General Procedure for Electro-reduced catalytic reaction In N_2-filled glovebox, a 20mL vial was charged with 0.1 mmol ketimine, 0.1 mmol diphenylacetylene, and a stir bar. In an H-Cell, one side was charged with 0.01 mmol precatalyst, a stir bar, and 5mL of 0.2 M TBAOTf in MeCN. A RVC working electrode was added. In the other side, an equivalent height of 0.2 M TBAOTf in MeCN was added, along with a stir bar, NiCr counter electrode and reference

electrode. A constant potential bulk electrolysis was conducted at 20mV more negative than the cathodic peak of the precatalyst. Live monitoring of the trace determines when the appropriate amount of charge has been passed to fully reduce the Fe(II) precatalyst to Fe(0). After this time, the electrolysis was stopped, electrodes removed, and working side solution transferred to the 20mL vial with the organic reagents and stirred for 24 h.

5.8 References-

1. Dombray, T.; Werncke, C. G.; Jiang, S.; Grellier, M.; Vendier, L.; Bontemps, S.; Sortais, J.; Sabo-Etienne, S.; Darcel, C. "Iron-Catalyzed C-H Borylation of Arenes", *J. Am. Chem. Soc.*, **2015**, 137, 4062-4065
2. Neumann, T.; Wowk, V.; Djebbar, F.; Chamoreau, L.; Lefevre, G. "Iron-Mediated Si-H Bond Activation: Synthesis, Characterization and Spectral Properties of a Series of $Fe^{II}(H)(SiR_3)(dmpe)_2$ Complexes", *Inorg. Chem.*, **2025**, 64, 22251-22261
3. Whittlesey, M. K.; Mawby, R. J.; Osman, R.; Perutz, R. N.; Field, L. D.; Wilkinson, M. P.; George, M. W. "Transient and Matrix Photochemistry of $Fe(dmpe)_2H_2$ (dmpe = $Me_2PCH_2CH_2PMe_2$): Dynamics of C-H and H-H Activation", *J. Am. Chem. Soc.*, **1993**, 115, 8627-8637
4. Ittel, S. D.; Tolman, C. A.; English. A. D.; Jesson, J. P. "The Chemistry of 2-Naphthyl Bis[bis(dimethylphosphino)ethane] Hydride Complexes of Fe, Ru, and Os. 2. Cleavage of sp and sp^3 C-H, C-O, and C-X Bonds. Coupling of Carbon Dioxide and Acetonitrile", *J. Am. Chem. Soc.*, **1978**, 7577-7585
5. Baker, M. V.; Field, L. D. "Reversible Metalation of Alkyl and Aryl Groups by a Coordinatively Unsaturated Iron Complex", *J. Am. Chem. Soc.*, **1986**, 5, 821-823
6. McWilliams, S.F.; Broere, D.L. J.; Halliday, C. J. V.; Bhutto, S. M.l Mercado, B. Q.; Holland, P. L. "Coupling dinitrogen and hydrocarbons through aryl migration", *Nature*, **2020**, 584, 221-226
7. Li, Y.; Hidalgo, N.; Bhutto, S. M.; Chew, N. B.; Mercado, B. Q.; Holland, P. L.; Chen, H. "Akali Metal Control of Triplet-Mediated C-H Activation in Iron-Mediated Coupling of Dinitrogen and Benzene", *Inorg. Chem.* **2025**, 64, 17387–17398

8. Messinis, A. M.; von Munchow, T.; Surke, M.; Ackermann, L. “Room temperature photo-promoted iron-catalysed arene C-H alkenylation without Grignard reagents”, *Nat. Cat.*, **2024**¸7, 273-284
9. Surke, M.; Simon, M. M.; Oliveira, J. C. A.; Ackermann, L. “Well-Defined Iron(0) Precatalysts for Grignard-Free C-H Alkenylation at Room Temperature”, *ACS Catal.*, **2025**, 12676-12683
10. Hata, G.; Kondo, H.; Miyake, A. “Ethylenebis (diphenylphosphine) Complexes of Iron and Cobalt. Hydrogen Transfer between the Ligand and Iron Stom”, *J. Am. Chem. Soc.*, **1968**, 90, 2278-2281
11. Azizian, H.; Morris, R. “Photochemical Synthesis and Reaction of $FeH(C_6H_4PPhCH_2CH_2PPh_2)(PPh_2CH_2CH_2PPh_2)$”, *Inorg. Chem.*, **1983**, 22, 6-9
12. DuBois, D.; Miedaner, A. “Synthesis, Characterization, and Electrochemical Studies of Iron, Cobalt, and Nickel Complexes of Polyphosphine Ligands.” *Inorg. Chem.*, **1986**, 25, 4642-4650
13. Patel, D. et. al. “Synthesis and characterisation of halide, separated ion pair, and hydride cyclopentadienyl iron bis(diphenylphosphino)ethane derivaties” *Dalton Trans*, **2015**, 44, 13159-14177